NMR INVESTIGATION OF QUADRUPOLAR NUCLEI IN MINERALOGY

BY

ZHI XU

A Thesis
Submitted to the Faculty of Graduate Studies
in Partial Fulfilment of the Requirements
for the Degree of

MASTER OF SCIENCE

Department of Geological Sciences
The University of Manitoba
Winnipeg, Manitoba

July, 1993

ISBN 0-315-86102-9

Name Xu Zhi

Dissertation Abstracts International is arranged by broad, general subject categories. Please select the one subject which most nearly describes the content of your dissertation. Enter the corresponding four-digit code in the spaces provided.

Geology
SUBJECT TERM

0370
SUBJECT CODE

U·M·I

Subject Categories

THE HUMANITIES AND SOCIAL SCIENCES

COMMUNICATIONS AND THE ARTS
Architecture 0729
Art History 0377
Cinema 0900
Dance 0378
Fine Arts 0357
Information Science 0723
Journalism 0391
Library Science 0399
Mass Communications 0708
Music 0413
Speech Communication 0459
Theater 0465

EDUCATION
General 0515
Administration 0514
Adult and Continuing 0516
Agricultural 0517
Art 0273
Bilingual and Multicultural 0282
Business 0688
Community College 0275
Curriculum and Instruction 0727
Early Childhood 0518
Elementary 0524
Finance 0277
Guidance and Counseling 0519
Health 0680
Higher 0745
History of 0520
Home Economics 0278
Industrial 0521
Language and Literature 0279
Mathematics 0280
Music 0522
Philosophy of 0998
Physical 0523
Psychology 0525
Reading 0535
Religious 0527
Sciences 0714
Secondary 0533
Social Sciences 0534
Sociology of 0340
Special 0529
Teacher Training 0530
Technology 0710
Tests and Measurements 0288
Vocational 0747

LANGUAGE, LITERATURE AND LINGUISTICS
Language
- General 0679
- Ancient 0289
- Linguistics 0290
- Modern 0291

Literature
- General 0401
- Classical 0294
- Comparative 0295
- Medieval 0297
- Modern 0298
- African 0316
- American 0591
- Asian 0305
- Canadian (English) 0352
- Canadian (French) 0355
- English 0593
- Germanic 0311
- Latin American 0312
- Middle Eastern 0315
- Romance 0313
- Slavic and East European 0314

PHILOSOPHY, RELIGION AND THEOLOGY
Philosophy 0422
Religion
- General 0318
- Biblical Studies 0321
- Clergy 0319
- History of 0320
- Philosophy of 0322

Theology 0469

SOCIAL SCIENCES
American Studies 0323
Anthropology
- Archaeology 0324
- Cultural 0326
- Physical 0327

Business Administration
- General 0310
- Accounting 0272
- Banking 0770
- Management 0454
- Marketing 0338

Canadian Studies 0385
Economics
- General 0501
- Agricultural 0503
- Commerce-Business 0505
- Finance 0508
- History 0509
- Labor 0510
- Theory 0511

Folklore 0358
Geography 0366
Gerontology 0351
History
- General 0578
- Ancient 0579
- Medieval 0581
- Modern 0582
- Black 0328
- African 0331
- Asia, Australia and Oceania 0332
- Canadian 0334
- European 0335
- Latin American 0336
- Middle Eastern 0333
- United States 0337

History of Science 0585
Law 0398
Political Science
- General 0615
- International Law and Relations 0616
- Public Administration 0617

Recreation 0814
Social Work 0452
Sociology
- General 0626
- Criminology and Penology 0627
- Demography 0938
- Ethnic and Racial Studies 0631
- Individual and Family Studies 0628
- Industrial and Labor Relations 0629
- Public and Social Welfare 0630
- Social Structure and Development 0700
- Theory and Methods 0344

Transportation 0709
Urban and Regional Planning 0999
Women's Studies 0453

THE SCIENCES AND ENGINEERING

BIOLOGICAL SCIENCES
Agriculture
- General 0473
- Agronomy 0285
- Animal Culture and Nutrition 0475
- Animal Pathology 0476
- Food Science and Technology 0359
- Forestry and Wildlife 0478
- Plant Culture 0479
- Plant Pathology 0480
- Plant Physiology 0817
- Range Management 0777
- Wood Technology 0746

Biology
- General 0306
- Anatomy 0287
- Biostatistics 0308
- Botany 0309
- Cell 0379
- Ecology 0329
- Entomology 0353
- Genetics 0369
- Limnology 0793
- Microbiology 0410
- Molecular 0307
- Neuroscience 0317
- Oceanography 0416
- Physiology 0433
- Radiation 0821
- Veterinary Science 0778
- Zoology 0472

Biophysics
- General 0786
- Medical 0760

EARTH SCIENCES
Biogeochemistry 0425
Geochemistry 0996
Geodesy 0370
Geology 0372
Geophysics 0373
Hydrology 0388
Mineralogy 0411
Paleobotany 0345
Paleoecology 0426
Paleontology 0418
Paleozoology 0985
Palynology 0427
Physical Geography 0368
Physical Oceanography 0415

HEALTH AND ENVIRONMENTAL SCIENCES
Environmental Sciences 0768
Health Sciences
- General 0566
- Audiology 0300
- Chemotherapy 0992
- Dentistry 0567
- Education 0350
- Hospital Management 0769
- Human Development 0758
- Immunology 0982
- Medicine and Surgery 0564
- Mental Health 0347
- Nursing 0569
- Nutrition 0570
- Obstetrics and Gynecology 0380
- Occupational Health and Therapy 0354
- Ophthalmology 0381
- Pathology 0571
- Pharmacology 0419
- Pharmacy 0572
- Physical Therapy 0382
- Public Health 0573
- Radiology 0574
- Recreation 0575
- Speech Pathology 0460
- Toxicology 0383

Home Economics 0386

PHYSICAL SCIENCES
Pure Sciences
Chemistry
- General 0485
- Agricultural 0749
- Analytical 0486
- Biochemistry 0487
- Inorganic 0488
- Nuclear 0738
- Organic 0490
- Pharmaceutical 0491
- Physical 0494
- Polymer 0495
- Radiation 0754

Mathematics 0405
Physics
- General 0605
- Acoustics 0986
- Astronomy and Astrophysics 0606
- Atmospheric Science 0608
- Atomic 0748
- Electronics and Electricity 0607
- Elementary Particles and High Energy 0798
- Fluid and Plasma 0759
- Molecular 0609
- Nuclear 0610
- Optics 0752
- Radiation 0756
- Solid State 0611

Statistics 0463

Applied Sciences
Applied Mechanics 0346
Computer Science 0984
Engineering
- General 0537
- Aerospace 0538
- Agricultural 0539
- Automotive 0540
- Biomedical 0541
- Chemical 0542
- Civil 0543
- Electronics and Electrical 0544
- Heat and Thermodynamics 0348
- Hydraulic 0545
- Industrial 0546
- Marine 0547
- Materials Science 0794
- Mechanical 0548
- Metallurgy 0743
- Mining 0551
- Nuclear 0552
- Packaging 0549
- Petroleum 0765
- Sanitary and Municipal 0554
- System Science 0790

Geotechnology 0428
Operations Research 0796
Plastics Technology 0795
Textile Technology 0994

PSYCHOLOGY
General 0621
Behavioral 0384
Clinical 0622
Developmental 0620
Experimental 0623
Industrial 0624
Personality 0625
Physiological 0989
Psychobiology 0349
Psychometrics 0632
Social 0451

NMR INVESTIGATION OF QUADRUPOLAR NUCLEI IN MINERALOGY

BY

ZHI XU

A Thesis submitted to the Faculty of Graduate Studies of the University of Manitoba in partial fulfillment of the requirements for the degree of

MASTER OF SCIENCE

ACKNOWLEDGEMENT

I would like to thank my supervisor, Dr. Barbara L. Sherriff, for introducing me into the fantastic world of solid state nuclear magnetic resonance and for all the opportunities she provided me. I could have never gone so far without her kind help and guidance. I am grateful to Dr. Ted Schaefer, who gave me tremendous help with his knowledge, and Dr. Brian Pettitt, who taught me the formal theory of quadrupolar interaction and gave the simulation software. Thanks also goes to Dave Teertstra, Jian-Jie Liang for helping to better understand the crystallography of minerals. Special thanks goes to Kirk Marat and Terry Wolowiec for setting up the equipments and pulsing programming. Bruker Ltd., Canada is thanked for the loan of the DOR probe.

I appreciate deeply the review of the thesis by Dr. Ted Schaefer, Dr. Norman M. Halden and Dr. K. S. Sharma.

Finally I would like to thank my wife, Yang Jin, for her help and understanding.

ABSTRACT

Nuclear magnetic resonance is one of the most powerful techniques in investigating the structure and dynamics of molecular systems in many fields. In this thesis solid state NMR is used to study problems in mineralogy.

The formal quantum mechanical theory of quadrupolar interactions is discussed in detail from first principles. Equations to calculate quadrupolar shifts of all the transitions are derived. The principles and techniques of magic angle spinning (MAS), double-rotation (DOR) and dynamic angle spinning (DAS) NMR are discussed and their advantages and limitations are compared.

MAS, DAS and DOR NMR are used to study the local atomic environments in tugtupite, $Na_8[Al_2Be_2Si_8O_{24}](Cl,S)_2$. The structure is found to be exceptionally well ordered with only one Si, Al, Na and Be environment. The quadrupolar parameters C_Q (quadrupolar coupling constant) and η (asymmetry parameter) of ^{23}Na and ^{27}Al were obtained by a comparison of a computer simulation of the MAS central transition line-shape at two different fields with experimental results and the results are verified in two ways.

^{27}Al DOR NMR spectra of the alumino-silicate polymorph minerals, kyanite, sillimanite and andalusite, show separately resolved peaks for the first time, relating to the crystallographically non-equivalent sites. The isotropic chemical shifts are calculated from the observed peak positions and they correlate closely with those found previously by simulation of MAS NMR spectra. The intensities of the four

non-equivalent sites in kyanite are found to have an exponential relationship with their corresponding quadrupolar coupling constants (C_Q).

DOR NMR at 8.4 T, MAS NMR at both 8.4 T and 11.7 T are applied to ^{23}Na and ^{27}Al nuclei to study cation ordering in the scapolite mineral series. Different ways of fitting peaks to the spectra have been done to investigate the possible explanations.

TABLE OF CONTENTS

LIST OF ABBREVIATIONS

NMR : nuclear magnetic resonance

MAS : magic angle spinning

DOR : double rotation

DAS : dynamic angle spinning

LAS : laboratory axis system

PAS : principle axis system

CSA : chemical shift anisotropy

FT : Fourier transform

FID : free induction decay

RF : radio frequency

PWHH: peak width at half height

TMS : tetramethylsilane

Ma : marialite

Me : meionite

QCC : quadrupolar coupling parameter

LIST OF FIGURES

LIST OF TABLES

CHAPTER ONE. INTRODUCTION TO NUCLEAR MAGNETIC RESONANCE IN SOLIDS

1.1. INTRODUCTION

About fifty years ago the phenomenon of nuclear magnetic resonance (NMR) was discovered independently by F. Bloch and E. M. Purcell in the United States of America.[1.1][1.2] Since then the NMR techniques have developed dramatically, especially after the early 1970s when R. Ernst and W. A. Anderson invented pulse Fourier Transform (FT) NMR.[1.3] Now NMR is one of the most powerful tools in investigating the structure and dynamics of molecular systems in chemistry, biochemistry, physics, material sciences, medicine, pharmacy, agriculture and mineralogy.

The objective of this study is to investigate the applicability of the newly developed double-angle techniques of double rotation (DOR)[1.4] and dynamic-angle spinning (DAS)[1.5] NMR for quadrupolar nuclei in alumino-silicate minerals.

This thesis is divided into six chapters. Chapter one explains the general theory of solid state NMR and the importance of the new techniques, DOR and DAS, for quadrupolar nuclei in solids. In chapter two, a formal quantum mechanical treatment of quadrupolar interactions is discussed in detail, including the first- and

second-order perturbation expansion and formulae to calculate the quadrupolar shifts in different strengths of the magnetic field. Chapter three contains the basic principles of magic angle spinning (MAS), DOR and DAS NMR and some practical experimental details.

In chapter four, a well-ordered mineral, tugtupite, is used to evaluate the utility of MAS, DAS, DOR and variable temperature MAS. Quadrupolar parameters are obtained through simulations of the MAS lineshape at two magnetic fields and the problem of chemical shift distributions is discussed. Chapter five describes the application of DOR NMR to ^{27}Al in the alumino-silicate polymorphs. The peaks due to different ^{27}Al environments are resolved for the first time and the isotropic chemical shifts are calculated. In chapter six, Al/Si ordering in the scapolite mineral series is examined using DOR and MAS and some new results are presented.

1.2. PRINCIPLES OF NUCLEAR MAGNETIC RESONANCE

Each element in the Periodic Table has at least one isotope which has a non-zero nuclear spin and a concomitant magnetic moment. When such a nucleus is placed in a magnetic field, B_0, its magnetic moment will interact with the magnetic field and attain a series of Zeeman energy levels. The Zeeman Hamiltonian of this interaction is[1.6]

$$H_{Zeeman} = - \gamma \hbar B_0 I_z \qquad (1.1)$$

where γ is the magnetogyric ratio of the nucleus, $\hbar$ is the Planck constant, B_0 is the

strength of the static magnetic field. In the laboratory axis system (LAS) the z-axis is vertical and the x- and y-axis are in the horizontal plane. B_0 is along z-axis in LAS and I_z is the projection of the nuclear spin I along the z direction.

When the nucleus is in the magnetic field, the nuclear spin undergoes a precession about B_0. The precession frequency is called the Larmor frequency (ω_I):

$$\omega_I = \gamma B_0 \tag{1.2}$$

The Larmor frequency of each isotope of the nucleus is different and as there is rarely overlap between frequencies, it is possible for isotopes to be investigated separately. The nuclear spin has a magnetic moment, μ.

A pulse of radio-frequency radiation at the Larmor frequency is generated by a small, time-dependent, magnetic field, B_1, which lies along the x-axis in the LAS. When this pulse is applied to the sample, the magnetic moment of the nuclear spin tips with respect to B_0. The tip angle (θ) is proportional to the strength and duration (t) of B_1:[1.7]

$$\theta = \gamma B_1 t \tag{1.3}$$

If θ is equal to 90°, the magnetic moment is rotated to the y-axis.

After the r. f. pulse is turned off, the magnetic moment of the nuclear spin dephases in the x-y plane (T_2 relaxation) and returns to the z-axis (T_1 relaxation). The precession of the magnetic moment during dephasing in the x-y plane is recorded as a function of the time to give a free induction decay (FID). The FID is then Fourier-transformed from the time domain to the frequency domain to give the NMR spectrum.

The major NMR interactions are Zeeman (H_z), dipole-dipole interaction (H_{DD}), chemical shift shielding (H_{CS}), J-coupling (H_J) and quadrupolar interaction (H_Q):[1.8]

$$H_{total} = H_Z + H_{DD} + H_{CS} + H_J + H_Q \qquad (1.6)$$

H_{DD} is the interaction between the dipoles of two nuclear spins. It depends on the magnitude and orientation of their magnetic moments and also on the length and orientation of the vector describing their relative positions. It is independent of the applied magnetic field strength.[1.8]

H_{CS} is the screening of B_0 at the nucleus by the surrounding electrons. It consists of a scalar isotropic value and a traceless anisotropic tensor, which is called the chemical shift anisotropy (CSA). The elements of the tensor depend on the orientation of the electrical charge distribution around the nucleus. The magnitude of H_{CS} is proportional to the applied magnetic field strength.[1.8]

H_J is the indirect coupling of two nuclear spins through the mediation of surrounding electrons. This weak coupling is important in liquids and is usually too small to be observed in solids. Like dipole-dipole interactions, it is also independent of the applied magnetic field strength.[1.8]

H_Q only exists for nuclei with spin > 1/2. It is due to the electrical interaction between the non-spherical, symmetrical nuclear electric charge distribution and the electric field gradient at the site of the nucleus. It is independent of the applied magnetic field strength.[1.8]

These interactions all depend on the local chemical environment of the

nucleus. NMR can be used to measure these interactions and gain information about structure.

The chemical shift (δ) is the difference between two resonant frequencies, measured in parts per million (ppm) of B_0 with respect to a reference signal (ν_R).[1.7]

$$\delta = (\nu_L - \nu_R)/\nu_R \tag{1.4}$$

where ν_L is the Larmor frequency of the peak; ν_R is the Larmor frequency of the reference. For ^{27}Al, the reference is $AlCl_3$ in a 1 M aqueous solution; for ^{23}Na, it is NaCl in a 1 M aqueous solution; for ^{29}Si, it is tetramethylsilane (TMS). If all the nuclei are completely relaxed, the areas under the peaks gives the relative populations of the nucleus at each magnetic environment.

The detectable NMR signal intensity is proportional to the population difference (ρ) of two adjacent energy levels and at room temperature, it is given by the equation:[1.6]

$$\rho \propto \mu_z B_0/kT \tag{1.5}$$

where ρ is the difference in population density; μ_z is the z-component of the nuclear magnetic moment; k is the Boltzmann constant; T is the sample temperature in degrees Kelvin.

Because of the small value for μ, at room temperature, $\mu_z B_0$ is much smaller than kT and NMR signal sensitivity is very low. For ^1H, which has the second largest μ of all isotopes, $\mu_z B_0/kT$ is only about 10^{-6} for a B_0 of 1 T (Nucleus ^3H has the largest μ). Factors affecting the NMR signal to noise ratio (S/N), include magnetic field strength, sample temperature, and sample volume.

One way to solve the problem of low sensitivity is to increase the magnetic field strength. NMR spectroscopists refer to magnetic field strengths by the Larmor frequency of ^1H at that particular magnetic field strength. The largest stable magnetic field is 750 MHz (or 17.6 T).

Another way is to collect and add a large number (N) of FID's before Fourier transformation. As the signals are added in phase and the noise is not, the signal to noise ratio can be improved by a factor of $N^{1/2}$.[1.7] In pulsed Fourier Transform NMR, one RF pulse can usually excite all the magnetic non-equivalent sites of interest, but between each experiment one has to wait long enough (3 to 5 times T_1) to let the system fully relax and reattain equilibrium. Therefore, for a nucleus with a slow relaxation, the total experimental time can be long.

1.3. SOLID STATE NMR

In liquids rapid random motion of molecules, such as Brownian motion, averages anisotropic dipole-dipole, quadrupolar, chemical shift, and J-coupling interactions. The resulting high resolution spectra yield isotropic chemical shifts and scalar J-couplings.[1.7]

In solids, the situation is different, as the atoms are located in a rigid structure. If magnetic nuclei are adjacent, it will result in strong homonuclear and heteronuclear dipole-dipole interactions (H_{DD}). These interactions are independent of the crystal orientation and they cause rapid transverse relaxation (T_2) and thus

large homogeneous line broadening.

Chemical shift and quadrupolar interactions are orientation dependent. Individual grains of powdered samples have random orientations and each orientation corresponds to a peak. The overall result of all possible orientations in space causes the overlapping of the numerous peaks and thus substantial line broadening.

In summary the anisotropies of chemical shift, dipole-dipole and quadrupolar interactions cause broad peaks and low resolution spectra of powder samples of solids.

Often the peaks in solid state NMR spectra are broad and overlapped so that they form featureless peaks, which makes it difficult to tell the number of magnetically non-equivalent sites.

The technique of magic angle spinning (MAS) can be used to average these anisotropies and improve resolution.[1.9] A rotor containing the powdered sample is spun around an axis at 54.7° with respect to B_0. If the sample spinning speed is much larger than the static peak linewidths, dipole-dipole interactions, the anisotropies of H_{CS} and first-order H_Q can be totally averaged to zero;[1.6] If the spinning speed is less than the width of the anisotropies, the spinning will modulate the anisotropies and give spinning side bands. At present the maximum spinning speed is about 20 kHz. For most spin-1/2 nuclei this speed is fast enough to average H_{DD} and H_{CS} and result in high resolution spectra, but for some nuclei, such as ^1H, the homonuclear dipole-dipole interactions are so large that peak linewidths in static

NMR are about 50 kHz. Even high speed MAS is not efficient to average them and numerous spinning side bands are present.[1.6]

A pulse sequence, called WAHUHA,[1.10] will flip the nuclear spins very quickly in spin space to average homonuclear dipole-dipole anisotropies. The pulse sequence is made up of numerous 90° pulse with a phase shift between them. One data point is acquired at the end of each cycle of the pulse sequence. Both the pulse length and the delay between the pulses are so short that the result of this is to make the nuclear spins rotate quickly around the axis of 54.7° with respect to B_0. Strong dipole-dipole interactions can be efficiently averaged. The combination of this technique with MAS can achieve high resolution NMR spectra even with large dipole-dipole interactions.[1.11]

In an NMR spectrum of a powder there are usually several peaks. Each peak represents a non-equivalent local magnetic environment. The linewidth shows the size of dipole-dipole interactions if there is no other reason for broadening.[1.6]

The lineshape of a peak is due to the powder pattern of CSA and anisotropy of quadrupolar interaction. The lineshapes are sensitive to the parameters of CSA and quadrupolar interaction. If a set of these parameters is selected and the orientation of a single crystal is known, the nuclear resonance frequency of the peak can be calculated. A powdered sample is made of many small crystals oriented at random. The powder pattern with a certain lineshape can be calculated if the parameters of CSA, quadrupolar interaction and the Euler angles, which are used to transform the principal axis systems between them, are known. Comparison of the

calculated lineshape with the NMR spectrum can verify if the parameters are correct.

1.4. SOLID STATE NMR OF QUADRUPOLAR NUCLEI

For nuclei with spin > 1/2 in solids the main broadening mechanisms are the first- and second-order anisotropies of quadrupolar interactions as these are usually much larger than other interactions, except the Zeeman interaction.

The quadrupolar interaction can cause very efficient relaxation and usually this is the dominant mechanism for relaxation for spin > 1/2 nuclei in solids.[1.8] The short relaxation times can broaden the NMR peaks. As quadrupolar interactions are orientation dependent, the random orientation of grains of powdered samples cause multiple overlapping peaks, giving broad lines.

Pulse sequences, such as WAHUHA and MREV-8, and MAS are not efficient in averaging quadrupolar anisotropies and not practical, as the very short relaxation time of quadrupolar nuclei does not allow time for the multiple pulses before the signal decays. MAS can only average the first order quadrupolar interactions.[1.4][1.5] For quadrupolar nuclei, such as ^{23}Na, ^{27}Al, ^{17}O, ^{11}B, the quadrupolar interactions are usually so large that second-order perturbations, which remain under MAS, cause the overlapping broad peaks.

Recently two kinds of double angle techniques, double-rotation (DOR) and dynamic-angle spinning (DAS), have been invented to solve this problem.[1.4][1.5] They can both average the second-order quadrupolar interaction anisotropies of non-

integer quadrupolar nuclei. They can also average dipole-dipole interactions and CSA's. This greatly improves the resolution of the spectra of quadrupolar nuclei.

REFERENCE FOR CHAPTER ONE

[1.1] F. Bloch, W. W. Hansen, and M. Packard : Nuclear induction Phys. Rev. **69**, 127 (1946).

[1.2] E. M. Purcell, H. C. Torrey, and R. V. Pound : Resonance absorption by nuclear magnetic moments in a solid Phys. Rev. **69**, 37 (1946).

[1.3] R. R. Ernst and W. A. Anderson : Application of Fourier transform spectroscopy to magnetic resonance Adv. Magn. Reson. **2**, 1 (1966).

[1.4] Y. Wu, B. Q. Sun, and A. Pines : NMR experiment with a new double rotor J. Magn. Reson. **89**, 297 (1990).

[1.5] K. T. Mueller, B. Q. Sun, C. G. Chings, J. W. Zwanziger, T. Terao, and A. Pines : Dynamic-angle spinning of quadrupolar nuclei J. Magn. Reson. **86**, 470 (1990).

[1.6] C. P. Slichter: Principles of Magnetic Resonance Third and Enlarged Edition. Springer-Verlag (1990).

[1.7] J. K. M. Sanders and B. K. Hunter: Modern NMR Spectroscopy: a guide for chemists Oxford Science Publication (1987).

[1.8] G. Engelhardt and D. Michael: High-Resolution Solid-State NMR of Silicates and Zeolites Wiley (1987).

[1.9] a. E. R. Andrew, A. Bradbury, and R. G. Eades : Nuclear magnetic resonance spectra from a crystal rotated at high speed Nature **182**, 1659 (1958).

b. I. J. Lowe : Free induction decays of rotating solids Phys. Rev. Lett. **2**,

285 (1959).

[1.10] a. J. S. Waugh, L. M. Huber, and U. Haeberlen : Approach to high-resolution NMR in solids Phys. Rev. Lett. **20**, 180 (1968).

b. U. Haeberlen and J. S. Waugh : Coherent averaging effects in magnetic resonance Phys. Rev. **173**, 453 (1968).

[1.11] B. C. Gerstein and C. R. Dybowski : Transient techniques in NMR of solids : An introduction to theory and practice Academic , Orlando, FL (1985).

CHAPTER TWO THEORY OF QUADRUPOLAR INTERACTIONS

In chapter one the classical pictures and general principles of NMR are introduced. This classical description (nuclear spin precession) is only useful for describing the NMR phenomena of non-coupled spin-half systems. For quadrupolar nuclei, quantum mechanics is needed to explain the observed behaviour. Therefore, a formal quantum mechanical treatment of quadrupolar nuclei is discussed in detail.

2.1. QUADRUPOLAR HAMILTONIAN

Quadrupolar nuclei have non-symmetrical nuclear charge distributions in space. If the surrounding electronic potential is not homogeneous, there will be an electric field gradient at the centre of the nucleus. This will cause quadrupolar interactions to occur. The interaction energy, E, of a nuclear charge with an external local electric field potential, V(x,y,z), is:[2.1]

$$E = \int \rho(x,y,z)\, V(x,y,z)\, d\tau \qquad (2.1)$$

where ρ(x,y,z) is the charge distribution density of the nucleus and dτ is the volume element and equals dxdydz. The integral is over all space.

If the potential, V(x,y,z), is expanded about the origin in terms of spatial

variables and substituted in equation (2.1),

$$\begin{aligned} E &= E^{(0)} + E^{(1)} + E^{(2)} + \cdots \\ &= V(0)\int \rho\, d\tau + \int \sum\nolimits_{\alpha} V_{\alpha}(0) x_{\alpha} \rho\, d\tau + \frac{1}{2}\int \sum\nolimits_{\alpha,\beta} V_{\alpha\beta}(0) x_{\alpha} x_{\beta} \rho\, d\tau + \cdots \end{aligned} \tag{2.2}$$

where x_α or x_β ($\alpha, \beta = 1, 2, 3$) stands for x, y, z and

$$V_{\alpha}(0) = \frac{\partial V(x,y,z)}{\partial x_{\alpha}}\Big|_{x,y,z=0} \qquad V_{\alpha\beta}(0) = \frac{\partial V(x,y,z)}{\partial x_{\alpha}\partial x_{\beta}}\Big|_{x,y,z=0} \ . \tag{2.3}$$

$E^{(0)}$ in equation (2.2) is the electrostatic energy of the nucleus taken as a point charge, which is a constant. $E^{(1)}$ is the electric dipole term. As all the nuclei have definite even parity (or inversion symmetry),[2.1] $\rho(x,y,z)$ is equal to $\rho(-x,-y,-z)$. In the same term, $V_\alpha(0)$ is a constant and x_α has odd parity; therefore, the integral over the whole space of this term is zero. $E^{(2)}$ in equation (2.2) is the electrical quadrupolar term (eQ: nuclear quadrupolar moment).

Conventionally, the quantity, $eQ_{\alpha\beta}$, is defined as:

$$eQ_{\alpha\beta} = \int (3x_{\alpha}x_{\beta} - \delta_{\alpha\beta} r^2)\, \rho(x,y,z)\, d\tau \ . \tag{2.4}$$

When α equals β, $\delta_{\alpha\beta}$ is 1; otherwise, it is zero. Rearranging the expression in terms of $Q_{\alpha\beta}$'s, gives:

$$\int x_{\alpha}x_{\beta}\, \rho(x,y,z)\, d\tau = \frac{1}{3}\left[eQ_{\alpha\beta} + \int \delta_{\alpha\beta} r^2\, \rho(x,y,z)\, d\tau\right] \ . \tag{2.5}$$

Substituting the above term into $E^{(2)}$ in equation (2.2), gives:

$$E^{(2)} = \frac{1}{6}\sum_{\alpha,\beta} [V_{\alpha\beta}(0)eQ_{\alpha\beta} + V_{\alpha\beta}(0)\delta_{\alpha\beta}\int r^2\rho(x,y,z)d\tau] \ . \qquad (2.6)$$

There are two coordinate systems used to describe the quadrupolar interactions: the laboratory axis system (LAS) and the principal axis system (PAS). Generally, they do not coincide.[2.2] In the LAS, the z-axis is along the direction of the applied static magnetic field $\mathbf{B}_0$. The PAS is chosen so that $V_{\alpha\beta}$ is diagonal: $V_{\alpha\beta} = \delta_{\alpha\beta} \cdot V_{\alpha\alpha}$. As there is no electronic charge at the nucleus, according to Laplace's equation,[2.3] $V_{\alpha\beta}$ is traceless:

$$\nabla^2 V(x,y,z) = 0 \qquad \sum_\alpha V_{\alpha\alpha}(x,y,z) = 0 \ . \qquad (2.7)$$

In equation (2.6), the term $\int r^2\rho(x,y,z)d\tau$ for the nucleus is a constant. Using equation (2.7), this term becomes zero. The higher order terms, such as $E^{(3)}$, are much smaller than $E^{(2)}$ in equation (2.6) and are not considered here. Thus, the first term in equation (2.6) is the only non-zero component of the quadrupolar coupling.

To obtain the quantum mechanical expression (H_Q) for the quadrupolar coupling, the classical coordinates, x, y, z, and the distance, r, are substituted by their quantum mechanical operators although their forms remain the same:

$$H_Q = \frac{1}{6}\sum_{\alpha,\beta} V_{\alpha\beta}eQ_{\alpha\beta}^{(op)} \qquad (2.8)$$

$$eQ_{\alpha\beta}^{(op)} = e\sum_k (3x_{\alpha k}x_{\beta k} - \delta_{\alpha\beta}r_k^2). \qquad (2.9)$$

The superscript (op) in equation (2.8) and (2.9) may be used to represent the quantum mechanical expression. The summation is over the protons (k) in the

nucleus, each with a charge, e.

To begin a quantum mechanical treatment, the first step is to select an eigenstate for H_Q. Here we choose $|Im\zeta>$ so that $H_Q|Im\zeta> = E_m|Im\zeta>$. 'I' is the total spin angular momentum of the nucleus; 'm' is the eigenvalue of the z-component of the total spin angular moment, an integer between -I and +I; ζ is a set of other quantum numbers which do not affect the nuclear spin; E_m is the corresponding eigenvalue of H_Q. Applying the extension of Wigner-Eckart theorem to $Q_{\alpha\beta}^{(op)}$, gives:[2.4]

$$(Im\zeta|e\sum_k (3x_\alpha x_\beta - \delta_{\alpha\beta} r_k^2)|In\zeta) = (Im\zeta|(3\frac{I_\alpha I_\beta + I_\beta I_\alpha}{2} - \delta_{\alpha\beta} I^2)|In\zeta)C \quad (2.10)$$

where C is a constant for all values of m, n, α and β. In order to calculate C, set m = n = I and $\alpha = \beta = z$, and define eQ, the quadrupolar moment:

$$\begin{aligned} eQ &= (II\zeta|e\sum_k (3z_k^2 - r_k^2)|II\zeta) \\ &= C(II\zeta|3I_z^2 - I^2|II\zeta) \\ &= CI(2I - 1) \end{aligned} \quad (2.11)$$

From equation (2.11), (2.10) and (2.9), gives:

$$C = \frac{eQ}{I(2I - 1)} \quad (2.12)$$

$$H_Q = \frac{eQ}{6I(2I - 1)} \sum_{\alpha,\beta} V_{\alpha\beta}(\frac{3}{2}(I_\alpha I_\beta + I_\beta I_\alpha) - \delta_{\alpha\beta} I^2). \quad (2.13)$$

In the PAS, by using the traceless and diagonal properties of $V_{\alpha\beta}$ and substituting $I^2 = I_x^2 + I_y^2 + I_z^2$ into equation (2.13):

$$H_Q = \frac{eQ}{4I(2I - 1)}[V_{zz}(3I_z^2 - I^2) + (V_{xx} - V_{yy})(I_x^2 - I_y^2)]. \qquad (2.14)$$

According to convention, the axes of the PAS are chosen to satisfy:[2.5]

$$V_{zz} \geq V_{xx} \geq V_{yy} .$$

Another two symbols, q, the field gradient, and η, the asymmetry parameter, are defined as:

$$q = V_{zz}/e \qquad \eta = (V_{xx} - V_{yy})/V_{zz} . \qquad (2.15)$$

η has a positive value between 0 and 1. Finally, the effective quadrupolar Hamiltonian in the PAS is:

$$H_Q = \frac{e^2qQ}{4I(2I - 1)}[(3I_z^2 - I^2) + \eta(I_x^2 - I_y^2)]. \qquad (2.16)$$

2.2. FIRST-ORDER PERTURBATION EXPANSION OF QUADRUPOLAR INTERACTIONS IN A STATIC MAGNETIC FIELD

2.2.1. Quadrupolar Hamiltonian in the LAS as Spherical Tensor

An alternative way of expressing the Hamiltonian is to use the Cartesian tensor. It can be shown that H_Q in equation (2.16) is the same as:

$$H_Q = \frac{e^2 Q}{2I(2I-1)} \hat{\imath} \cdot q \cdot \hat{\imath}. \qquad (2.17)$$

q is the electric field gradient. It satisfies: $\nabla\nabla V \equiv eq$ and is a second-order tensor; $\hat{\imath}$ is a first-rank tensor (a vector). In the PAS, **q** is traceless and diagonal:

$$q_{xx} + q_{yy} + q_{zz} = 0 \text{ and } q_{\alpha\beta} = \delta_{\alpha\beta} \cdot V_{\alpha\alpha}.$$

It is possible to transform H_Q from PAS to LAS using the spherical tensor form of H_Q. The general formula for transforming the above quantity $\mathbf{I} \cdot \mathbf{q} \cdot \mathbf{I}$ to a spherical tensor is:[2.6]

$$I \cdot q \cdot I = \sum_{m,m'} \sum_{L,M} (-1)^M C(11L;mm'M) q_M^{(L)} I^{(-m)} I^{(-m')} \qquad (2.18)$$

where $q_M^{(L)}$ and $I^{(m)}$ are the second- and first-rank spherical tensors, respectively. C(11L;mm'M) are the Clebsch-Gordan coefficients, non-zero condition when m+m'=M. The relationships between the first-, second-rank spherical tensors and their Cartesian representations are as follows:

$$I^{(1)} = -\frac{1}{\sqrt{2}} I_+ = -\frac{1}{\sqrt{2}} (I_x + iI_y) \quad I^{(-1)} = \frac{1}{\sqrt{2}} I_- = \frac{1}{\sqrt{2}} (I_x - iI_y) \quad I^{(0)} = I_z$$

$$q_0^{(0)} = -\frac{1}{\sqrt{3}} (q_{xx} + q_{yy} + q_{zz}) \quad q_0^{(1)} = \frac{1}{\sqrt{2}} i(q_{xy} - q_{yx}) \quad q_{\pm 1}^{(1)} = \mp \frac{1}{2} i[q_{yz} - q_{zy} \pm i(q_{zx} - q_{xz})]$$
$$q_0^{(2)} = \frac{1}{\sqrt{6}} (2q_{zz} - q_{xx} - q_{yy}) \quad q_{\pm 1}^{(2)} = \mp \frac{1}{2} [q_{xz} + q_{zx} \pm i(q_{yz} + q_{zy})] \quad q_{\pm 2}^{(2)} = \frac{1}{2} [q_{xx} - q_{yy} \pm i(q_{xy} + q_{yx})] \qquad (2.19$$

In the PAS, using the definition: $q_{zz} = q$ and $\eta = (q_{xx} - q_{yy})/q_{zz}$, we have:

$$q_0^{(2)} = \frac{\sqrt{6}}{2}q \quad q_{\pm1}^{(2)} = 0 \quad q_{\pm2}^{(2)} = \frac{\eta q}{2}. \tag{2.20}$$

It can be seen that $q_0^{(0)}$, $q_0^{(1)}$ and $q_{\pm1}^{(1)}$ are all zero. Thus, in equation (2.18), we can set L = 2. In C(11L;mm'M) there are only two independent parameters, m and m'. Defining a new term: c(m,m') = $\sqrt{6}\cdot$C(11L;mm'M), gives:[6]

$$c(m,m') = \sqrt{\frac{[2+(m+m')]![2-(m+m')]!}{(1+m)!(1-m)!(1+m')!(1-m')!}} \tag{2.21}$$

$$m, m' = -1, 0, 1.$$

By substituting the above into equation (2.18) and noticing that c(m,m')=c(-m,-m'), we have:

$$\begin{aligned} I\cdot q\cdot I &= \frac{1}{\sqrt{6}}\sum_{m,m'=-1}^{1}(-1)^{(m+m')}c(m,m')q_{m+m'}^{(2)}I^{(-m)}I^{(-m')} \\ &= \frac{1}{\sqrt{6}}\sum_{-m,-m'=1}^{-1}(-1)^{(-m-m')}c(-m,-m')q_{-m-m'}^{(2)}I^{(m)}I^{(m')} \\ &= \frac{1}{\sqrt{6}}\sum_{m,m'=-1}^{1}(-1)^{(-m-m')}c(m,m')q_{-m-m'}^{(2)}I^{(m)}I^{(m')} \end{aligned}$$

The quadrupolar interaction Hamiltonian in the PAS is:

$$H_Q = \frac{e^2Q}{\sqrt{6}2I(2I-1)}\sum_{m,m'=-1}^{1}(-1)^{-m-m'}c(m,m')q_{-m-m'}^{(2)}I^{(m)}I^{(m')}. \tag{2.22}$$

Consider the Cartesian form of the scalar term $\mathbf{I}\cdot\mathbf{q}\cdot\mathbf{I}$ in equation (2.17). In the LAS (x',y',z'), it retains the same form: $\mathbf{I'}\cdot\mathbf{q'}\cdot\mathbf{I'}$;[2,7] $\mathbf{q'}$ is still traceless but no longer diagonal and vector $\mathbf{I'}$ is: ($I_{x'}$,$I_{y'}$,$I_{z'}$). Using the same procedure as equation (2.17)

to (2.22), we can transform the Cartesian expression, I'·**q**'·I', to its corresponding spherical tensor form. The spherical tensor form of H_Q in the LAS is the same as that in equation (2.22).

$$H_Q = \frac{e^2 Q}{\sqrt{6}2I(2I-1)} \sum_{m,m'=-1}^{1} (-1)^{-m-m'} c(m,m') q^{(2)}_{-m-m'} I^{(m)} I^{(m')}. \qquad (2.23)$$

The transformation from the LAS (x',y',z') to the PAS (x,y,z) is a consecutive rotation $\Omega_q = \Omega(\alpha_q,\beta_q,\gamma_q)$ where α_q, β_q, γ_q are the rotational Euler angles (Fig. 2. 1). The D-matrix is used to transform the spherical tensor from the PAS to the LAS. One important property of the D-matrix is as follows:[2.6]

$$D_{m,n}^{(L)*}(\Omega) = (-1)^{m-n} D_{-m,-n}^{(L)}(\Omega) . \qquad (2.24)$$

Here we want to represent $q'^{(2)}_n$ in terms of $q^{(2)}_n$ and the D-matrix. Using the property of spherical tensors under rotation, noticing $q^{(2)}_n = q^{(2)}_{-n}$ and the non-zero condition for $q^{(2)}_n$ is that n is even number, we have:

$$\begin{aligned} q^{(2)}_{-m-m'} &= \sum_{n=-2}^{2} q^{(2)}_n D^{(2)*}_{n,-m-m}(\Omega_q) = \sum_{n=-2}^{2} (-1)^{n+m+m'} q^{(2)}_n D^{(2)}_{-n,m+m}(\Omega_q) \\ &= \sum_{n=-2}^{2} (-1)^{m+m'} q^{(2)}_{-n} D^{(2)}_{n,m+m}(\Omega_q) = \sum_{n=-2}^{2} (-1)^{m+m'} q^{(2)}_n D^{(2)}_{n,m+m}(\Omega_q) \end{aligned} \qquad (2.25)$$

Substituting the above into equation (2.23), the quadrupolar Hamiltonian in the LAS can be expressed as:

$$H_q = \frac{e^2 Q}{\sqrt{6}2I(2I-1)} \sum_{m,m'=-1}^{1} \sum_{n=-2}^{2} c(m,m') q^{(2)}_n D^{(2)}_{n,m+m}(\Omega_q) I^{(m)} I^{(m')}. \qquad (2.26)$$

In order to simplify the notations, we use the quantities without the prime to

denote the components of the spherical tensor in the LAS. Equation (2.26) is further simplified and made useful for applications by defining the dimensionless quantities:

$$q_n = \frac{q_n^{(2)}}{q_0^{(2)}} = \frac{q_n^{(2)}}{\sqrt{6}/2q} = \begin{array}{ll} 1 & \text{if } n=0 \\ 0 & \text{if } n=\pm 1 \\ \eta/\sqrt{6} & \text{if } n=\pm 2 \end{array} \tag{2.27}$$

and the quadrupolar angular frequency

$$\omega_q = \frac{3e^2qQ/\hbar}{2I(2I-1)}. \tag{2.28}$$

Finally, the quadrupolar interaction Hamiltonian in the LAS as spherical tensor form is as follows:

$$H_q = \frac{\hbar\omega_q}{6} \sum_{m,m'=-1}^{1} \sum_{n=-2}^{2} c(m,m')q_n D^{(2)}_{n,m+m'}(\Omega_q) I^{(m)} I^{(m')}. \tag{2.29}$$

2.2.2. The First-order Perturbation Expansion

For modern FT-NMR the static magnetic field is very strong and the Zeeman energy is usually much larger than quadrupolar interactions. Nuclear quadrupolar interactions can be treated as perturbations of the Zeeman energy. In other words the nuclear spins are still quantized along B_0 or the z direction of the laboratory frame and the eigenstates for the new Hamiltonian, including quadrupolar interactions, are the same as those for the Zeeman interactions. Although this approximation does not hold when the quadrupolar interactions are of the same

magnitude as the Zeeman energy, in the following discussion the approximation is assumed to be valid.

For the first-order expansion there are only diagonal terms and m+m' is always zero. Using equation (2.20) and equation (2.21), we find c(0,0) = c(1,-1) = c(-1,1) = 1 and

$$\begin{aligned}
&\sum_{m,m'=-1,m+m'=0}^{1} c(m,m')\langle M|I^{(m)}I^{(m')}|M\rangle \\
&=c(0,0)\langle M|I_zI_z|M\rangle-\frac{1}{2}c(1,-1)\langle M|I_+I_-|M\rangle-\frac{1}{2}c(-1,1)\langle M|I_+I_-|M\rangle \\
&=2M^2-\frac{1}{2}(I(I+1)-M(M+1))-\frac{1}{2}(I(I+1)-M(M-1)) \\
&=3M^2-I(I+1)
\end{aligned} \tag{2.30}$$

where $|M\rangle$ is the eigenstate of $\{I^2 \& I_z\}$.

$$I_{\pm}|M\rangle = \sqrt{I(I+1)-M(M\pm1)}\,|M\pm1\rangle. \tag{2.31}$$

According to perturbation theory, the first-order quadrupolar energy level shifts are given by the matrix element of the quadrupolar interaction H_q between their eigenstates:

$$\begin{aligned}
E_M^{(1)} &= \langle M|H_q|M\rangle \\
&= \frac{\hbar\omega_q}{6}\sum_{m,m'=-1\,m+m'=0}^{1}\sum_{n=-2}^{2} c(m,m')q_nD_{n,0}^{(2)}(\Omega_q)\langle M|I^{(m)}I^{(m')}|M\rangle \\
&= \frac{\hbar\omega_q}{2}[M^2-\frac{I(I+1)}{3}]\sum_{n=-2}^{2} q_nD_{n,0}^{(2)}(\Omega_q)
\end{aligned} \tag{2.32}$$

The resonance energies of transitions between adjacent levels in the spin manifold (remember that M=I is the lowest Zeeman state) are shifted by the amounts:

$$\begin{aligned}\Delta E^{(1)}(M-1\rightarrow M) &= -(M-1/2)\hbar\omega_q \sum_{n=-2}^{2} q_n D^{(2)}_{n,0}(\Omega_q) \\ &= -(M-1/2)\hbar\omega_q[\frac{\eta}{\sqrt{6}}(D^{(2)}_{-2,0}(\Omega_q)+D^{(2)}_{2,0}(\Omega_q))+D^{(2)}_{0,0}(\Omega_q)]\end{aligned} \tag{2.33}$$

Notice:[2.6]

$$D^{(2)}_{\pm 2,0}(\Omega_q)=\sqrt{\frac{3}{8}}Sin^2\beta_q e^{\pm i2\gamma_q} \quad D^{(2)}_{\pm 1,0}(\Omega_q)=-\sqrt{\frac{3}{8}}Sin2\beta_q e^{\pm i\gamma_q} \quad D^{(2)}_{0,0}(\Omega_q)=(3Cos^2\beta_q-1)/2 \tag{2.34}$$

Substituting the above into equation (2.33), gives:

$$\Delta E^{(1)}(M-1\rightarrow M) = -\frac{1}{2}(M-\frac{1}{2})\hbar\omega_q[(3Cos^2\beta_q-1)+\eta Sin^2\beta_q Cos(2\gamma_q)]. \tag{2.35}$$

If M=1/2 in the above equation, we find that $\Delta E^{(1)}(-1/2\Leftrightarrow 1/2)$ becomes zero. Therefore, the transition from -1/2 $\Leftrightarrow$ 1/2 is not affected by the first-order quadrupolar interactions and the central transition of half-integer quadrupolar nuclei has a much narrower linewidth than those of the other transitions.

2.3 SECOND-ORDER QUADRUPOLAR INTERACTION EXPANSION

According to the second-order perturbation theory, the second-order quadrupolar interaction is:[2.8]

$$\Delta E^{(2)}_M = \sum_{n\neq M} \frac{|<M|H_q|n>|^2}{E^{(0)}_M - E^{(0)}_n} \tag{2.36}$$

$$E_M^{(0)} = -M\hbar\omega_I$$

where ω_I is the Larmor frequency of the nucleus in radiant. For $n \neq M$, the only non-zero terms of $<M|H_q|n>$ are:

$$<M|H_q|M-2> \quad <M|H_q|M-1> \quad <M|H_q|M+1> \quad <M|H_q|M+2>.$$

Now we can define four factors C_1, C_2, C_3 and C_4 as follows:

$$C_1 = |<M|I^{(-1)}I^{(-1)}|M+2>|^2 = (1/4)\cdot[I(I+1) - (M+2)(M+1)][I(I+1) - (M+1)M]$$

$$C_2 = |<M|I^{(+1)}I^{(+1)}|M-2>|^2 = (1/4)\cdot[I(I+1) - (M-2)(M-1)][I(I+1) - (M-1)M]$$

$$C_3 = |<M|I^{(-1)}I^{(0)}+I^{(0)}I^{(-1)}|M+1>|^2 = (1/2)\cdot[I(I+1) - (M+1)M](2M+1)^2$$

$$C_4 = |<M|I^{(+1)}I^{(0)}+I^{(0)}I^{(+1)}|M-1>|^2 = (1/2)\cdot[I(I+1) - (M-1)M](2M-1)^2 .$$

Also: $c(1,1)=c(-1,-1)=\sqrt{6}$ $c(1,0)=c(0,1)=c(-1,0)=c(0,-1)=\sqrt{3}$, we have:

From equation (2.29) it can be seen that:

$$\begin{aligned} |<M|H_q|M+2>|^2 &= C_1\left(\frac{\hbar\omega_q}{6}\right)^2 \left|\sum_n C(-1,-1)q_n D^{(2)}_{n,-2}(\Omega_q)\right|^2 \\ &= C_1\frac{(\hbar\omega_q)^2}{36}|C(-1,-1)|^2\left|\sum_n q_n D^{(2)}_{n,-2}(\Omega_q)\right|^2 = C_1\frac{(\hbar\omega_q)^2}{6}\left|\sum_n q_n D^{(2)}_{n,-2}(\Omega_q)\right|^2 \end{aligned} \tag{2.37}$$

similarly,

$$|<M|H_q|M-2>|^2 = C_2\frac{(\hbar\omega_q)^2}{6}\left|\sum_n q_n D^{(2)}_{n,2}(\Omega_q)\right|^2$$

$$\begin{aligned} |<M|H_q|M+1>|^2 &= C_3\frac{(\hbar\omega_q)^2}{12}\left|\sum_n q_n D^{(2)}_{n,-1}(\Omega_q)\right|^2 \\ |<M|H_q|M-1>|^2 &= C_4\frac{(\hbar\omega_q)^2}{12}\left|\sum_n q_n D^{(2)}_{n,1}(\Omega_q)\right|^2. \end{aligned} \tag{2.38}$$

By defining two other coefficients, A and B, in the following, using equation (2.24), it can be proved that:

$$
\begin{aligned}
A &= |\textstyle\sum_n q_n D^{(2)}_{n,-2}(\Omega_q)|^2 \\
&= \textstyle\sum_{n,n'} q_n q_{n'} D^{(2)}_{n,-2}(\Omega_q) D^{(2)*}_{n',-2}(\Omega_q) \\
&= \textstyle\sum_{n,n'} q_n q_{n'} D^{(2)*}_{-n,2}(\Omega_q) D^{(2)}_{-n',2}(\Omega_q)
\end{aligned}
\tag{2.39}
$$

Making the change n→ -n and n'→ -n' and noticing that $q_n = q_{-n}$, $q_{n'} = q_{-n'}$, the above equation is simplified to:

$$
\begin{aligned}
A &= \textstyle\sum_{n,n'} q_n q_{n'} D^{(2)*}_{n,2}(\Omega_q) D^{(2)}_{n',2}(\Omega_q) \\
&= |\sum_{n=-2}^{2} q_n D^{(2)}_{n,2}(\Omega_q)|^2
\end{aligned}
\tag{2.40}
$$

Therefore, the angular-dependent part of $<M|H_q|M+2>$ is the same as that of $<M|H_q|M-2>$. The same is true for B:

$$
\begin{aligned}
B &= |\textstyle\sum_n q_n D^{(2)}_{n,-1}(\Omega_q)|^2 \\
&= |\textstyle\sum_n q_n D^{(2)}_{n,1}(\Omega_q)|^2
\end{aligned}
\tag{2.41}
$$

The summations of n and n' in the above equations (2.39), (2.40) and (2.41) are all -2, 0, 2. Thus, from equation (2.36):

$$
\begin{aligned}
\Delta E^{(2)}_M &= \frac{|<M|H_q|M-2>|^2}{E^{(0)}_M - E^{(0)}_{M-2}} + \frac{|<M|H_q|M-1>|^2}{E^{(0)}_M - E^{(0)}_{M-1}} + \frac{|<M|H_q|M+1>|^2}{E^{(0)}_M - E^{(0)}_{M+1}} + \frac{|<M|H_q|M+2>|^2}{E^{(0)}_M - E^{(0)}_{M+2}} \\
&= \frac{1}{2\hbar\omega_I}(|<M|H_q|M+2>|^2 - |<M|H_q|M-2>|^2) + \frac{1}{\hbar\omega_I}(|<M|H_q|M+1>|^2 - |<M|H_q|M-1> \\
&= \frac{1}{2\hbar\omega_I} \cdot \frac{(\hbar\omega_q)^2}{6}(C_1 A - C_2 A + C_3 B - C_4 B)
\end{aligned}
\tag{2.42}
$$

From the definitions of C_1, C_2, C_3 and C_4, it is found that:

$$
C_1 - C_2 = M[2M^2 + 1 - 2I(I+1)] \quad C_3 - C_4 = M[4I(I+1) - 8M^2 - 1] \ ; \tag{2.43}
$$

therefore, substituting the above into equation (2.42), gives:

$$\Delta E_M^{(2)} = \frac{\hbar\omega_q^2 M}{12\omega_I}[(2M^2+1-2I(I+1))A + (4I(I+1)-8M^2-1)B]. \qquad (2.44)$$

Changing, M → (M - 1), gives:

$$\Delta E_{M-1}^{(2)} = \frac{\hbar\omega_q^2 (M-1)}{12\omega_I}[(2(M-1)^2+1-2I(I+1))A + (4I(I+1)-8(M-1)^2-1)B].$$

$$\begin{aligned}\Delta E_q^{(2)}(M-1\rightarrow M) &= \Delta E_{M-1}^{(2)} - \Delta E_M^{(2)} \\ &= \frac{\hbar\omega_q^2}{12\omega_I}[(-6M^2+6M-3+2I(I+1))A + (24M^2-24M+9-4I(I+1))B]\end{aligned} \qquad (2.45)$$

Considering the special case of the central transition (-1/2 ⇔ 1/2), M = 1/2:

$$\begin{aligned}\Delta E_q^{(2)}(-\frac{1}{2}\rightarrow\frac{1}{2}) &= \frac{\hbar\omega_q^2}{12\omega_I}[(2I(I+1)-\frac{3}{2})A + (3-4I(I+1))B] \\ &= \frac{\hbar\omega_q^2}{6\omega_I}[I(I+1)-\frac{3}{4}](A-2B)\end{aligned} \qquad (2.46)$$

Using the known expression for the D-matrix,[2.6]

$$D_{\pm2,2}^{(2)}(\Omega_q)=\frac{1}{4}(1\pm Cos\beta_q)^2 e^{i(2\alpha_q\pm2\gamma_q)} \quad D_{\pm2,1}^{(2)}(\Omega_q)=\pm\frac{1}{2}(1\pm Cos\beta_q)Sin\beta_q e^{i(\alpha_q\pm2\gamma_q)}$$

$$D_{0,2}^{(2)}(\Omega_q)=\sqrt{\frac{3}{8}}(Sin\beta)^2 e^{i2\alpha_q} \quad D_{0,1}^{(2)}(\Omega_q)=-\sqrt{\frac{3}{8}}Sin2\beta\, e^{i\alpha_q} \qquad (2.47)$$

the quantity (A - 2B) is:

$$A - 2B = F_1(\gamma_q)(Cos\beta_q)^4 + F_2(\gamma_q)(Cos\beta_q)^2 + F_3(\gamma_q) \qquad (2.48)$$

where

$$F_1(\gamma_q) = \frac{27}{8} - \frac{9\eta}{4}Cos(2\gamma_q) + \frac{3\eta^2}{8}(Cos(2\gamma_q))^2$$
$$F_2(\gamma_q) = -\frac{15}{4} + \frac{\eta^2}{2} + 2\eta Cos(2\gamma_q) - \frac{3\eta^2}{4}(Cos(2\gamma_q))^2$$
$$F_3(\gamma_q) = \frac{3}{8} - \frac{\eta^2}{3} + \frac{\eta}{4}Cos(2\gamma_q) + \frac{3\eta^2}{8}(Cos(2\gamma_q))^2$$

It is interesting to notice that angle α_q is not present in either equation (2.48) or (2.35) though the Euler angle set (α_q, β_q, γ_q) is used to perform the transformation from the PAS to the LAS. The orientation of the PAS z-axis in the LAS can therefore be described by two polar angles, β_q and γ_q. The energy of quadrupolar interaction is quantized along the z-axis in the PAS. Therefore the quadrupolar perturbation is only determined by the orientation of the z-axis of the PAS or the two angular parameter β_q and γ_q, independent of α_q.

Under an isotropic, dynamical averaged system, such as in a liquid, we have to integrate β_q and γ_q over all space. That is:

$$(\Delta E_q^{(2)}(-\frac{1}{2}\rightarrow\frac{1}{2}))_0 = \frac{\hbar\omega_q^2}{6\omega_I}[I(I+1) - \frac{3}{4}]\frac{1}{4\pi}\int_0^{2\pi}\int_0^{\pi}(A-2B)Sin\beta_q d\beta_q d\gamma_q. \qquad (2.49)$$

Using the results:

$$\int_0^{2\pi}Cos(2\gamma_q)d\gamma_q = 0 \qquad \int_0^{2\pi}(Cos(2\gamma_q))^2 d\gamma_q = \pi$$

gives:

$$\int_0^{\pi}(Cos\beta_q)^4 Sin\beta_q d\beta_q = \frac{2}{5} \qquad \int_0^{\pi}(Cos\beta_q)^2 Sin\beta_q d\beta_q = \frac{2}{3} \tag{2.50}$$

$$\frac{1}{4\pi}\int_0^{2\pi}\int_0^{\pi}(A - 2B)Sin\beta_q d\beta_q d\gamma_q = -\frac{1}{5}(1 + \frac{\eta^2}{3}). \tag{2.51}$$

Therefore the isotropic second-order shift of central transition of quadrupolar nucleus is:

$$\delta_Q = \frac{(\Delta E_q^{(2)}(-\frac{1}{2}\rightarrow\frac{1}{2}))_0}{\hbar\omega_I} = -\frac{\omega_q^2}{30\omega_I^2}[I(I+1)-\frac{3}{4}](1+\frac{\eta^2}{3}) \tag{2.52}$$

Generally, we have to find the expressions of A and B, and use equation (2.50) to calculate the isotropic second-rank shift for non-central transitions. From the known result of second-order D-matrix, we have:

$$\begin{aligned} A &= \frac{1}{24}[9-8\eta^2-54\eta Cos2\gamma_q+17\eta^2(Cos2\gamma_q)^2](Cos\beta_q)^4 \\ &+\frac{1}{12}[-9+10\eta^2+24\eta Cos2\gamma_q-17\eta^2(Cos2\gamma_q)^2](Cos\beta_q)^2 \\ &+\frac{1}{24}[9-8\eta^2+6\eta Cos\gamma_q+17\eta^2(Cos\gamma_q)^2]-2\eta Cos2\gamma_{qCos}\beta_q(Sin\beta_q)^2 \end{aligned}$$

$$\begin{aligned} B = -\frac{1}{6}[9+\eta^2-\eta^2(Cos2\gamma_q)^2](Cos\beta_q)^4 + \frac{1}{6}[9+\eta^2-2\eta^2(Cos2\gamma_q)^2](Cos\beta_q)^2 \\ +\frac{\eta^2}{6}(Cos\gamma_q)^2 - \eta Cos2\gamma_q Cos\beta_q(Sin\beta_q)^2 \end{aligned} \tag{2.53}$$

Using the same integral as mentioned above, we have:

$$\langle A\rangle_0=\int_0^{2\pi}\int_0^{\pi} A\,Sin\beta_q\,d\beta_q\,d\gamma_q=\frac{1}{5}(1+\frac{\eta^2}{3}) \quad \langle B\rangle_0=\int_0^{2\pi}\int_0^{\pi} B\,Sin\beta_q\,d\beta_q\,d\gamma_q=\frac{1}{5}(1+\frac{\eta^2}{3}).$$

(2.54)

Thus, the isotropic second-order quadrupolar shift for all single quantum transitions are:

$$\begin{aligned}\delta_M &= \frac{\Delta E_q^{(2)}(M-1\rightarrow M)}{\hbar\omega_q} \\ &= \frac{\omega_q^2}{30\omega_I^2}(1+\frac{\eta^2}{3})[9M^2-9M+3-I(I+1)]\end{aligned} \tag{2.55}$$

According to convention, a parameter C_Q, called the quadrupolar coupling constant, is defined as:

$$C_Q = (e^2qQ)/h\ . \tag{2.56}$$

Since $h = 2\pi\cdot\hbar$, it is possible to substitute C_Q into equation (2.28),

$$\omega_q = \frac{6\pi C_Q}{2I(2I-1)}. \tag{2.57}$$

Using $\omega_I = 2\pi\nu_I$ and substituting the above into equation (2.55):

$$\delta_M = \frac{3C_Q^2}{40I^2(2I-1)^2\nu_I^2}(1+\frac{\eta^2}{3})[9M^2-9M+3-I(I+1)] \tag{2.58}$$

where δ_M is in parts per million (ppm) and C_Q and ν_I are in MHz. This is the usual formula for quadrupolar interactions quoted in the literature.[2.5]

REFERENCE FOR CHAPTER TWO

[2.1] C. P. Slichter: Principles of Magnetic Resonance Third and Enlarged Edition. Springer-Verlag (1990).

[2.2] W. P. Power, R. E. Wasylishen, S. Mooibroek, B. A. Pettitt and W. Danchura : Simulation of NMR powder line shapes of quadrupolar nuclei with half-integer spin at low-symmetry sites J. Am. Chem. Soc. **94**, 591 (1990).

[2.3] D. S. Jones: The Theory of Electromagnetism Oxford: Pergamon Press (1964).

[2.4] G. H. Duffey: Applied Group Theory for Physicists and Chemists England Cliffs, NJ: Prentice Hall (1992).

[2.5] G. Engelhardt, D. Michael: High-resolution Solid-state NMR of Silicates and Zeolites. Wiley, J. & Sons (1987).

[2.6] D. M. Brink and G. R. Satchler : Angular momentum Second Edition Oxford: Clarendon Press (1968).

[2.7] J. G. Simmonds : A Brief on Tensor Analysis New York: Springer-Verlag (1982).

[2.8] J. J. Sakurai: Modern Quantum Mechanics Menlo Park, Calif.: Benjamin/Cummings (1985).

CHAPTER THREE. PRINCIPLES AND TECHNIQUES OF MAS, DOR AND DAS

The main factors causing line-broadening in solid state NMR spectra are dipole-dipole interaction (H_{DD}), chemical shift anisotropy (H_{CS}) and quadrupolar interaction (H_Q). To improve the spectral resolution these must be averaged to anisotropic values. Fast Magic Angle Spinning (MAS) can average H_{DD}, H_{CS} and H_Q to the first-order. Double rotation (DOR) and Dynamic Angle Spinning (DAS) can average H_{DD} and H_{CS} to the first-order and H_Q to the second-order. Therefore, we can obtain high-resolution NMR spectra for nuclei with large quadrupolar interactions by using DOR and DAS.

3.1. MAGIC ANGLE SPINNING (MAS)

3. 1. 1. Theory

The dipole-dipole interaction between two nuclei is:[3.1]

$$H_D = \frac{\gamma_1 \gamma_2 \hbar^2}{r_{12}^3}(A + B + C + D + E + F) \tag{3.1}$$

where

$$A = I_{1z}I_{2z}[1 - 3(Cos\theta_{12})^2] \qquad B = \frac{1}{2}(I_{1z}I_{2z} - \hat{I}_1 \cdot \hat{I}_2)[1 - 3(Cos\theta_{12})^2]$$

$$C = -\frac{3}{2}(I_1^+ I_{2z} + I_{1z}I_2^+)Sin\theta_{12}Cos\theta_{12}e^{-i\phi_{12}} \qquad D = -\frac{3}{2}(I_1^- I_{2z} + I_{1z}I_2^-)Sin\theta_{12}Cos\theta_{12}e^{+i\phi_{12}}$$

$$E = -\frac{3}{4}I_1^+ I_2^+ (Sin\theta_{12})^2 e^{-2i\phi_{12}} \qquad F = -\frac{3}{4}I_1^- I_2^- (Sin\theta_{12})^2 e^{+2i\phi_{12}}.$$

Here r_{12} is the distance between spin 1 and 2; θ and ϕ are the polar angles of the radius vector $\mathbf{r_{12}}$ with respect to x, y and z (Fig. 3. 1); γ_1 and γ_2 are the magnetogyric ratios of nuclei 1 and 2.

When considering the first-order perturbation of H_{DD} with respect to H_Z, only the secular terms, A and B, in equation (3.1) are important. Thus,

$$H_D = \frac{\gamma_1 \gamma_2 \hbar^2}{r_{12}^3}\frac{1}{2}[1 - 3(Cos\theta)^2](3I_{1z}I_{2z} - \hat{I}_1 \cdot \hat{I}_2). \tag{3.2}$$

Now to consider the effect of sample rotation on first-order dipolar splitting; the relative orientations of $\mathbf{B_0}$, $\mathbf{r_{12}}$ and the fixed axis of rotation **R**, are shown in Figure 3. 2, where the angle between **R** and $\mathbf{B_0}$ is θ ; the rotor rotational angle is $\phi'_{12}(t)$. The angle is time-dependent and equal to $\omega_r t$, where ω_r is the rotor spinning speed in radians. It can be proved that:[3.2]

$$Cos\theta_{12} = Cos\theta'_{12}Cos\theta + Sin\theta'_{12}Sin\theta Sin(\omega_r t). \tag{3.3}$$

Substitution of equation (3.3) into $(1 - 3Cos^2\theta_{12})$, gives:

Fig. 3. 1. Relationship between rectangular coordinates x, y, z and the polar coordinates r, θ, ϕ (copy from ref. [3. 1]).

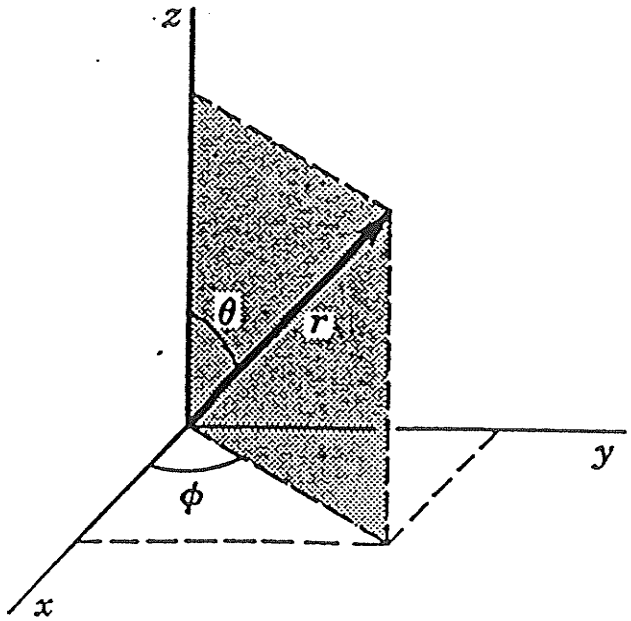

Fig. 3. 2. The relative orientations of $\mathbf{r}_{12}$, $\mathbf{B}_0$ and the rotational axis **R**. (copy from ref. [3. 1])

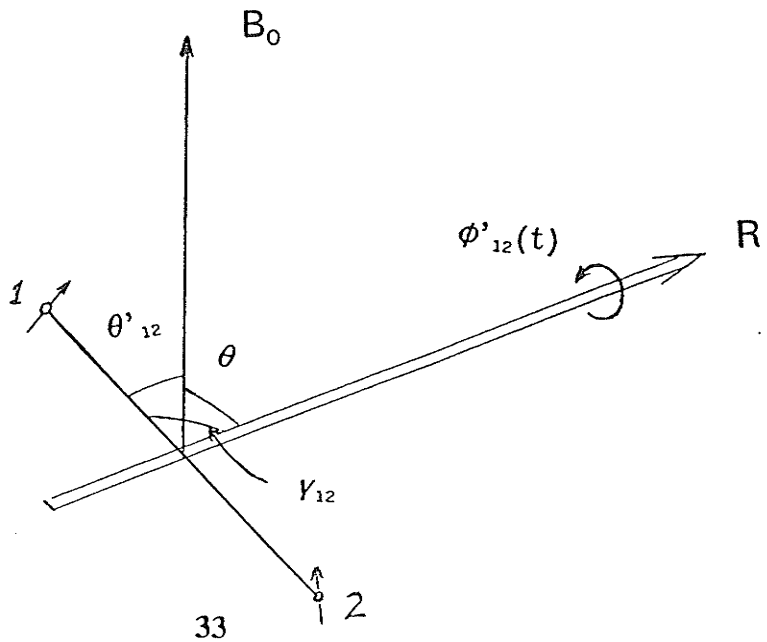

$$1-3(Cos\theta_{12})^2=\frac{1}{2}[3(Cos\theta)^2-1][3(Cos\theta'_{12})^2-1]-\frac{3}{2}Sin2\theta Sin2\theta'_{12}Cos(\omega_r t) \\ -\frac{3}{2}(Sin\theta)^2(Sin\theta'_{12})^2Cos(2\omega_r t). \tag{3.4}$$

The chemical shift interaction is a second-order tensor, like the quadrupolar interaction. It has its own principle axis system (PAS), in which the chemical shift interaction is diagonal. One third of the trace of the chemical shift tensor is defined as the isotropic chemical shift, σ_{is}. In the PAS, the anisotropic chemical shift (CSA) has three components which are along the x, y and z axes. After subtracting σ_{is} from each of the three components, the remaining part can be defined as σ_{11}, σ_{22} and σ_{33} which satisfy:

$$\sigma_{11} + \sigma_{22} + \sigma_{33} = 0 \tag{3.5}$$

According to convention, the PAS is selected as: $\sigma_{33} \geq \sigma_{11} \geq \sigma_{22}$. Two parameters are defined to represent the chemical shift anisotropic tensor, σ_{cs} and η_{cs}:

$$\sigma_{cs} = \sigma_{33} \quad \eta_{cs} = (\sigma_{11} - \sigma_{22})/\sigma_{33} \tag{3.6}$$

where $0 \leq \eta_{cs} \leq 1$.

The transformation from the PAS to the laboratory axis system (LAS) is through a set of Euler angles (α, β, γ), which are the same angles used for the transformation of quadrupolar interaction in chapter Two. Because the chemical shift interaction is very small compared to the Zeeman energy, first-order perturbation can be used to represent the corresponding Hamiltonian, H_{cs}. The first-order perturbation of the chemical shift interaction is:

$$H_{cs} = \gamma B_0 I_z \sigma_{zz}$$
$$\sigma_{zz} = \sigma_{is} + \frac{1}{2}\sigma_{cs}[3(Cos\beta)^2 - 1 + \eta_{cs}(Sin\beta)^2 Cos2\gamma]. \quad (3.7)$$

To consider the effect of sample spinning, we use the same notation of fixed-axis-rotation as that in dipole-dipole interaction, where θ is the angle between **R** and $\mathbf{B_0}$ and $\phi(t)$, the sample rotational angle is ω_r. According to the transformation theory of spherical tensors, it can be proved that:[3.1]

$$\sigma_{zz} = \sigma_{is} + C_0 + C_1 Cos\omega_r t + S_1 Sin\omega_r t + C_2 Cos2\omega_r t + S_2 Sin2\omega_r t \quad (3.8)$$

$$C_0 = \frac{1}{2}[3(Cos\theta)^2 - 1][3(Cos\beta)^2 - 1 + \eta_{cs}(Sin\beta)^2 Cos2\gamma]. \quad (3.9)$$

where C_1, C_2, S_1 and S_2 are expressions containing α, β, γ and θ.[3.1]

When the sample is spinning around **R**, equation (3.4) can be averaged over the rotational period ($2\pi/\omega_r$). If the rotor spinning speed, ω_r , is much larger than the dipolar splitting linewidth, only the first, time-independent term on the right side of equation (3.4) and (3.9), remains; the other terms in the two equations vanish. Therefore,

$$H_D^{rot} = \frac{1}{2}[3(Cos\theta)^2 - 1]\frac{\gamma_1\gamma_2\hbar^2}{r_{12}^3}\frac{1}{2}[3(Cos\theta'_{12})^2 - 1](3I_{1z}I_{2z} - \hat{I}_1\cdot\hat{I}_2) \quad (3.10)$$

$$H_{cs}^{rot} = \gamma B_0 I_z[\sigma_{is} + \frac{1}{2}(3(Cos\theta)^2 - 1)(3(Cos\beta)^2 - 1 + \eta_{cs}(Sin\beta)^2 Cos2\gamma)]. \quad (3.11)$$

From the above equations it can be seen that the width of the central line is reduced by a factor of (1/2)($3Cos^2\theta$ - 1). If θ is set to 54.7°, then ($3Cos^2\theta$ - 1) is equal to

zero; the dipole-dipole interaction is removed and CSA is averaged to an isotropic value.

If the sample spinning speed is smaller than, or equal to, the dipolar splitting and the CSA linewidth, the time-dependent terms over the rotational period in equation (3.4) and C_1, C_2, S_1, S_2 in equation (3.8) do not average to zero. The contribution of these terms will give rise to spinning side bands; the frequency difference between them and the centre peak will be equal to the sample spinning speed, ω_r.

For the first-order quadrupolar perturbation, equation 2.35 can be compared with equation 3.7 as the angular dependent parts are the same. Thus, when the effect of fixed-axis-rotation is considered and the linewidth caused by the first-order quadrupolar interactions will be reduced by the factor $(1/2)(3\text{Cos}^2\theta - 1)$. Fast MAS can average the first-order anisotropies of quadrupolar interactions. For the central transition of half-integer nuclei, the first-order quadrupolar perturbation, $\Delta E^{(1)}_{-1/2\leftrightarrow 1/2}$ is zero.

3. 1. 2. Instrumentation

The MAS probe used in this study is a high speed probe made by Doty Scientific Ltd. There are two air lines, one providing bearing air pressure and the other driving air pressure. The rotor is 5 mm in diameter, made of either silicon nitride or zirconia. When both the bearing and the driving air pressure approaches 40 psi, the rotor spinning speed reaches approximately 14 kHz. The rotor spinning

stability is about 20 Hz at 10 kHz. To discriminate between central bands and spinning side bands, the samples can be spun at different speeds. The central bands will remain in the same position while the spinning side bands will move.

The bearing air pressure is turned on at 0.5 bar to start the spinning, then turn on the drive air is slowly turned on. If the rotor does not spin well, the sample may be repacked. Sometimes lowering the bearing pressure will the sample to spin. Also cleaning the air lines of the probe with some alcohol may start the sample spinning.

3. 2. DOUBLE ANGLE ROTATION (DOR)

3. 2. 1. Theory

For half-integer quadrupolar nuclei, the central transition ($-1/2 \leftrightarrow 1/2$), which is not affected by first-order quadrupolar interactions, is detected. However, often the quadrupolar interactions are so strong that second-order quadrupolar effects for the central transition must be taken into account. Samoson et al. have shown that MAS methods can not average completely the line broadening caused by anisotropies of the second-order quadrupolar interactions.[3.4][3.5]

The effect of fixed-axis-rotation on second-order quadrupolar interaction of the central transition can be found, using the method described in the previous section. The fixed axis **R** is inclined at an angle θ to the external field $\mathbf{B}_0$; the rotational angle is $\phi(t) = \omega_r t$. Equation (2.46) can be expressed as:[3.6]

$$a_{ij} = a_{ij}^{(4)} P_4(Cos\theta) + a_{ij}^{(2)} P_2(Cos\theta). \qquad (3.13)$$

$$\nu^{(2)}_{-1/2\leftrightarrow 1/2} = \nu^{(2)}_{is} + A\sum_{i,j=0}^{2} a_{ij}Cos(2i\beta_q)Cos(2j\gamma_q) + B(\omega_r t) + C(2\omega_r t)$$

$$where \qquad A = \left(\frac{C_Q}{2I(2I-1)}\right)^2 \frac{4I(I+1)-3}{32\nu_I} \qquad (3.12)$$

In equation (3.12), $\nu_{is}^{(2)}$ is the second-order quadrupolar shift; ν_I is the Larmor frequency; $B(\omega_r t)$ and $C(2\omega_r t)$ are the time-dependent terms, which only contribute to spinning side bands under fast sample spinning. The term, C_Q, is the quadrupolar coupling constant.

In equation (3.13), $a_{ij}^{(2)}$ and $a_{ij}^{(4)}$ are constants containing the asymmetry parameter, η; they are listed in Table 3. 1. The terms, $P_2(Cos\theta)$ and $P_4(Cos\theta)$, are the second and fourth Legendre polynomials:

$$P_2(Cos\theta) = \frac{1}{2}[3(Cos\theta)^2 - 1] \qquad P_4(Cos\theta) = \frac{1}{8}[35(Cos\theta)^4 - 30(Cos\theta)^2 + 3] \qquad (3.14)$$

The time-independent term in equation (3.12) determines the line width of the central transition under fixed-axis-rotation. The dependence of the frequency on $P_4(Cos\theta)$ in equation (3.14) gives a broadened spectrum after averaging over β_q and γ_q. In fact, no single angle may be chosen so that both $P_2(Cos\theta)$ and $P_4(Cos\theta)$ are simultaneously zero. Consequently, MAS (where $\theta = 54.74°$, the root of $P_2(Cos\theta)$) will not completely narrow the line broadening of quadrupolar interaction to the second order. One solution is to rotate the sample around two angles simultaneously so that the angles are roots of $P_2(Cos\theta) = 0$ and $P_4(Cos\theta) = 0$. This is the principle of double rotation.

From $P_2(\cos\theta) = 0$, we have: $\theta = 54.74°$, the magic angle.

From $P_4(Cos\theta) = 0$, we have:

$$35(Cos\theta)^4 - 30(Cos\theta)^2 + 3 = 0$$

$$(Cos\theta)^2 = \frac{30 \pm 4\sqrt{30}}{70}.$$

Notice that $0 \leq \theta \leq 90°$ and $0 \leq Cos\theta \leq 1$, thus,

$$Cos\theta_1 = 0.8611 \qquad \theta_1 = 30.56°$$

$$Cos\theta_2 = 0.3400 \qquad \theta_2 = 70.12°.$$

Table 3. 1. Coefficients in the Anisotropic Frequency Cosine Expansion of the central transition of second-order quadrupolar interaction.[3.6]

i	j	$a_{ij}^{(4)}$	$a_{ij}^{(2)}$
0	0	$(81/1120)(18+\eta^2)$	$-(12/7)(1-\eta^2/3)$
0	1	$(9/56)(18+\eta^2)$	$-(36/7)(1-\eta^2/3)$
0	2	$(9/32)(18+\eta^2)$	0
1	0	$(81\eta)/56$	$(24\eta)/7$
1	1	$(27\eta)/14$	$-(24\eta)/7$
1	2	$-(27\eta)/8$	0
2	0	$(27\eta^2)/32$	0
2	1	$-(9\eta^2)/8$	0
2	2	$(9\eta^2)/32$	0

3. 2. 2. Instrumentation and Technique

A DOR probe, loaned from Bruker spectrospin Canada Ltd., uses the pair of angles, 54.74° and 30.56°, for the outer rotor and inner rotor respectively (Fig. 3. 3). There are four air lines: outer bearing and drive , and inner bearing and drive. The spinning inner rotor has the tendency to change its orientation when a torque is exerted on it. This makes the DOR probe very difficult to design. Wu et al [3.7] showed that the torque can be reduced to a tolerably small value when the ratio of the inner and outer rotor spinning speed, ω_1/ω_2, approaches a certain fixed value that depends on the structure of the inner rotor.[3.7] This is incorporated in the design of the DOR probe used in this study where the ratio of the inner and outer rotor spinning speeds is 5 to 1.

Due to the critical balance of the inner and outer rotor, the outer rotor spinning speed cannot be high; the maximum is about 1200 Hz. The Bruker probe could maintain a speed of 1100 Hz for about two minutes. The low spinning speed causes spectra to be complicated by numerous spinning side bands due to the remaining quadrupolar and dipole-dipole interactions, and chemical shift anisotropies. The signal to noise ratio is low because the filling factor of the DOR probe is small compared to MAS probes. In order to increase the intensity of central band and simplify the spectra, the technique of synchronization was used in which the pulses are synchronised with the period of rotation to eliminate the odd-numbered sidebands.[3.7] The pulse programs are shown diagrammatically in Figure 3. 4.

D_5 is a circuit delay, which depends on the probe, the spectrometer and

Fig. 3. 3. The relative orientations of the inner rotor, outer rotor and the external magnetic field $\mathbf{B_0}$.

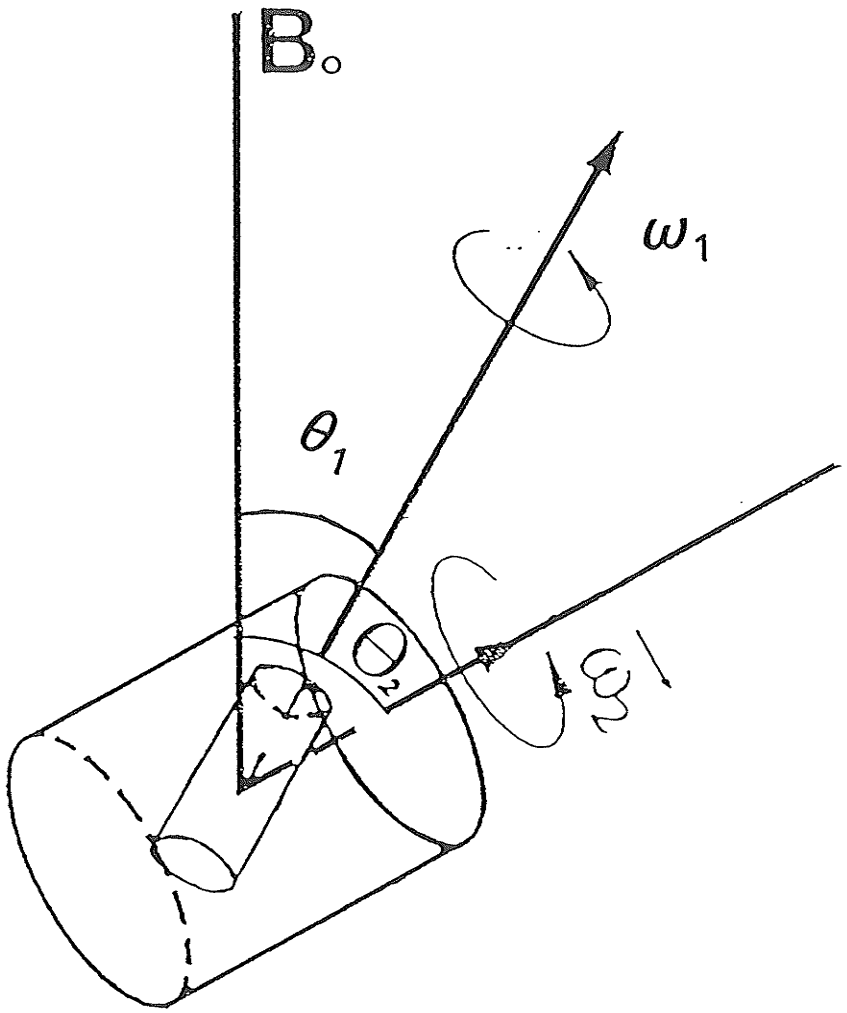

Θ_2: 54.7° , magic angle.

Θ_1: 30.6° , one root of $P_4(\mathrm{Cos}\Theta) = 0$.

Fig. 3. 4. Pulse diagram for DOR NMR experiments.

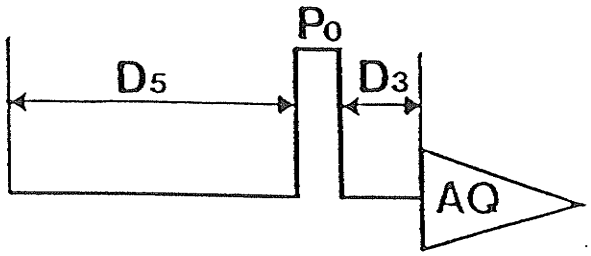

(a) (a) experiment 1, VD set as 0 μs;

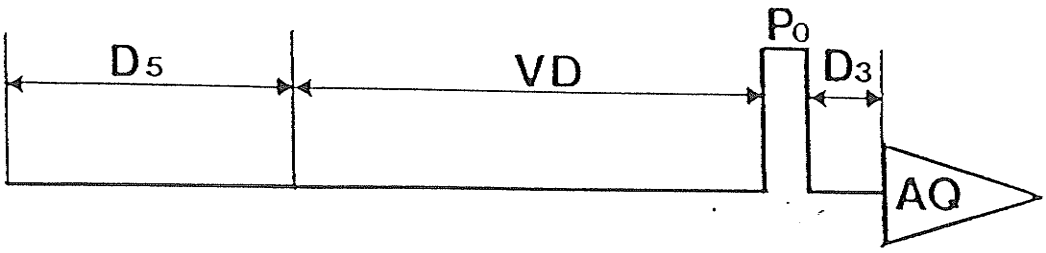

(b)

(b) experiment 2, VD is half the period of rotation of the outer rotor.

spinning speed of outer rotor, to allow the synchronization of the RF pulse with the rotation of the outer rotor.

VD is a time delay which is equal to either zero or half the period of rotation of the outer rotor.

P_0 is the excitation pulse (2 μs).

D_3 is a delay for the ring-down of the probe (15 μs).

The synchronization procedure consists of two experiments. In the first experiment, VD is set to zero (Fig. 3. 4a); in the second, VD is set to half the period of one rotation of the outer rotor (Fig. 3. 4b). At the beginning of the P_0 pulse in the second experiment, the relative position of the inner rotor is 180° from that in the first experiment. FID's are acquired at these two positions and added prior to Fourier Transformation.

Careful packing of the sample and correct adjustment of the position of the inner rotor with respect to the outer rotor are needed to start the rotors spinning. To begin the experiment, the first thing is to check the maximum outer rotor spinning speed:

1. Tune to ^{23}Na and put a sample of NaCl powder. Adjust the position of the outer rotor within the probe and make sure that the inner rotor is approximately at magic angle with respect to the external magnetic field;

2. Turn on the inner bearing air to 1.0 bar and start the inner drive air slowly. One can hear the sound of inner rotor spinning at about 0.4 bar or even lower. If the rotor starts spinning at 0.5 bar or higher, it is better not to run the sample higher

than 800 Hz;

3. Increase the inner drive air pressure to 1.0 bar and acquire an FID. From the spinning side bands of NaCl, one can know the inner rotor spinning speed. If the inner rotor is at a proper position with respect to the outer rotor, the spinning speed could be around 5 kHz. If the detected speed is below 4.4 kHz, it is better not to try to run the outer rotor higher than 800 Hz.

The next thing is to measure D_5 at different outer rotor spinning speeds. Use the packed NaCl sample and connect the four air lines:

1. Turn on the inner bearing air to 1.2 bar and start the inner drive air until one can hear the sound of spinning;

2. Turn on the outer bearing air to 2.8 bar and start the outer drive air slowly. Soon one can hear the spinning sound of the outer rotor. Now increase the pressures of the inner and outer drive air simultaneously. As the outer rotor picks up the speed, the sound becomes progressively louder. If there is some abrupt change of the sound frequency, it often means that the inner rotor has crashed and stopped spinning.

3. Once the outer rotor reaches the required frequency, select a value for D_5 and acquire an FID. From the FID, one can tell whether the inner rotor is spinning or not. After Fourier Transformation, one can find from the size of the odd-numbered spinning side bands if the proper D_5 value has been selected.

Once D_5 is obtained, one can begin an experiment. Often it can be difficult to determine whether or not the inner rotor is spinning, especially at high speeds,

and to maintain the speed for very long owing to the critical balance of the inner and outer driving air pressure at high speed of spin. For this reason, an MAS spectrum is acquired first in order to obtain the best parameters for the DOR experiment and minimize the duration of the DOR experiment. Different outer rotor spinning speeds can be used to distinguish the central bands from spinning side bands.

3. 3. DYNAMIC ANGLE SPINNING (DAS)

3. 3. 1. Theory

The basic premise of averaging out the second-order quadrupolar anisotropies in equation (3.13) is to make the angle θ time-dependent by moving the spinning axis. In order to do this, we require that over the time of experiment (T) for l = 2 and l = 4:[8]

$$\int P_l(Cos\theta)\, W(\theta)\, d\theta = \int_0^T P_l(Cos\theta(t))\, dt = 0 \qquad (3.15)$$

where $W(\theta)$ is a weighted function describing the distribution of angles.

In DAS experiments, a set of N discrete angles are found such that:

$$\sum_{i=1}^{N} P_2(Cos\theta_i)\, t_i = \sum_{i=1}^{N} P_4(Cos\theta_i)\, t_i = 0 \qquad (3.16)$$

where t_i is the fraction of time spent at each angle. The simplest case is that N equals 2. Then we have:

spinning speed of outer rotor, to allow the synchronization of the RF pulse with the rotation of the outer rotor.

VD is a time delay which is equal to either zero or half the period of rotation of the outer rotor.

P_0 is the excitation pulse (2 μs).

D_3 is a delay for the ring-down of the probe (15 μs).

The synchronization procedure consists of two experiments. In the first experiment, VD is set to zero (Fig. 3. 4a); in the second, VD is set to half the period of one rotation of the outer rotor (Fig. 3. 4b). At the beginning of the P_0 pulse in the second experiment, the relative position of the inner rotor is 180° from that in the first experiment. FID's are acquired at these two positions and added prior to Fourier Transformation.

Careful packing of the sample and correct adjustment of the position of the inner rotor with respect to the outer rotor are needed to start the rotors spinning. To begin the experiment, the first thing is to check the maximum outer rotor spinning speed:

1. Tune to ^{23}Na and put a sample of NaCl powder. Adjust the position of the outer rotor within the probe and make sure that the inner rotor is approximately at magic angle with respect to the external magnetic field;

2. Turn on the inner bearing air to 1.0 bar and start the inner drive air slowly. One can hear the sound of inner rotor spinning at about 0.4 bar or even lower. If the rotor starts spinning at 0.5 bar or higher, it is better not to run the sample higher

$$\begin{aligned} P_2(Cos\theta_1)t_1 + P_2(Cos\theta_2)t_2 &= 0 \\ P_4(Cos\theta_1)t_1 + P_4(Cos\theta_2)t_2 &= 0 \end{aligned} \tag{3.17}$$

If $t_1 = t_2$ is chosen, for the first equation in the above equations

$$(Cos\theta_2)^2 = \frac{2}{3} - (Cos\theta_1)^2 \tag{3.18}$$

Substituting 3.18 into the second term in equation (3.17), after some derivation, gives:

$$\begin{aligned} 45(Cos\theta_1)^4 - 30(Cos\theta_1)^2 + 1 &= 0 \\ (Cos\theta_1)^2 &= \frac{5 \pm 2\sqrt{5}}{15} \end{aligned} \tag{3.19}$$

The solution of the above equation is a pair of complimentary angles: $\theta = 37.38°$ or $\theta = 79.19°$. Substituting the results of θ_1 into equation (3.18), gives:

$$\theta_1 = 37.38°, \theta_2 = 79.19° \quad \text{or} \quad \theta_1 = 79.19°, \theta_2 = 37.38° \tag{3.20}$$

This is the solution for one-angle flipping DAS experiment. In practice, the sample is spun at 37.38° for time τ, then it is flipped to 79.19° for another time τ. At the end of the second τ time period, an FID is acquired and the rotor switched back to 37.38°, waiting for the beginning of another experiment. In this experiment, the second-order quadrupolar anisotropies of the central transition have been averaged to isotropic values.

3. 3. 2. Technique

One practical limitation of the DAS technique is the length of time, about 20 ms, required for flipping the stator between two angles. Thus the DAS technique

may only be used for nuclei with spin lattice relaxation times greater than 0.1 seconds. Quadrupolar interactions provide the dominant relaxation mechanism for quadrupolar nuclei in solids. As this is extremely efficient, the relaxation time of some quadrupolar nuclei, such as ^{27}Al, is typically of the order of tens of milliseconds,[3.9] and therefore is too short for the DAS technique to be used.

Another problem with this pulse sequence is that neither of these two angles is the magic angle. Thus the broadenings caused by dipole-dipole interactions and chemical shift anisotropies are not efficiently averaged. One way to solve the second problem was presented again by Mueller et al. in an experiment called a pure-phase absorption.[3.9]

In this experiment, the rotor flips among three angles, allowing the acquisition of the FID to be at the magic angle. The time τ is incrementally increased between subsequent experiments. The Fourier Transformation of the acquired MAS FID gives the F_2 dimension of the two-dimensional plot, which contains both the isotropic and anisotropic second-order quadrupolar interactions. Fourier Transformation of equivalent points from spectra with different values of τ gives the F_1 dimension, which contains only isotropic interactions and can separate peaks due to corresponding sites.[3.8] The projection of each of these peaks onto the F_2 dimension will result in normal MAS spectra, which can be used to obtain the quadrupolar interaction parameters by correlating the shape of each peak with the computer-simulated spectrum.[3.8][3.10]

In practice, the rotor was spun at 37.4° for time τ, flipped to 79.2° for another

period τ then flipped to 54.7° while an FID was acquired. A 90° pulse was applied just before each rotor-flip in order to rotate the transverse magnetization to the z-axis for storage. Immediately after the flip, a 90° pulse with an opposite phase was used to recover the magnetization.[3.8] After the acquisition of the FID, the spinning axis was returned to 37.4°. The 90° pulses used are soft pulses, in order to excite only the central transition.[3.8]

To set up a DAS experiment, the first thing is to calibrate the magic angle:

1. Connect all the lines and circuits and tune to ^{79}Br; put in sample KBr and spinning the sample at about 5 kHz;

2. Enter the 'gs' mode and watch the spikes on the FID; use the 'arrow' keys on the keyboard to change the magic angle slightly until the spikes reach the maximum; save the number of steps; from this value and a reference rod inside the probe, the computer can calibrate any other angles accurately.

The next step is to do one MAS experiment to choose the proper parameters. Then one has to calibrate the 90° pulse lengths at 37.38°, 54.74° and 79.19° separately. Soft pulses have to be used in order to excite only the central transitions of half-integer quadrupolar nuclei.[3.7] Finally, one has to set up a two-dimensional pulse sequence using a proper phase cycling to start the whole experiment.

3. 4. COMPARISON OF MAS, DAS AND DOR TECHNIQUES TO OBTAIN PARAMETERS FROM QUADRUPOLAR NUCLEI

Magic Angle Spinning can efficiently average the broadening effects due to dipole-dipole interactions and chemical shift anisotropy, but not those resulting from second-order quadrupolar interactions. As second-order quadrupolar interactions are inversely proportional to the strength of the magnetic field, the parameters C_Q and η can be calculated for simple spectra from the computer simulation of MAS spectra obtained at two magnetic field strengths. The isotropic chemical shift can be obtained by calculating the quadrupolar shift and subtracting it from the observed shift.

A comparison of the ^{23}Na peak widths of tugtupite in the DOR (68 Hz) and DAS (240 Hz) spectra (Table 4. 2) shows that the DOR technique is more efficient at averaging second-order quadrupolar interaction anisotropies and narrowing the peak (See chapter four). The spin-lattice relaxation times of quadrupolar nuclei are usually very short; during the periods of flipping of the rotor axis in the DAS experiments, some of the longitudinal and transverse magnetization will be lost. The averaging methods, which are based on equal magnetizations before and after the flip of the rotor axis, therefore, will no longer be precise. In the DOR experiments, the homonuclear dipole-dipole interactions are averaged more completely because multiple terms, such as $I_{1x}I_{2y}I_{3y}$, are not refocused during the MAS acquisition in DAS experiments.[3.11]

The length of time (40 ms) required for a flip of the rotor axis in DAS experiments confines its application to non-integer quadrupolar nuclei, such as ^{17}O,

^{23}Na and ^{87}Rb, with relatively long T_1 relaxation times. DOR can be used for nuclei with much more rapid relaxation, as the minimum time required for the acquisition of the free induction decay is not as limited.

For DOR experiments, the outer rotor, which is at the magic angle, spins at 1 kHz. This is not fast enough to average anisotropy in the chemical shift and dipole-dipole interactions greater than 1 kHz. In pure-phase absorption DAS experiments, the sample can spin at 14 kHz. As the acquisition is at the magic angle, this technique is more efficient than DOR at averaging chemical shift anisotropy.

DOR is the most difficult experiment to perform technically, especially at high-speed spinning of the outer rotor, owing to the critical balance of the inner and outer rotor. In DOR experiments, short pulse-lengths can be used to excite only the centre bands, which reduces the delay required for relaxation of nuclei between pulses, enhances the sensitivity of detection,[3.12] and shortens the duration of the experiment. DAS experiments can take up to 14 hours in comparison to DOR experiments, which can be performed in one hour.

DAS is the preferred technique for quadrupolar nuclei with long T_1 relaxation times, relatively small quadrupolar interactions, small homonuclear dipole-dipole interactions and large anisotropies in chemical shifts. The DOR technique is preferred for quadrupolar nuclei with large quadrupolar and homonuclear dipole-dipole interactions and small chemical shift anisotropies. MAS at two fields can be used to calculate quadrupolar parameters, but only for spectra of simple structures that do not give overlapping peaks.

REFERENCE FOR CHAPTER THREE

[3.1] M. Mehring: High Resolution NMR in Solids Second and Enlarged Edition. Springer-verlag (1983).

[3.2] U. Haeberlen : High-resolution NMR in solids; Supplement 1 to Advances in Magnetic Resonance Academic, New York (1976).

[3.3] C. P. Slichter: Principles of Magnetic Resonance Third and Enlarged Edition. Springer-Verlag (1990).

[3.4] E. Kundla, A. Samoson and E. Lippmaa : High-resolution NMR of quadrupolar nuclei in rotating solids Chem. Phys. lett. **83**, 229 (1981).

[3.5] A. Samoson, E. Kundla and E. Lippmaa : High-resolution MAS-NMR of quadrupolar nuclei in powders J. Magn. Reson. **49**, 350 (1982).

[3.6] K. T. Mueller, Y. Wu, B. F. Chmelka, J. Stebbins and A. Pines : High-resolution oxygen-17 NMR of solid silicates J. Am. Chem. Soc. **113,** 32 (1991).

[3.7] Y. Wu, B. Q. Sun, and A. Pines : NMR experiments with a new double rotor. J. Magn. Reson. **89**, 297 (1990).

[3.8] K. T. Mueller, B. Q. Sun, C. G. Chings, J. W. Zwanziger, T. Terao, and A. Pines: Dynamic-angle spinning of quadrupolar nuclei J. Magn. Reson. **86**, 470 (1990).

[3.9] K. T. Mueller, E. W. Wooten, and A. Pines : Pure-absorption-phase dynamic -angle spinning J. Magn. Reson. **92**, 620 (1991).

[3.10] Z. W. Zheng, Z. H. Gan, N. K. Sethi, D. W. Alderman and D. M. Grant : An

efficient simulation of variable-angle spinning lineshapes for the quadrupolar nuclei with half-integer spin J. Magn. Reson. **95**, 509 (1991).

[3.11] J. H. Baltisberger, S. L. Gann, E. W., Wooten, T. H. Chang, K. T. Mueller, and A. Pines (1993): ^{87}Rb Dynamic-Angle Spinning NMR of Inorganic Rubidium Salts, preprint.

[3.12] D. Shaw, D. (1976): Fourier Transform NMR Spectroscopy Elsevier Scientific Publishing Company, Amsterdam.

CHAPTER FOUR ^{23}Na ^{27}Al ^{9}Be ^{29}Si NMR STUDY OF TUGTUPITE

4. 1. STRUCTURE OF TUGTUPITE

Tugtupite, $Na_8[Al_2Be_2Si_8O_{24}](Cl,S)_2$, is a well-ordered cubic tectosilicate mineral which crystallizes in space group I4.[4.1] Si, Be and Al, in tetrahedral coordination with four oxygen atoms, form the framework of the structure (Fig. 4. 1). There is a four-membered ring containing two Si, one Be and one Al atoms normal to the a axis, a four-membered ring containing four Si atoms perpendicular to the c axis, and a six-membered ring containing four Si, one Al and one Be atoms at the corners. Na and Cl are inside the cages, and the Cl atoms are either at the corners or the centre of the unit cell. Na is in five-fold coordination with one Cl and four O atoms.[4.2]

From X-ray diffraction results, it is not clear if there is any disorder of Si, Al and Be within the tetrahedral site. Different NMR techniques were used to study ^{9}Be, ^{23}Na, ^{27}Al and ^{29}Si nuclei in tugtupite in order to obtain the values of isotropic chemical shifts, C_Q and η, and to evaluate the degree of atomic order in the structure.

As tugtupite is an extremely well ordered aluminosilicate mineral, it was also used to investigate the limitations and possibilities of the various NMR techniques in the determination of isotropic chemical shift, C_Q and η parameters from

Fig. 4. 1. The crystal structure of tugtupite.

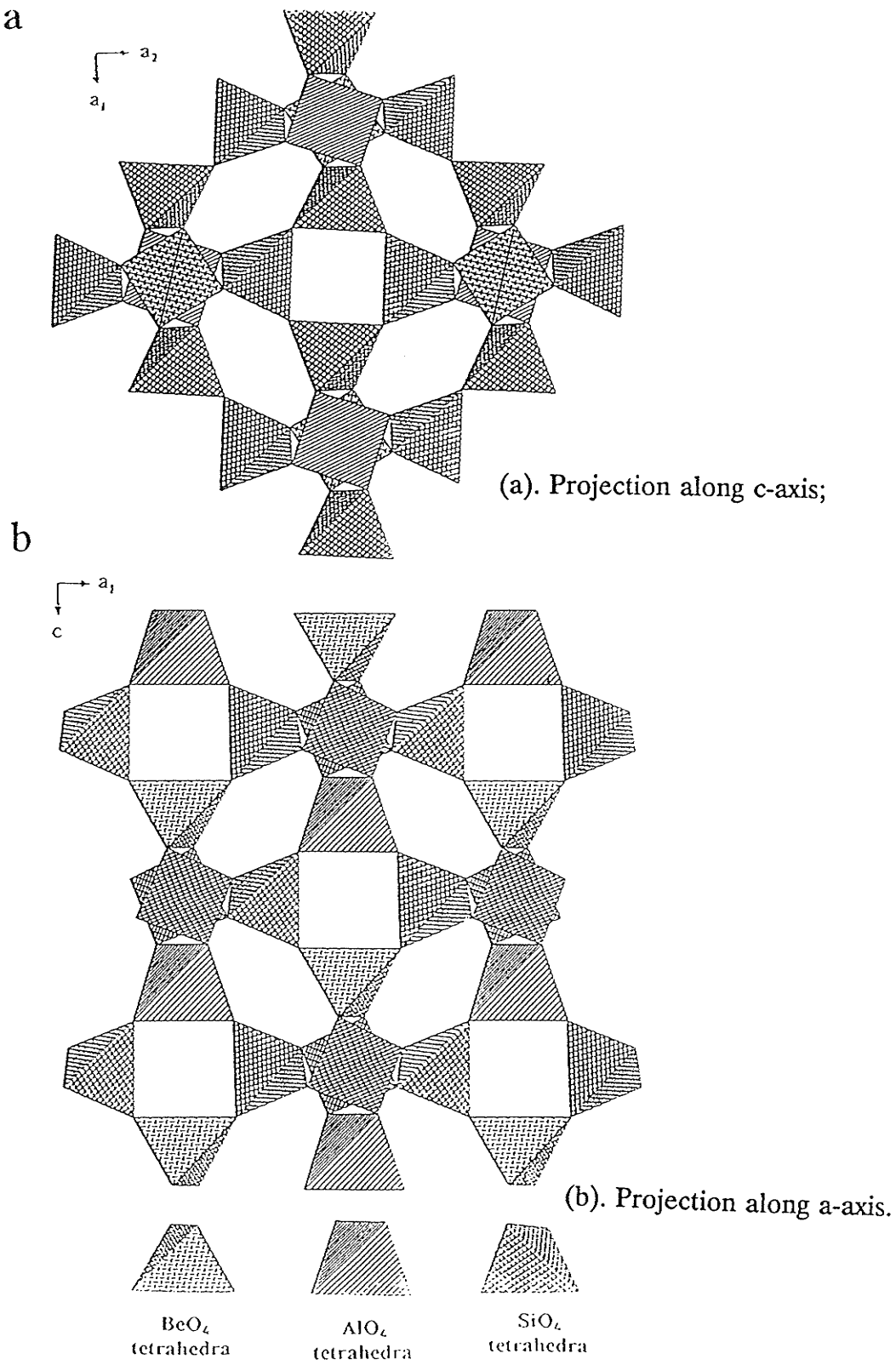

quadrupolar nuclei.

4. 2. EXPERIMENTAL

Tugtupite from Ilimaussaq, Narssaq Kommune, South Greenland (Royal Ontario Museum, sample number: M32790) was finely ground prior to packing into the NMR rotors. It is from the same locality as the sample analyzed by Danø.[4.1] The NMR spectra were acquired using a Bruker AMX-500 console with an 8.4 T wide-bore magnet and an 11.7 T narrow-bore magnet. MAS spectra were acquired at both fields using a high-speed MAS probe with 5-mm diameter rotors from Doty Scientific Ltd. The experimental parameters are listed in Table 4. 1. MAS spectra for ^{23}Na were obtained at -35, -52, -80 and -110°C at 132.3 MHz. The spectra were recorded with reference to $^{23}Na^{+}$ in a 0.1 M aqueous solution of NaCl, $^{27}Al(H_2O)_6$ in an aqueous solution of $AlCl_3$, $^{9}Be^{2+}$ in an aqueous solution of $Be(NO_3)_2$ solution, and ^{29}Si in tetramethylsilane (TMS).

^{23}Na and ^{27}Al DOR spectra were acquired at a magnetic field of 8.4 T using a Bruker DOR probe with an outer rotor spinning speed of 800 Hz. The delay between pulses was 2 s; short pulse-lengths of 2 μs were used for both ^{23}Na and ^{27}Al to excite the central transitions only.[4.3]

The DAS experiments of ^{23}Na were run at a magnetic field of 8.4 T . The sample was packed in a 5-mm rotor which was spun at 6.9 kHz around an axis

TABLE 4. 1. MAS EXPERIMENTAL PARAMETERS OF ^{23}Na, ^{27}Al, ^{9}Be AND ^{29}Si.

	$P_1(\mu s)$	D_1 (s)	Spectra Width(Hz)	Number of Scans	Line Broadening(Hz)	Spinning Speed(kHz)	Larmor Frequency(MHz)
^{23}Na	0.4	2.0	20000	500	50	8.7	95.22
^{23}Na	0.4	1.0	125000	500	50	8.7	95.22
^{23}Na	0.4	2.0	20000	404	20	9.7	132.30
^{23}Na	0.4	1.0	125000	400	20	9.7	132.30
$^{23}Na^{a}$	0.6	1.0	20000	300	50	6.0	132.30
^{27}Al	0.4	0.5	20000	600	10	8.7	93.80
^{27}Al	1.0	0.5	125000	904	20	8.7	93.80
^{27}Al	0.4	0.5	20000	547	10	9.7	130.32
^{27}Al	1.0	0.5	125000	800	10	9.7	130.32
^{9}Be	0.2	0.1	31250	5294	0	9.0	70.28
^{29}Si	2.0	30	10000	1235	30	7.1	99.35

D_1: relaxation delay between pulses; P_1: pulse length.
[a]: ^{23}Na MAS experiments at low temperatures.

capable of being flipped from 23° to 85° with respect to the magnetic field. Sixteen FIDs were recorded for each experiment, with 256 points being collected in the F_1 dimension and 512 in the F_2 dimension. The pulse lengths of 90°, measured at the three rotor flip angles of 37.38°, 54.74° and 79.19°, were 3.8 μs, 2.1 μs and 2.0 μs, respectively.[4.4] The time delay for switching between two angles was 50 ms. The duration of τ was increased by 2 μs between successive experiments. The relaxation delay between pulses was 3 s. A narrow spectral width of 20,000 Hz was chosen to just cover the frequency range containing the peaks in order to obtain sufficient resolution in the F_1 dimension and reduce the duration of the experiment.

The central transition lineshapes for non-integer quadrupolar nuclei were simulated using a computer program which modified after "SECQUAD" written by W. P. Power and R. E. Wasylishen.[4.5] In this simulation, spinning speeds were considered to be infinitely large, so that spinning sidebands did not need to be considered. The lineshapes were assumed to be only due to second-order quadrupolar interactions, as for non-integer quadrupolar nuclei, the central transitions are not affected by first-order quadrupolar interactions.

4. 3. RESULTS AND DISCUSSION

4. 3. 1. ^{29}Si

The ^{29}Si MAS spectrum has one narrow peak at -95.1 ppm with a linewidth

of 70 Hz (30 Hz line broadening) (Table 4. 2, Fig. 4. 2). This shows that ^{29}Si is in a single site, which is tetrahedrally coordinated with one Al, one Be and two Si atoms. There is no Si/Al disorder among the tetrahedral sites (Fig. 4. 1). Using the crystal-structure data of Hassan & Grundy [4.2] and the empirical relationship derived by Sherriff et al.,[4.6] the peak position was calculated to be at -94.5 ppm, which was very close to the experimental result.

4. 3. 2. ^{9}Be

The MAS NMR spectrum gave one extremely narrow ^{9}Be peak at -2.1 ppm, with 22 Hz width at half peak maximum (0 Hz line broadening) (Table 4. 2, Fig. 4. 3). ^{9}Be is therefore in a single symmetrical tetrahedral environment, with a small field gradient and therefore quadrupolar interactions. The spinning sidebands are due to first order splitting and indicate that C_Q is of the order of 9 kHz. The structure refinement from single-crystal X-ray diffraction data shows that the site is very symmetrical, with the four Be-O bond lengths of 1.631(2) Å, four O-Be-O bond angles of 107.7(1)°, and two of 113.5(1)°.[4.2]

4. 3. 3. ^{23}Na

There is one peak with two maxima in the ^{23}Na MAS spectra at both 95.2 MHz and 132.3 MHz. DOR NMR was used to determine whether the two maxima are due to two Na peaks or one peak with a quadrupolar shape. The DOR spectrum gave a single peak at 1.8 ppm, with a peak width at half height of 68 Hz (Table 4.

Table 4. 2. The NMR results of tugtupite.

	δ_{obs} (ppm)*	linewidth (Hz)	C_Q (MHz)	η	δ_{iso}(ppm)
^{29}Si MAS, 11.7 T	- 95.1	70 lb=30			- 95.1
^{9}Be MAS, 11.7 T	- 2.1	22 lb=0			- 2.1
^{23}Na MAS, 8.43 T	2.0	830 lb=50	1.27	0.48	6.8
^{23}Na MAS, 11.7 T	4.4	590 lb=20	1.27	0.48	6.9
^{23}Na DAS, 8.43 T	2.1	240 lb=20	1.27	0.48	6.9
^{23}Na DOR, 8.43 T	1.8	68 lb=10	1.27	0.48	6.6
^{27}Al MAS, 8.43 T	62.3	180 lb=10	1.70	0.19	64.2
^{27}Al MAS, 11.7 T	63.3	140 lb=20	1.70	0.19	64.2
^{27}Al DOR, 8.43 T	62.5	43 lb=10	1.70	0.19	64.4

*: δ_{obs} are the observed shifts of the centres of gravity of the central bands.

Fig. 4. 2. ^{29}Si MAS spectrum of tugtupite at 11.7 T spinning at 7.1 KHz.

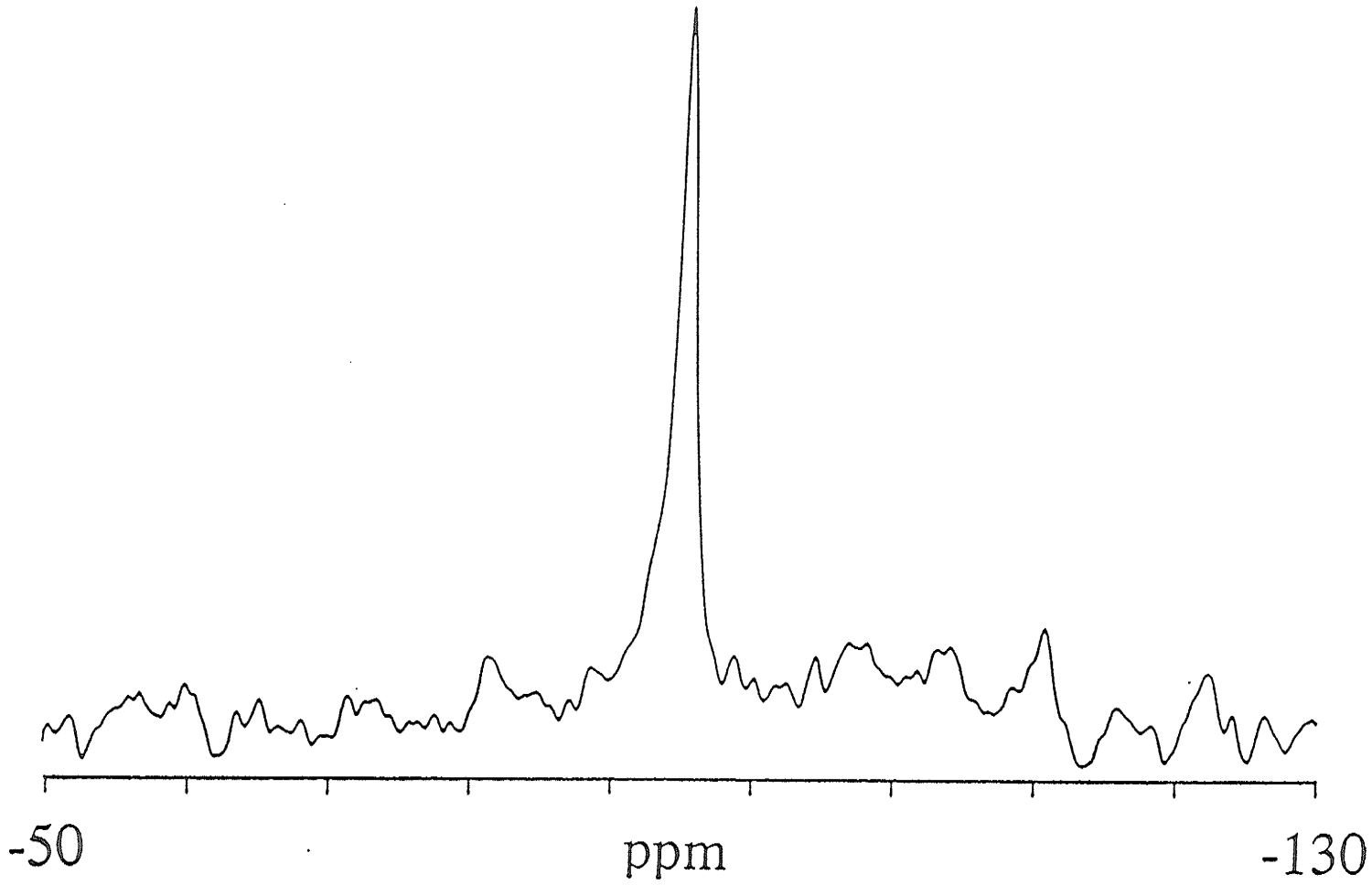

Fig. 4. 3. ^{9}Be MAS spectrum of tugtupite at 11.7 T spinning at 9.0 KHz.

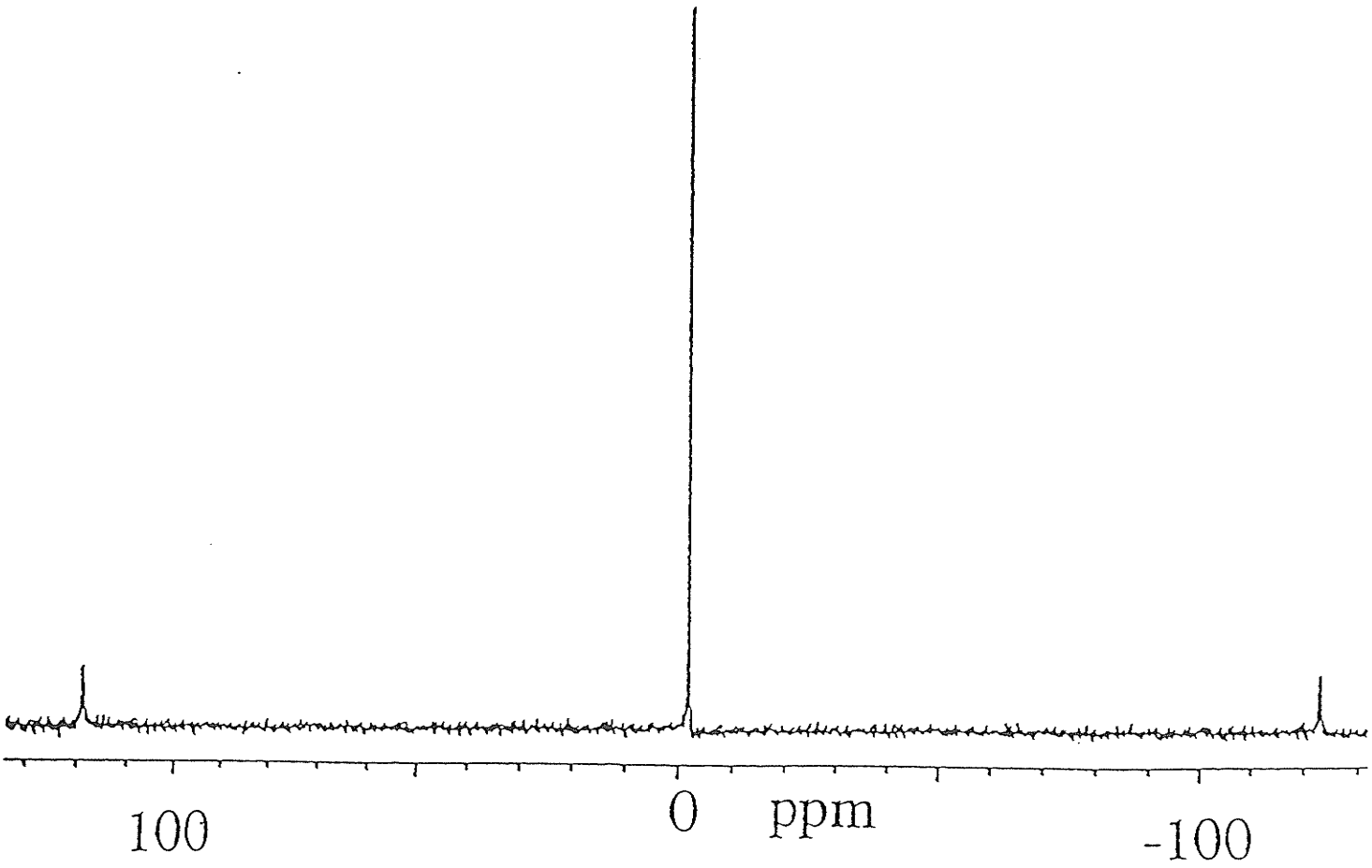

2, Fig. 4. 4), showing that there is one ^{23}Na environment in tugtupite.

For quadrupolar nuclei in a single site, the second moment of the central transition in MAS spectra will be inversely proportional to the strength of the magnetic field if the peak width is only caused by the second-order quadrupolar interactions.[4.7] Therefore, by comparing the widths of MAS central transitions at different strengths of magnetic field, it is possible to determine if the lineshapes are caused only by second-order quadrupolar interaction anisotropy. For ^{23}Na, the ratio of the linewidths for the field strengths of 11.7 T and 8.4 T is 570 : 780 or 0.73 (Table 4. 2). As this result is close to the ratio of the strengths of the magnetic field of 0.72, the ^{23}Na MAS lineshapes are considered to be caused solely by the second-order quadrupolar interactions.

The quadrupolar parameters C_Q and η were found by comparison of the MAS experimental results with computer simulations of the central transition lineshape. The quadrupolar parameters for C_Q of 1.27 MHz, and η of 0.48, were required to produce simulations with the same lineshapes as the experimental spectra recorded at both magnetic field strengths (Fig. 4. 5).

To verify these parameters, the difference between the peak positions at the two fields was calculated in the following manner and compared to experimental results. For a quadrupolar nucleus, the centre of gravity of a single MAS peak (δ_{obs}) is a resultant of the quadrupolar shift (δ_Q) and isotropic chemical shift (δ_{iso}).

$$\delta_{obs} = \delta_Q + \delta_{iso} \qquad (4.1)$$

For central transitions of a non-integer quadrupolar nucleus with spin I, the first-

Fig. 4. 4. ^{23}Na DOR spectrum of tugtupite at 8.4 T with the outer rotor spinning at 800 Hz.

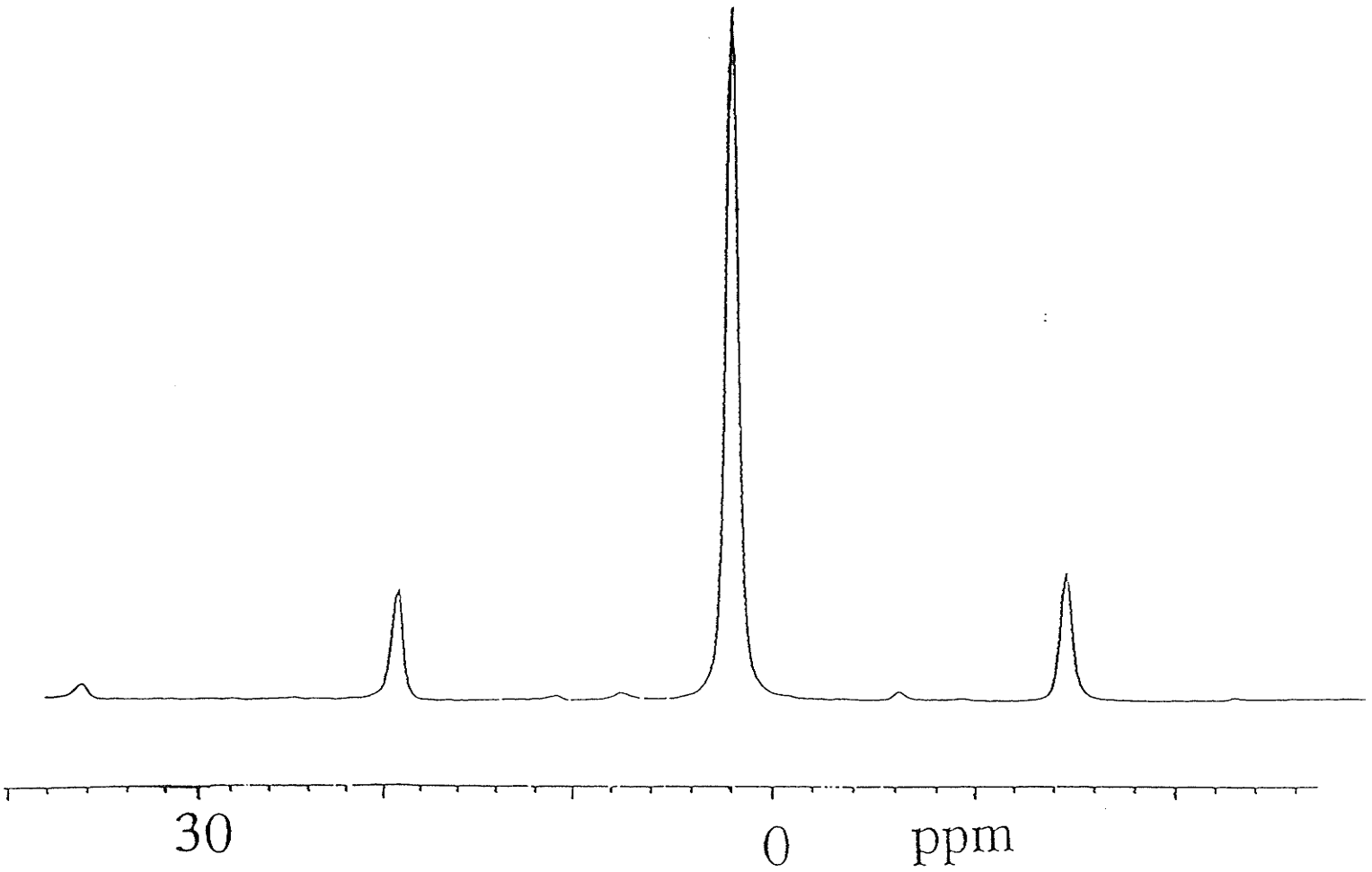

Fig. 4. 5. ^{23}Na MAS spectra of tugtupite.

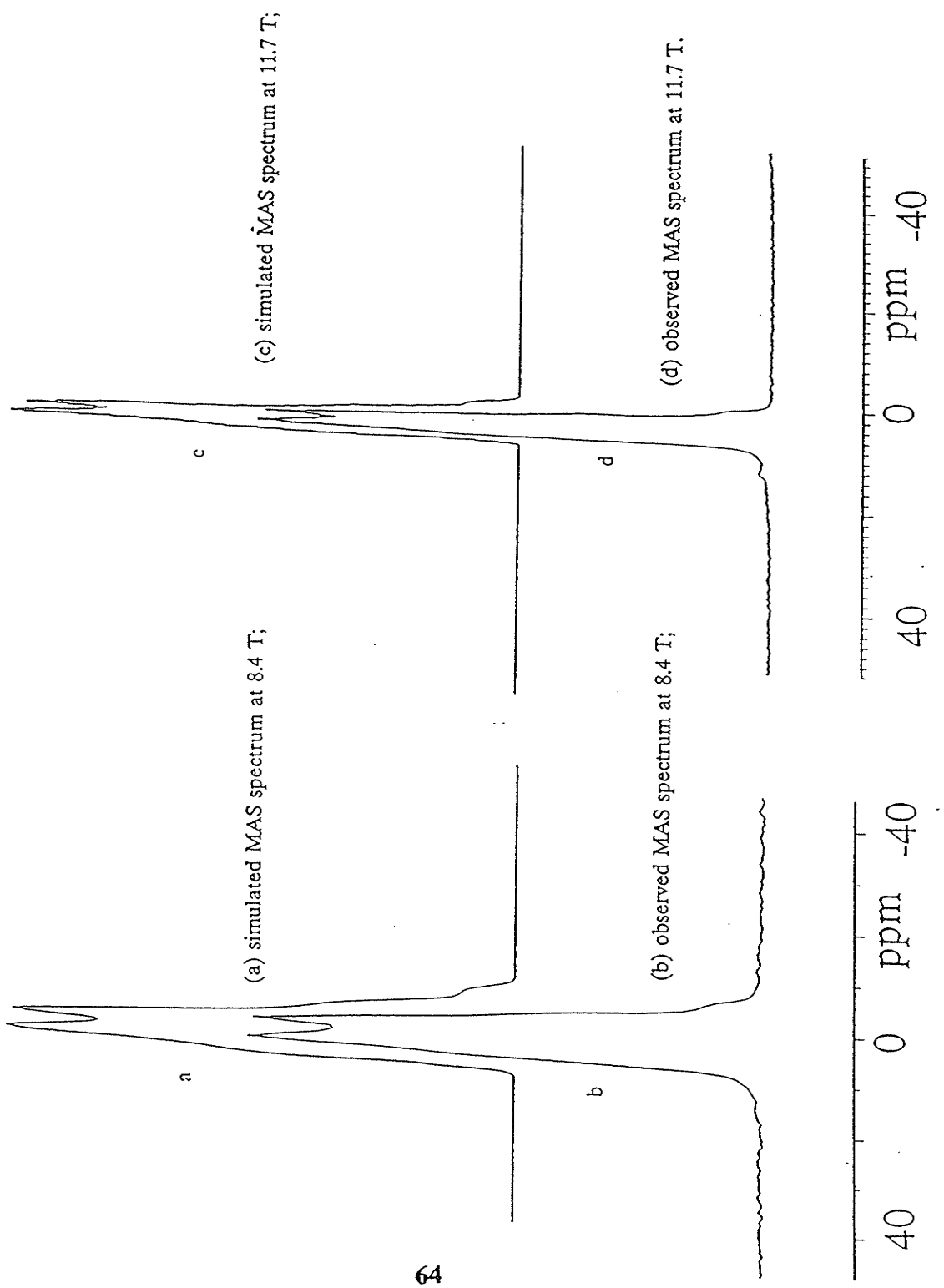

order quadrupolar shift is zero, and according to equation (2.58) the second-order quadrupolar shift is given by:

$$\delta_{Q1,2} = -3 \cdot 10^6 \cdot C_Q^2 (I(I+1)-3/4)(1+\eta^2/3)/(40I^2(2I-1)^2\nu^2_{1,2}) \qquad (4.2)$$

where $\nu_{1,2}$ is the Larmor frequency (MHz) at two different values of the magnetic field.

If one defines:

$$\Delta\delta_Q = \delta_{Q1} - \delta_{Q2} \qquad (4.3)$$

$$\Delta\delta_{iso} = \delta_{iso1} - \delta_{iso2} \qquad (4.4)$$

$$\Delta\delta_{obs} = \delta_{obs1} - \delta_{obs2} \qquad (4.5)$$

Then $$\Delta\delta_{obs} = \Delta\delta_{iso} + \Delta\delta_Q \qquad (4.6)$$

As the isotropic chemical shifts are independent of the strength of the magnetic field, they will be the same in both fields, and $\Delta\delta_{iso}$ will be zero. Therefore,

$$\Delta\delta_{obs} = \Delta\delta_Q \qquad (4.7)$$

If ν_1 is greater than ν_2, then from equation (4.2) and (4.3):

$$\Delta\delta_Q = -3[I(I+1)-3/4](1+\eta^2/3)C_Q^2 \cdot 10^6(1/\nu^2_1 - 1/\nu^2_2)/[40I^2(2I-1)^2] \qquad (4.8)$$

For ^{23}Na at the two field strengths of 8.4 T and 11.7 T, equation (4.8) becomes

$$\Delta\delta_Q = 1.329 \cdot C_Q^2 \cdot (1 + \eta^2/3) \quad \text{ppm.} \qquad (4.9)$$

By substituting the values of 1.27 for C_Q and of 0.48 for η, from the simulations of the MAS spectra, into expression (4.9), $\Delta\delta_Q$ is calculated to be 2.3 ppm. This compares favourably to the observed value of 2.4 $\pm$ 0.1 ppm.

The F_1 projection of the DAS spectrum showed only one ^{23}Na peak, with a linewidth of 240 Hz (Table 4. 2, Fig. 4. 6). As the spectral width was 20000 Hz and

Fig. 4. 6. Two-dimensional plot of ^{23}Na DAS spectrum of tugtupite at 8.4 T with one dimensional projections along the F_1 and F_2 axes and projections of the four points of the F_1 peak onto the F_2 dimension.

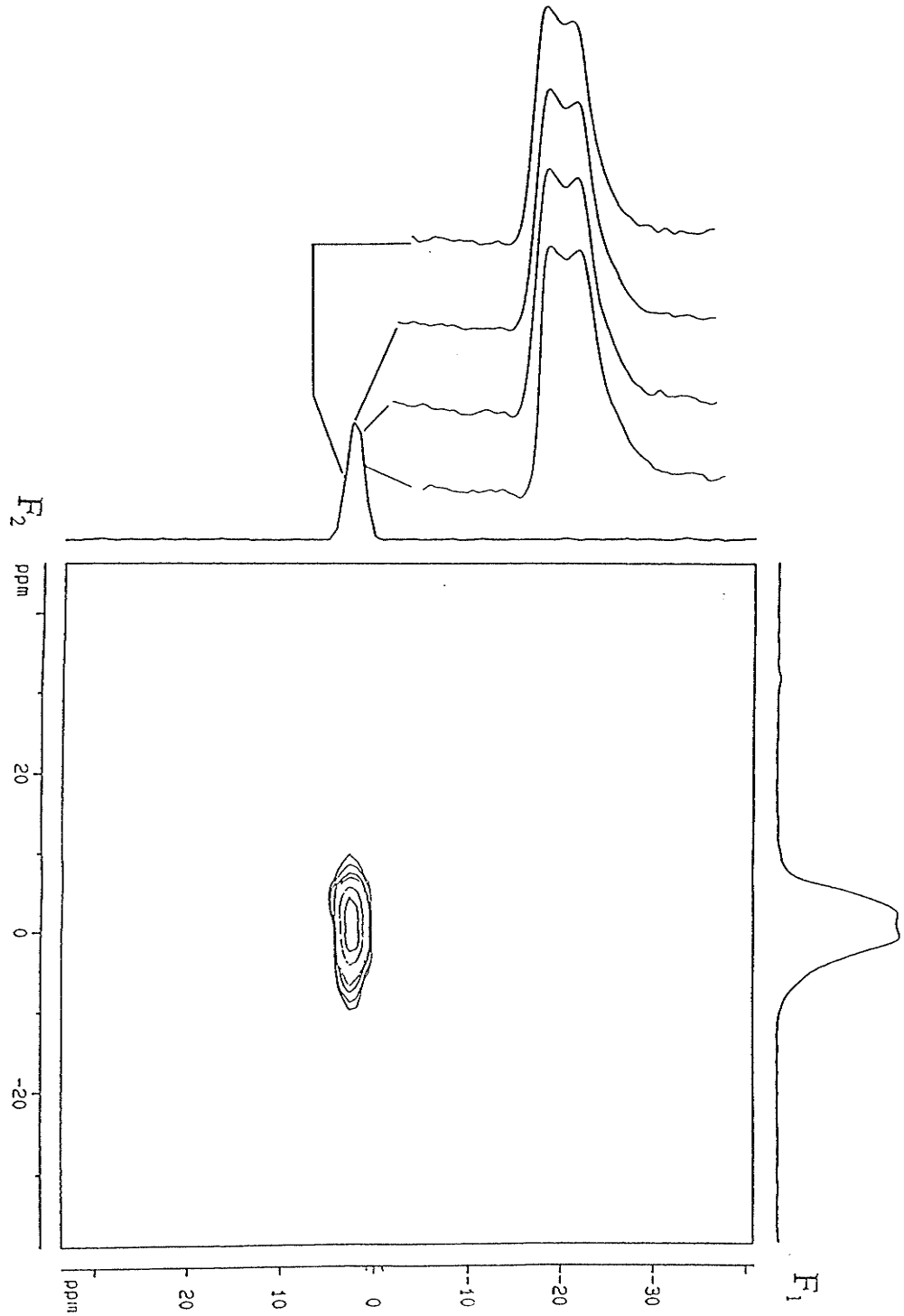

the number of points on F_1 was 256, the difference in frequency between two adjacent points was 78 Hz. There were only four points for the F_1 peak above the half-intensity of the peak. The projection of these four points on F_2 resulted in similar MAS spectra with the same lineshapes but different intensities (Fig. 4. 6). The shape of the peaks was found to be similar to that obtained in MAS experiment (Fig. 4. 5), though the resolution was lower. The computer simulation of these peaks gave the same values of C_Q and η as the MAS experiments. This finding shows that there is only one ^{23}Na site and no distribution of ^{23}Na chemical shift in tugtupite at room temperature.

^{23}Na MAS NMR spectra obtained at -35, -52, -80 and -110°C have exactly the same peak positions, lineshapes and linewidths as those measured at room temperature (Fig. 4. 7). Therefore, there is no phase change affecting the Na site between +25°C and -110°C.

4. 3. 4. ^{27}Al

The width of the ^{27}Al MAS peak at 130.3 MHz was found to be 140 Hz, which is relatively narrow for ^{27}Al in solids, indicating that the Al tetrahedrally coordinated site is very symmetrical, with a small gradient in electric field and, therefore, small ^{27}Al quadrupolar interactions. The structural refinement from single crystal data shows this high symmetry, with four Al-O bond lengths of 1.748(2) Å, four O-Al-O angles of 109.0(1)° and two of 110.5(1)°.[4.2]

There is one peak with two maxima in the ^{27}Al MAS spectra recorded at both

Fig. 4. 7. ^{23}Na low-temperature MAS spectra of tugtupite at:

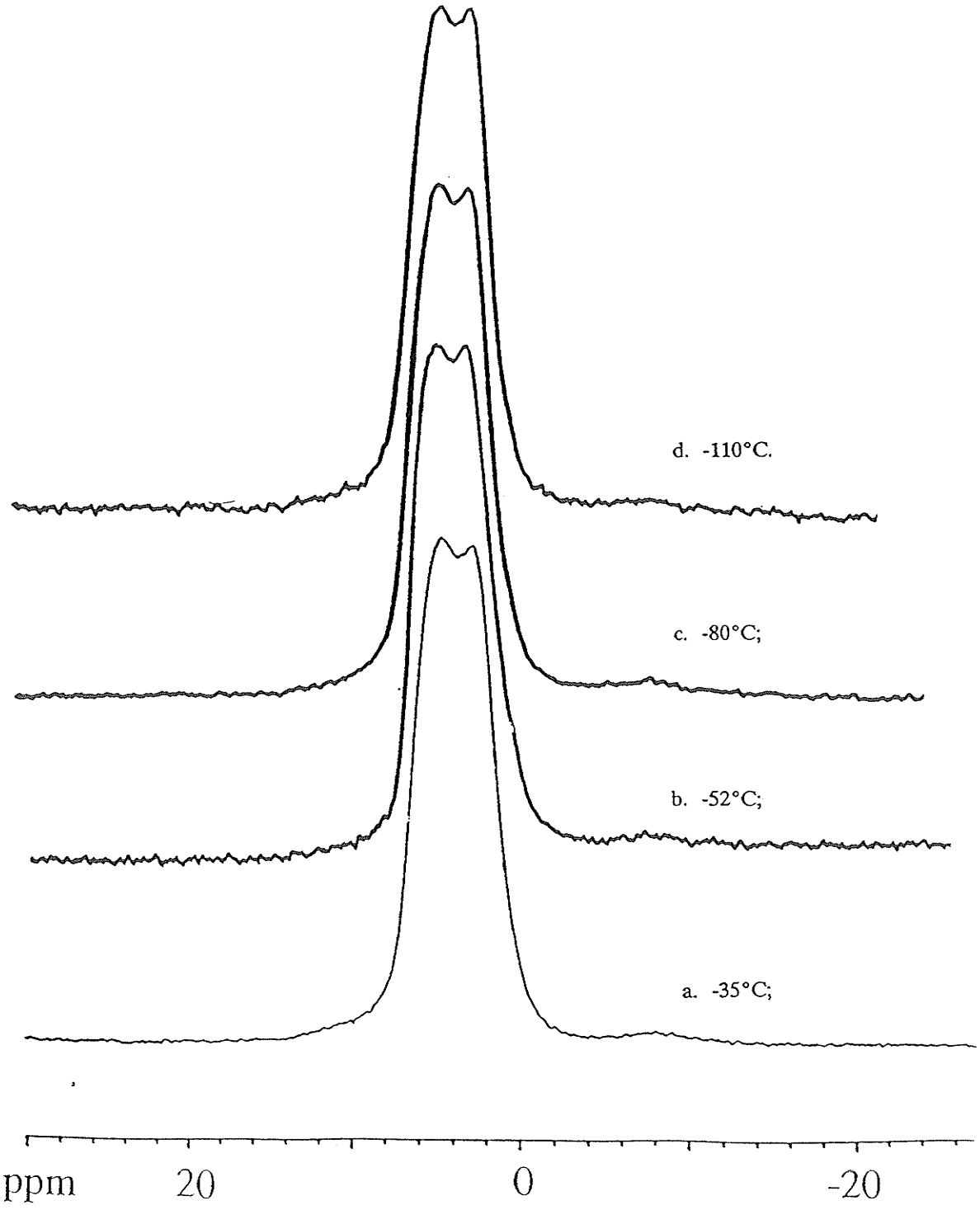

strengths of magnetic field (Table 4. 2, Fig. 4. 8). ^{27}Al DOR was used to determine whether this is due to two Al peaks or to one peak with a quadrupolar lineshape. The DOR spectrum has one symmetrical peak with a width at half maximum of only 43 Hz (line broadening of 10 Hz) (Table 4. 2, Fig. 4. 9), indicating that there is one ^{27}Al environment in tugtupite.

The ratio of the widths of the ^{27}Al MAS peaks at 11.7 T and 8.4 T, is 120 : 170 or 0.73 (Table 4. 2), which is close to the ratio of the strengths of the magnetic fields of 0.72. This indicates that the linewidth is due mainly to the second-order quadrupolar interaction.

The quadrupolar parameters of 1.70 MHz for C_Q and of 0.19 for η were used to simulate the MAS spectra at the two field strengths (Fig. 4. 8). These values were verified by a comparison of the peak positions at the two fields. From equation (4.8) for ^{27}Al with magnetic field strength of 11.7 T and 8.4 T:

$$\Delta\delta_Q = 0.328 \cdot C_Q^2 \cdot (1 + \eta^2/3) \quad \text{ppm} \qquad (4.10)$$

Using values for C_Q of 1.70 MHz and for η of 0.19, $\Delta\delta_Q$ is found to equal 0.96 ppm. This is slightly higher than the measured difference between MAS chemical shifts obtained at the two magnetic field strengths of 0.8 ppm.

For nuclei with spin 5/2, such as ^{27}Al, the values of C_Q and η obtained from a simulation of the MAS spectra can be verified in a second way. The first pair of spinning sidebands can each be resolved into two peaks, due to the sidebands of the central transition and of the inner satellite $\pm 1/2 \Leftrightarrow \pm 3/2$ transitions. For nuclei with a spin of 5/2, these satellite transitions have small second moments and sufficient

Fig. 4. 8. ^{27}Al MAS spectra of tugtupite and simulations.

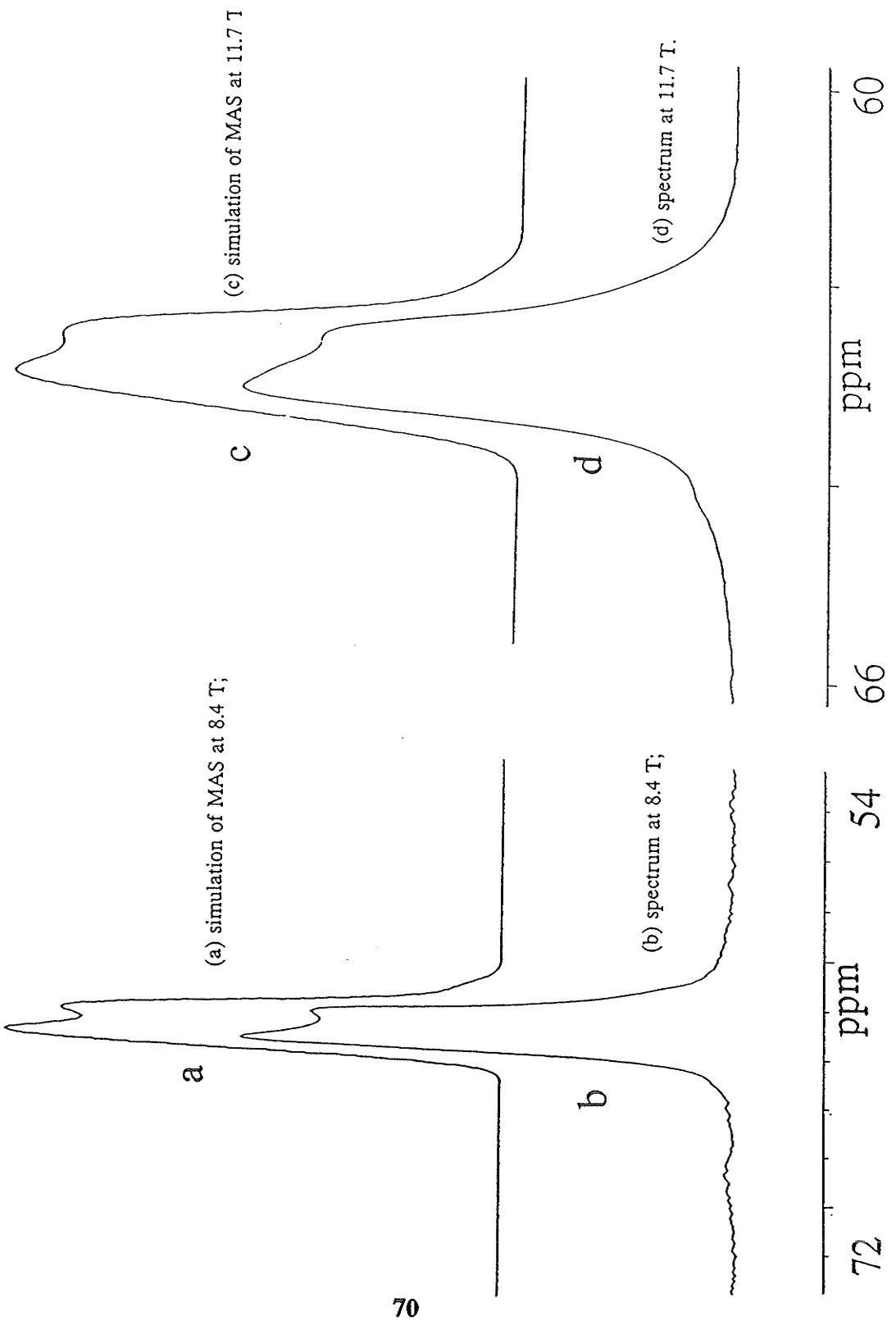

Fig. 4. 9. ^{27}Al DOR spectrum of tugtupite at 8.43 T with outer rotor spinning at 800 Hz.

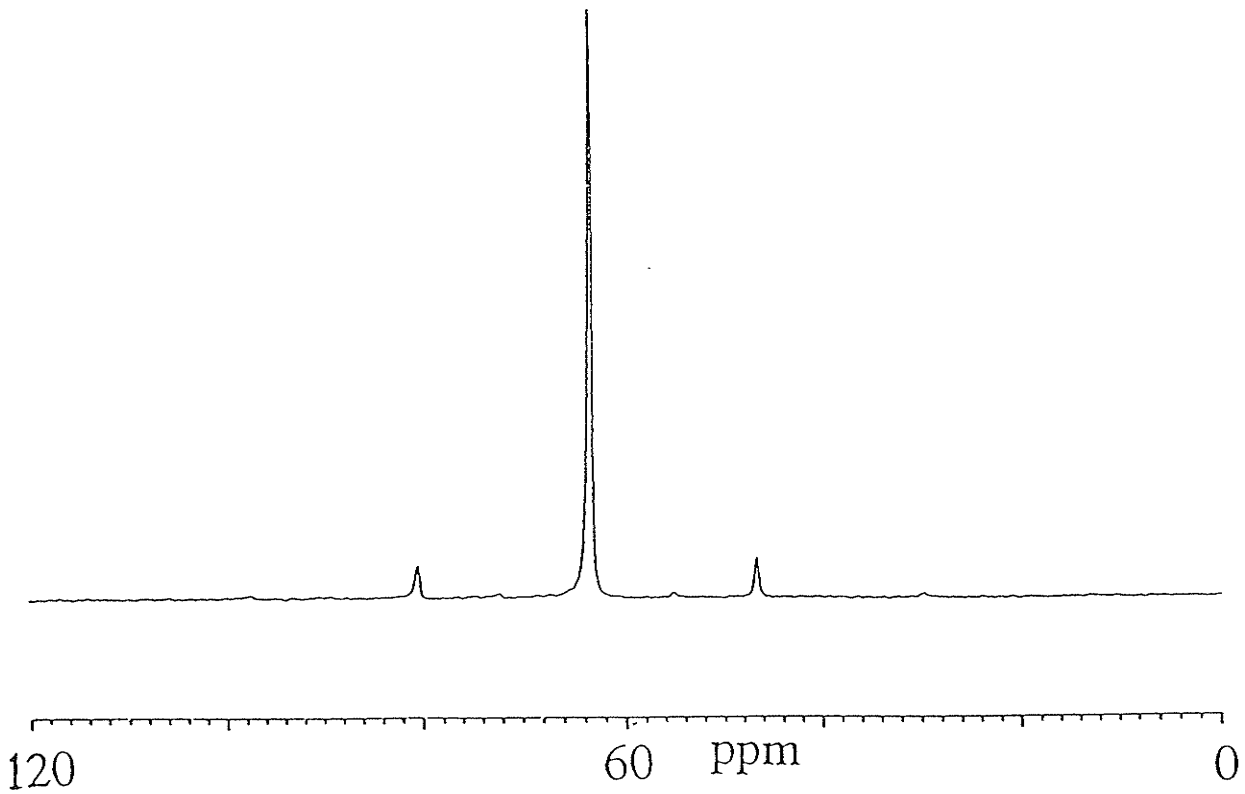

intensity to be observed. For nuclei with spin 3/2, such as ^{23}Na, the intensity of this transition is too small for observation of the sidebands.[4.8] The difference in peak position between $\pm 1/2 \Leftrightarrow \pm 3/2$ and $+1/2 \Leftrightarrow -1/2$ transitions can be measured for the first pair of spinning sidebands. The second-order quadrupolar shift of non-central transitions can be expressed as:

$$\delta_Q = -3 \cdot 10^6 \cdot C_Q^2[I(I+1)-9m(m-1)-3](1+\eta^2/3)/[40 \cdot \nu_0^2 I^2(2I-1)^2] \qquad (4.11)$$

For a nuclear spin I of 5/2, the value of the difference in position between the $\pm 1/2 \Leftrightarrow \pm 3/2$ and the central $-1/2 \Leftrightarrow +1/2$ transition is:

$$\Delta\delta_Q = 27 \cdot 10^3 \cdot C_Q^2(1 + \eta^2/3)/(4 \cdot \nu_0^2) \qquad (4.12)$$

Substitution of the value of 1.70 MHz for C_Q and of 0.19 for η obtained from the simulation of MAS lineshapes gives:

$\Delta\delta_Q = 2.24$ ppm at 8.4 T magnetic field

$\Delta\delta_Q = 1.16$ ppm at 11.7 T magnetic field.

The measured differences were found to be:

$\Delta\delta_{obs} = 2.5 \pm 0.2$ ppm at 8.4 T magnetic field

$\Delta\delta_{obs} = 1.2 \pm 0.2$ ppm at 11.7 T magnetic field.

This verifies that the simulated quadrupolar parameters of ^{27}Al in tugtupite is correct.

4. 4. CONCLUSION

Si is in a single tetrahedrally coordinated site in tugtupite, and there is no Si/Al disorder. Be is in a single extremely symmetrical environment that has no

measurable electric field gradient. There is only one site for both ^{23}Na and ^{27}Al, with no distribution in ^{23}Na chemical shift. For ^{23}Na, δ_{iso} is 6.9 ppm, C_Q is 1.27 MHz and η is 0.48. For ^{27}Al in a symmetrical tetrahedral AlO_4 site, δ_{iso} is 64.2 ppm, C_Q is 1.70 MHz, and η is 0.19. These results were verified by comparison of the calculated and observed differences in chemical shift at two strengths of the magnetic field. There is no phase change involving Na between 23° and -110°C.

MAS is efficient at averaging the broadening due to anisotropy of chemical shift and dipole-dipole interactions. The quadrupolar parameters C_Q and η may be obtained from a computer simulation of the MAS lineshape. Both DOR and DAS techniques are able to reduce the anisotropy due to second-order quadrupolar interactions. DAS provides an additional dimension that enables the simultaneously study of the lineshapes for different sites.

REFERENCE FOR CHAPTER FOUR

[4.1] M. Dano : The crystal structure of tugtupite - a new mineral Acta Crystallogr. **20**, 812-816 (1966).

[4.2] I. Hassan and H. D. Grundy : The crystal structure and thermal expansion of tugtupite Can. Mineral. **29**, 385-390 (1991).

[4.3] A. Samoson and E. Lippmaa : Excitation phenomena and line intensities in high -resolution NMR powder spectra of half-integer quadrupolar nuclei Phys. Rev. B **28**, 6567-6570 (1983).

[4.4] a. K. T. Mueller, B. Q. Sun, C. G. Chingas, J. W. Zwanziger, T. Terao and A. Pines : Dynamic-angle spinning of quadrupolar nuclei J. Magn. Reson. **86**, 470-497 (1990).

b. K. T. Mueller, E. W. Wooten and A. Pines : Pure-absorption-phase dynamic -angle spinning J. Magn. Reson. **92**, 620-627 (1991).

[4.5] W. P. Power, R. E. Wasylishen, S. Mooibroek, B. A. Pettitt and W. Danchura : Simulation of NMR powder line shapes of quadrupolar nuclei with half-integer spin at low-symmetry J. Am. Chem. Soc. **94**, 591-597 (1990).

[4.6] B. L. Sherriff, H. D. Grundy and J. S. Hartman : The relationship between ^{29}Si MAS NMR chemical shift and silicate mineral structure Eur. J. Mineral. **3**, 751-768 (1991).

[4.7] D. Freude, J. Haase, J. Klinowski, T. A. Carpenter and G. Ronikier : NMR line shifts caused by the second-order quadrupolar interaction Chem. Phys. Lett.

119, 365-368 (1985).

[4.8] A. Samoson : Satellite transition high-resolution NMR of quadrupolar nuclei in powders Chem. Phys. Lett. **119**, 29-32 (1985).

CHAPTER FIVE. ^{27}Al DOR NMR STUDY OF THE Al_2SiO5 POLYMORPHS

5 .1. STRUCTURE OF THE Al_2SiO_5 POLYMORPHS

The three alumino-silicate polymorphs kyanite, andalusite and sillimanite (Al_2SiO_5) are used by petrologists to determine the pressure and temperature of formation of rocks, due to their abundance in metamorphic rocks and their well characterized pressure and temperature ranges.[5.1] They are an interesting group of minerals to study using ^{27}Al NMR as they have a variety of Al sites and coordinations.

In kyanite there are four distinct octahedral aluminum sites, each characterized by different average Al-O bond lengths (Table 5 .1).[5.1] There are two different tetrahedral silicon sites, with identical average Si-O bond lengths (Table 5 .1). $Al_{(1)}$ and $Al_{(2)}$ octahedra share edges and form chains parallel to the c-axis. Si tetrahedra and $Al_{(3)}$, $Al_{(4)}$ octahedra cross-link the chains (Fig. 5. 1).[5.2] As the mean Al-O bond distance, the polyhedral volumes and sites energies of the $Al_{(1)}O_6$ and $Al_{(4)}O_6$ octahedra are very similar (Table 5. 1), they may be considered as identical from the point of crystal chemistry. The $Al_{(2)}O_6$ and $Al_{(3)}O_6$ octahedra are also

Table 5.1. Aluminum sites in the Al_2SiO_4 polymorphs. Bond distances are in angstroms.[5.1]

End -member	Andalusite		Sillimanite		Kyanite			
Site	Al1	Al2	Al1	Al2	Al1	Al2	Al3	Al4
C. N.	6	5	6	4	6	6	6	6
Point Sym.	2	m	1	m	1	1	1	1
Distance	1.827	1.816	1.914	1.751	1.874	1.934	1.986	1.816
(O-Al)	1.891	1.840	1.868	1.711	1.884	1.881	1.924	1.998
	2.086	1.899	1.954	1.796	1.971	1.889	1.862	1.846
		1.814			1.987	1.914	1.968	1.911
					1.847	1.930	1.883	1.933
					1.848	1.925	1.885	1.875
Mean O -Al	1.935	1.836	1.912	1.764	1.902	1.913	1.918	1.896
σ	0.121	0.036	0.039	0.041	0.062	0.023	0.050	0.065
Ploy. Vol.	9.539	5.153	9.175	2.791	8.977	9.136	9.164	8.921
Q. E.	1.011	--	1.011	1.006	1.016	1.014	1.018	1.014
Ang. Var.	18.0	--	36.4	20.5	47.7	50.2	57.0	42.5
Site Energy	-2490	-2569	-2573	-2526	-2532	-2563	-2543	-2531

C.N. = coordination number, Mean O-Al = mean cation-oxygen bond distance, σ = standard deviation of mean cation-oxygen bond distance, Poly. Vol. = polyhedral volume, Q.E. = quadratic elongation of polyhedra, Ang. Var. = angular variation of polyhedra. Site Energy is the electrostatic energy (in kcal) for one mole of sites.

Fig. 5. 1. The crystal structure of kyanite (projection along the c-axis).

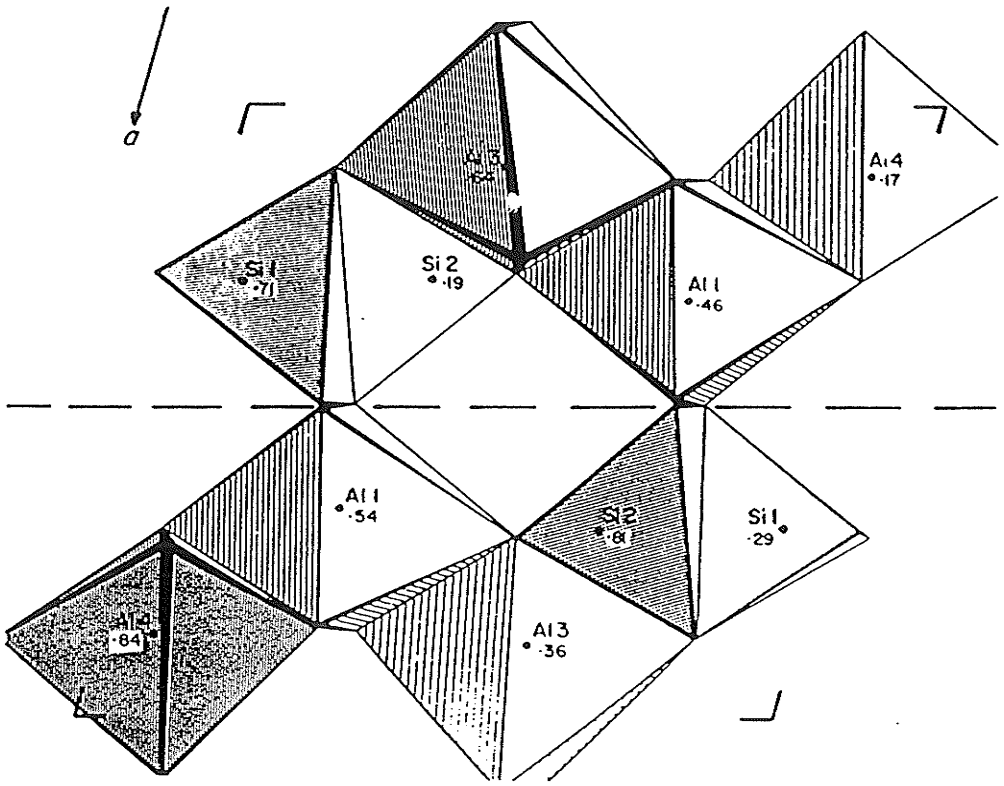

similar (Table 5. 1).

In andalusite, there is one octahedral and one five-coordinated Al site. Andalusite consists of edge-shared chains of AlO_6 octahedra, which are parallel to the c-axis. The chains are cross-linked through SiO_4 tetrahedral and penta-coordinated aluminum (Fig. 5 .2).[5.3] From the Al-O bond lengths in Table 5.1, it can be seen that the octahedra are distorted from ideal O_h symmetry, which will lead to a large electric field gradient at Al nucleus and hence a large quadrupolar interaction for ^{27}Al.

In sillimanite, there are two distinct octahedral Al sites. The structure of sillimanite is similar to that of andalusite: chains of edge-sharing AlO_6 octahedra parallel to the c-axis, which are cross-linked through double chains of tetrahedra containing Si and Al (Fig. 5. 3).[5.4]

The Al_2SiO_5 polymorphs have been extensively studied[5.1] and well characterized crystallographically and by single crystal[5.5] and MAS NMR[5.6][5.7][5.8]. Single crystal ^{27}Al NMR provides the quadrupolar parameters of C_Q and η for all the non-equivalent Al sites. ^{27}Al MAS NMR obtained at a high magnetic field strength can narrow some of the quadrupolar lines enough to resolve separate peaks. However, it is not possible to assign the isotropic chemical shifts of all the non-equivalent sites as MAS can not average all the anisotropies of the second-order quadrupolar interaction. DOR and DAS can be used to solve this problem. For quadrupolar nucleus ^{27}Al in solids, the relaxation time is typically of the order of tens of milliseconds, which is too short for the DAS technique to be used.[5.9][5.10] The

Fig. 5. 2. The crystal structure of andalusite (projection along the a-axis).

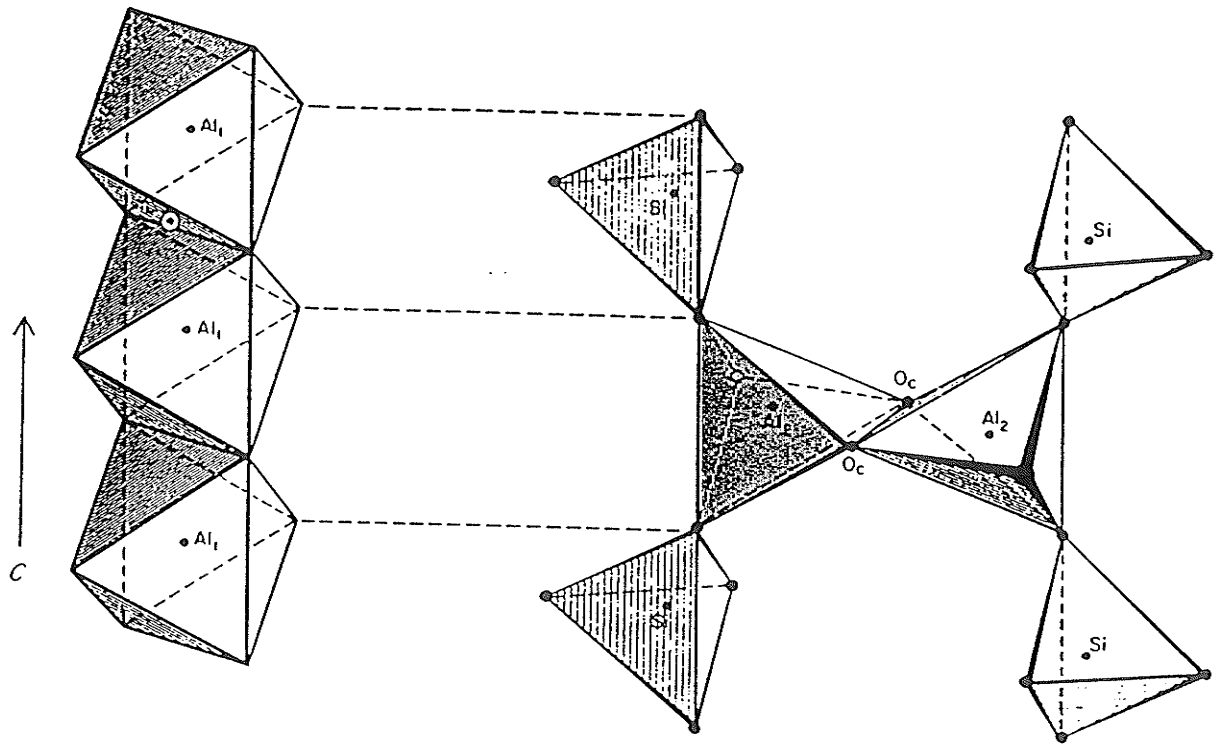

Fig. 5. 3. The crystal structure of sillimanite (projection along the a-axis).

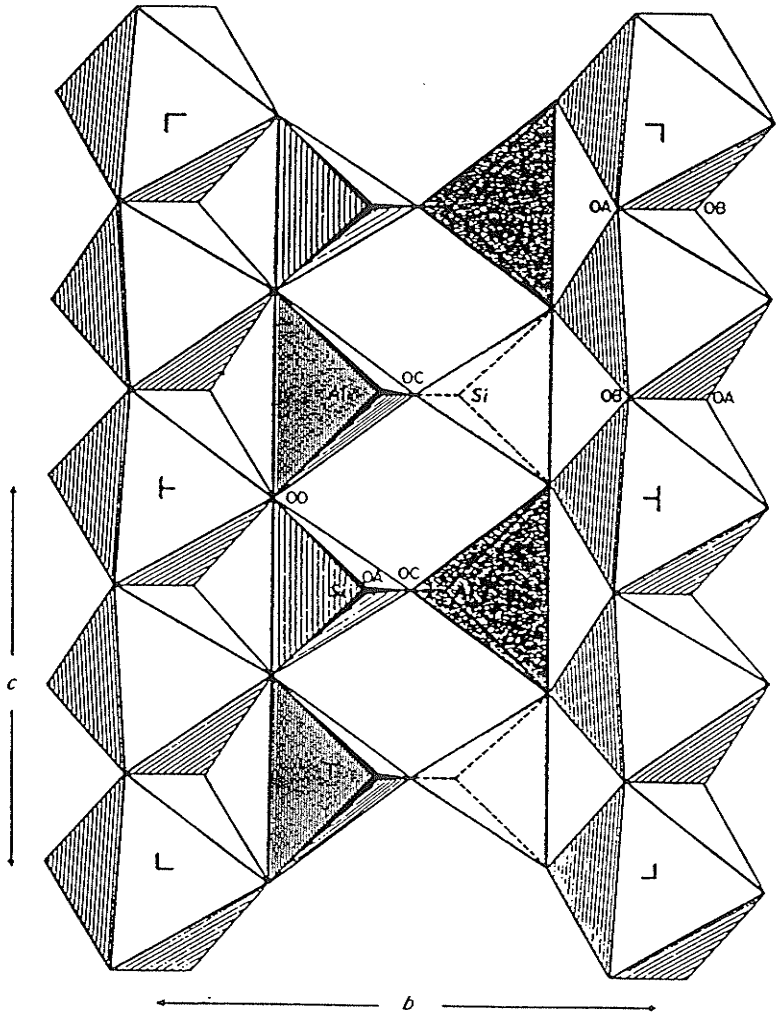

DOR probe does not have such a problem and can be used to obtain high resolution ^{27}Al spectra.

5 .2. EXPERIMENTAL

Samples of the minerals kyanite (E 2912, from Pfitschthal, Tyrol), andalusite (BLS 218, from Minas Geras, Brazil) and sillimanite (BLS 144, from Dillan, Montana) were finely ground prior to carefully packing them into the inner rotor.

The spectra were acquired on a Bruker AMX-500 console with an 8.42 T wide bore magnet. 2 μs pulse lengths were used, as the 90° pulse length measured on 1 M $AlCl_3 \cdot 6H_2O$ aqueous solution was 20 μs. The ^{27}Al spectral reference was 1M $AlCl_3 \cdot 6H_2O$ solution. The FID's were Fourier Transformed with a line broadening of 10 Hz. Peak positions are accurate to $\pm$ 0.1 ppm.

Spectra were acquired at different spinning speeds of the outer rotor to distinguish the outer rotor spinning sidebands from centre bands. The inner rotor spinning speed of between 5 and 7 kHz changes with the outer rotor spinning speed to maintain a stable spinning configuration.[5.11] The spinning sidebands from the inner rotor do not interfere with the centre bands in these spectra, as they are very small and spaced at intervals of over 55 ppm. The outer rotor speeds for the kyanite spectra were 800 Hz, 1000 Hz and 1100 Hz, for sillimanite, 800 Hz, 900 Hz and 1000 Hz and for andalusite, 800 Hz and 1000 Hz. Synchronisation technique removed odd

numbered spinning sidebands.

Equivalent points in two spectra of each mineral acquired at different outer rotor spinning speeds were multiplied together. If the sidebands are narrow and do not overlap in the two spectra, the equivalent points on the sidebands will be multiplied by zero and the spinning sidebands will be eliminated. As the centre bands are present in both spectra, this multiplication will result in their intensity being squared.

5. 3. RESULTS AND DISCUSSION

The measured peak positions in the DOR spectra (δ_{obs}) are the sum of two effects: isotropic chemical shift (δ_{iso}) and isotropic second-order quadrupolar shift (δ_Q).

$$\delta_{obs} = \delta_Q + \delta_{iso}. \tag{5.1}$$

The isotropic second-order quadrupolar shift can be calculated from equation (2.58):

$$\delta_Q = -3[I(I+1)-3/4](1+\eta^2/3)C^2_Q \cdot 10^6/[40I^2(2I-1)^2\nu^2_0] \tag{5.2}$$

where C_Q is the quadrupolar coupling constant in MHz (e^2qQ/h) and η is the quadrupolar asymmetry parameter ($(V_{xx} - V_{yy})/V_{zz}$). For ^{27}Al, I = 5/2 and ν_0 = 93.803 MHz at a magnetic field of 8.42 T, therefore

$$\delta_Q = - 0.6826(1 + \eta^2/3)C^2_Q. \tag{5.3}$$

The C_Q and η values used in equation (5.3) were calculated from single-crystal

NMR studies[5.5] and from simulated spectra fitted to MAS spectra.[5.6] Observed peak positions, quadrupolar parameters and calculated isotropic chemical shifts are shown in Table 5. 2.

By the comparison of DOR spectra of kyanite at three different spinning speeds, it is possible to identify four peaks relating to the four octahedrally coordinated Al sites (Fig. 5 .4). The sidebands move out from the centre bands as the outer rotor spinning speed increases and only the peaks at -6.5, -25.3, -51.7 and -56.2 ppm remain static. Another way to distinguish the four centre bands is to multiply together the spectra acquired with outer rotor spinning speeds of 800 Hz and 1100 Hz (Fig. 5 .5).

Two peaks at 31.7 ppm and -51.6 ppm relating to the tetrahedrally and octahedrally coordinated Al sites respectively, are found in the spectrum of sillimanite (Fig. 5. 6). For andalusite only one peak at 9.6 ppm due to the five-coordinate Al can be found (Fig. 5 .7). The quadrupolar coupling constant of the octahedrally coordinated site is too large, at 15.5 MHz, to be resolved by the DOR technique with the present spinning speed capability.

Several factors need to be considered in the interpretation of the relative intensity of different peaks in DOR NMR spectra. One factor is the excitation of satellites. For nuclei with non-integral spins only the central transitions ($-1/2 \rightarrow +1/2$) are not affected by the first-order quadrupolar interactions and can be used to study the relative population of different sites. According to the NMR nutation study by Samoson et al.[5.12] a small flip angle of the magnetization will suppress the

Table 5. 2. Isotropic chemical shifts (δ_{iso}), quadrupolar coupling constants (C_Q) and asymmetry parameters (η) for Al sites of kyanite, sillimanite and andalusite.

	C_Q(MHz)	η	δ_{iso}(ppm)	δ_Q*(ppm)	δ_{obs}(ppm)	δ_{iso}(ppm)
kyanite						
octahedral	3.70[b]	0.89[b]	5.0[b]	-11.81	-6.5	5.3
octahedral	6.53[b]	0.59[b]	7.5[b]	-32.48	-25.3	7.2
octahedral	9.37[b]	0.38[b]	13[a]	-62.81	-51.7	11.1
octahedral	10.04[b]	0.27[b]	15[a]	-70.48	-56.2	14.3
sillimanite						
tetrahedral	6.77[b]	0.532[b]	64.5[b]	-34.24	31.7	65.9
octahedral	8.93[b]	0.462[b]	4.0[b]	-58.31	-51.6	6.7
andalusite						
5-coordinate	5.73[a]	0.7[a]	35[a]	-26.0	79.6	35.7
octahedral	15.5[a]	0.0[a]	10[a]	-164.00		

a:from Raymond, M. Phys. Rev. B. 3, 3692 (1971) [5.5].

b: from Alemany, L.B. et al. Chem. Phys. Lett. 177, 301 (1991) [5.6].

*:calculated

Fig. 5. 4. DOR NMR spectra of kyanite. Centre bands are labelled with arrows.

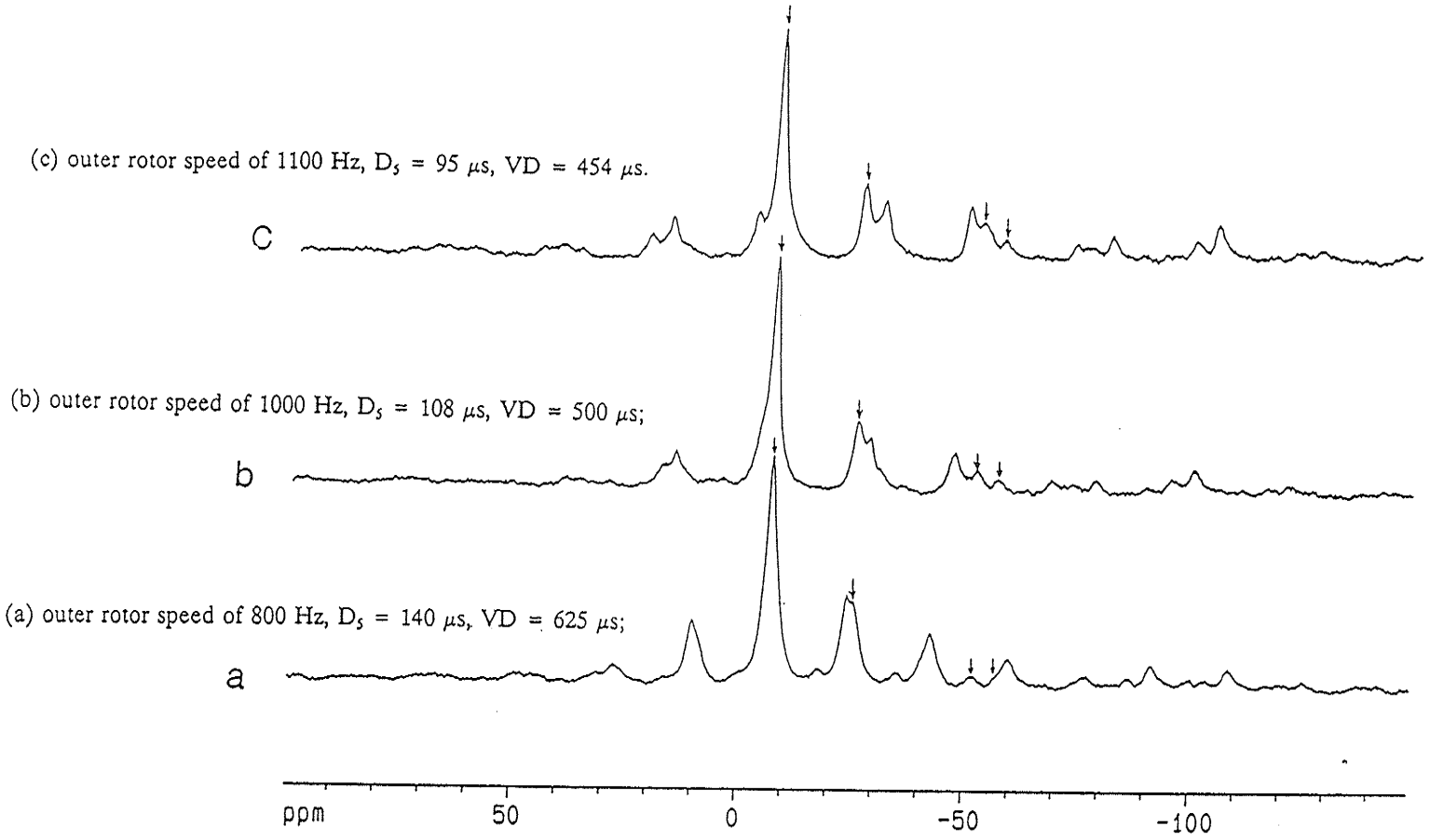

Fig. 5. 5. The results of the multiplication of DOR NMR spectra of kyanite with outer rotor spinning speeds of 800 Hz and 1100 Hz.

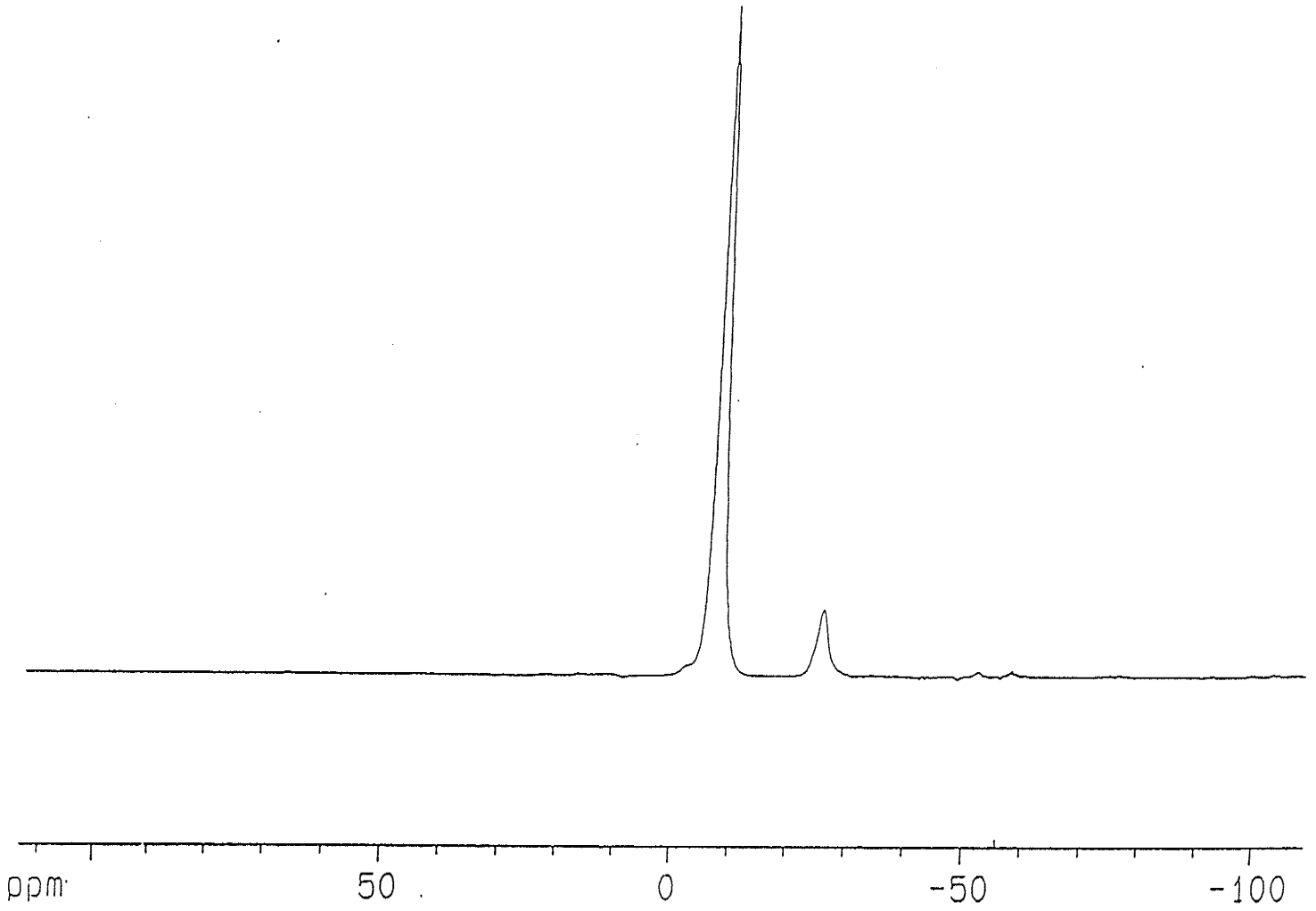

Fig. 5. 6. DOR NMR spectra of sillimanite. Centre bands are labelled with arrows.

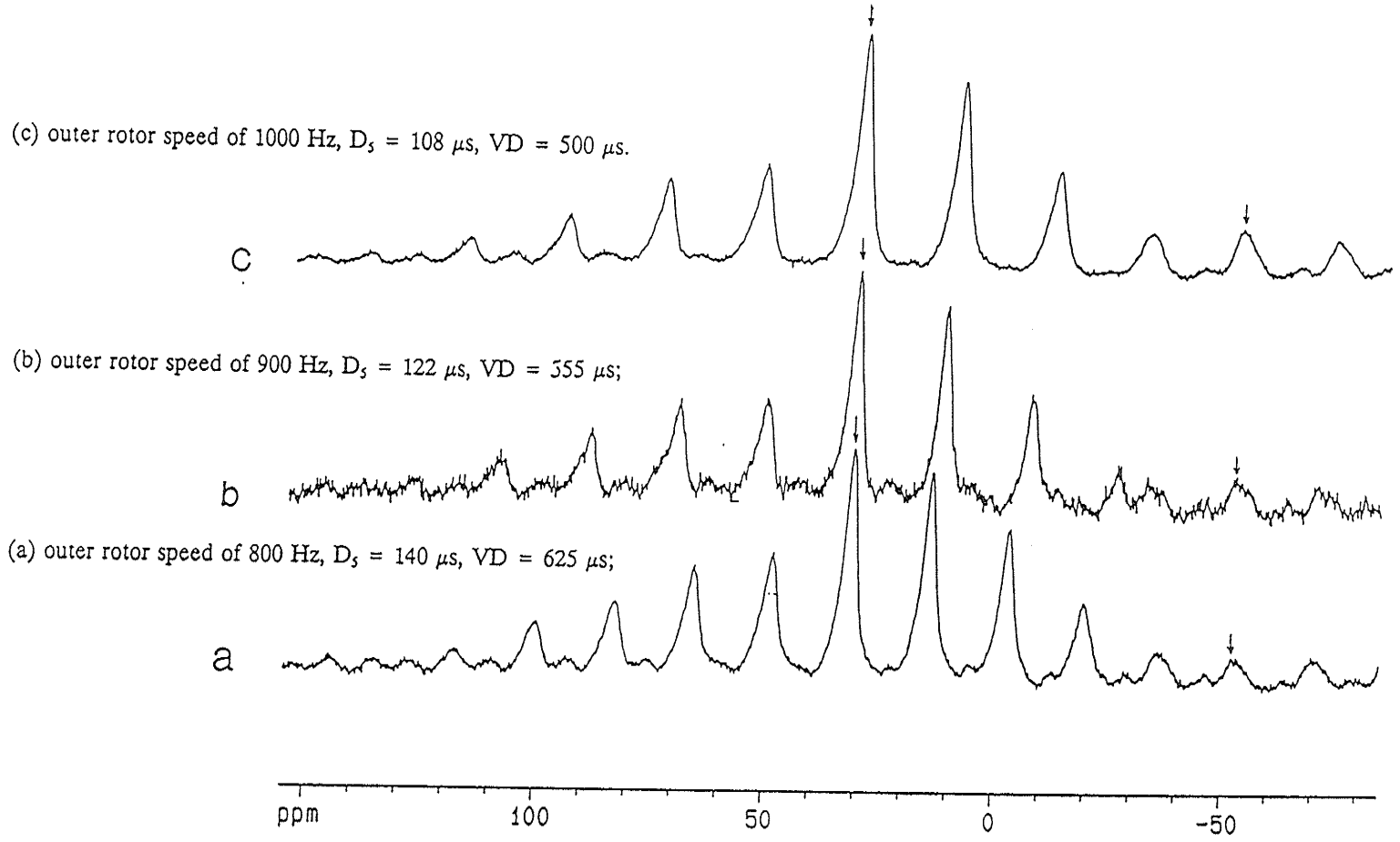

Fig. 5. 7. DOR NMR spectra of andalusite. The centre band is labelled with an arrow.

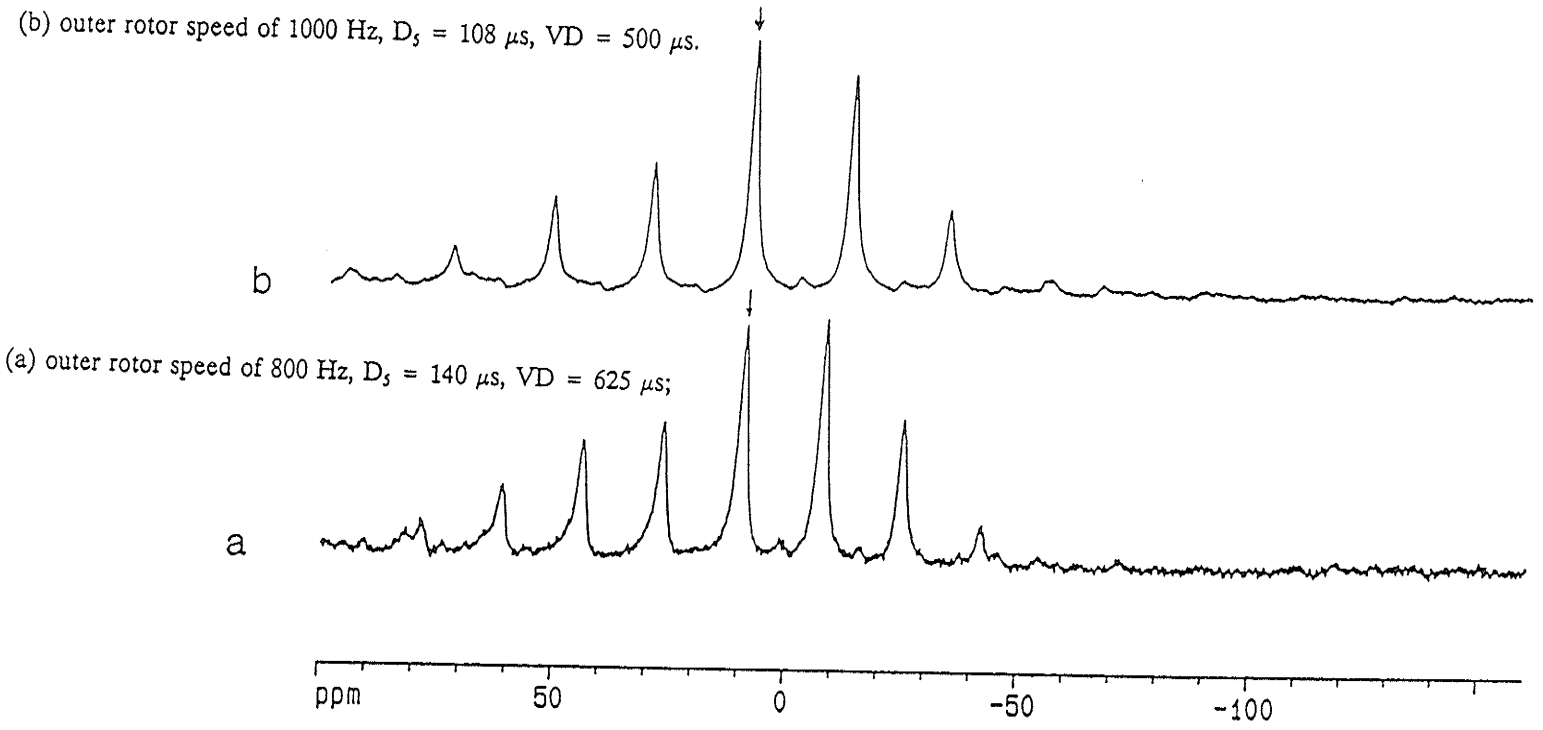

excitation of satellites. In our experiments the pulse length of 2 μs should allow less than five percent of the satellite non-central transitions to contribute to the central transition.

Al sites have different symmetries and distortions and hence different quadrupolar coupling constants and asymmetry parameters. As the dominant relaxation mechanism is quadrupolar interaction, this can lead to different spin lattice relaxation times for individual sites in a mineral. By using a small flip angle and a relatively long time delay (D_1 = 1 s) between pulses,[5.9] complete relaxation of all sites is allowed and this effect should be minimized in our experiments.

Other factors to be considered in the interpretation of relative peak intensity and broadening are chemical shift anisotropy (CSA), dipole-dipole, quadrupolar-dipole and quadrupolar interactions. For ^{27}Al in alumino-silicate minerals the quadrupolar interactions have the largest effect on line broadening, as dipole-dipole, quadrupolar-dipole interactions and CSA are relatively small.[5.6] However, the low spinning speed of outer rotor, which is less than 1.1 kHz at the Magic Angle, makes it difficult to reduce all of the non-quadrupolar interactions to isotropic values. This inefficiency of averaging CSA results in a large number of outer rotor spinning sidebands. For sillimanite (Fig. 5 .6) and andalusite (Fig. 5 .7) the large CSA of ^{27}Al in both sites gives rise to intense spinning sidebands. With the increase of DOR outer rotor spinning speeds, more intensity goes into the centre bands and the intensity ratio between the centre bands and sidebands becomes larger.

The remaining broadening and low intensity of peaks could be related to short

transverse relaxation times (T_2). When T_2 is of comparable length to the delay (D_3) for the ring-down of the probe, much of the signal may be lost before acquisition of the FID. Therefore the sites with larger quadrupolar coupling constants will produce wider peaks and smaller relative intensities. This could be one reason for the irregularly coordinated AlO_6 site in andalusite not being observed. Also the quadrupolar coupling constant for the octahedral site in andalusite might be so large (15.5 MHz) that quadrupolar interactions higher than second-order have to be considered. Thus, DOR may not be sufficient to resolve the peak.

The spectra of kyanite have narrower peaks and also a lower number and intensity of spinning side bands than those of sillimanite and andalusite. The kyanite spectrum, with an outer rotor spinning speed of 1100 Hz, was used to study the intensities of different Al sites. In kyanite there are four octahedral sites with the equal Al occupancies[5.2] which should theoretically give peaks of equal intensities. The relationship between the relative intensities of the four ^{27}Al peaks and quadrupolar coupling constants was investigated. A plot of relative intensities of the central isotropic lines (not including the sidebands) (I) against C_Q in MHz for kyanite can be fitted to the exponential curve using a least-square method, with standard deviation of 0.02 (Fig. 5 .8):

$$I = 3.57 \exp(-0.352C_Q) \qquad (5.4)$$

For sillimanite the centre band intensity of ^{27}Al peaks is again greater for the site with the smaller quadrupolar coupling constant. The difference in signal intensity in kyanite and sillimanite is therefore mathematically related to the quadrupolar

Fig. 5. 8. A plot of the relative intensities (I) of the four ^{27}Al peaks in kyanite against the quadrupolar coupling constants (C_Q) in MHz.

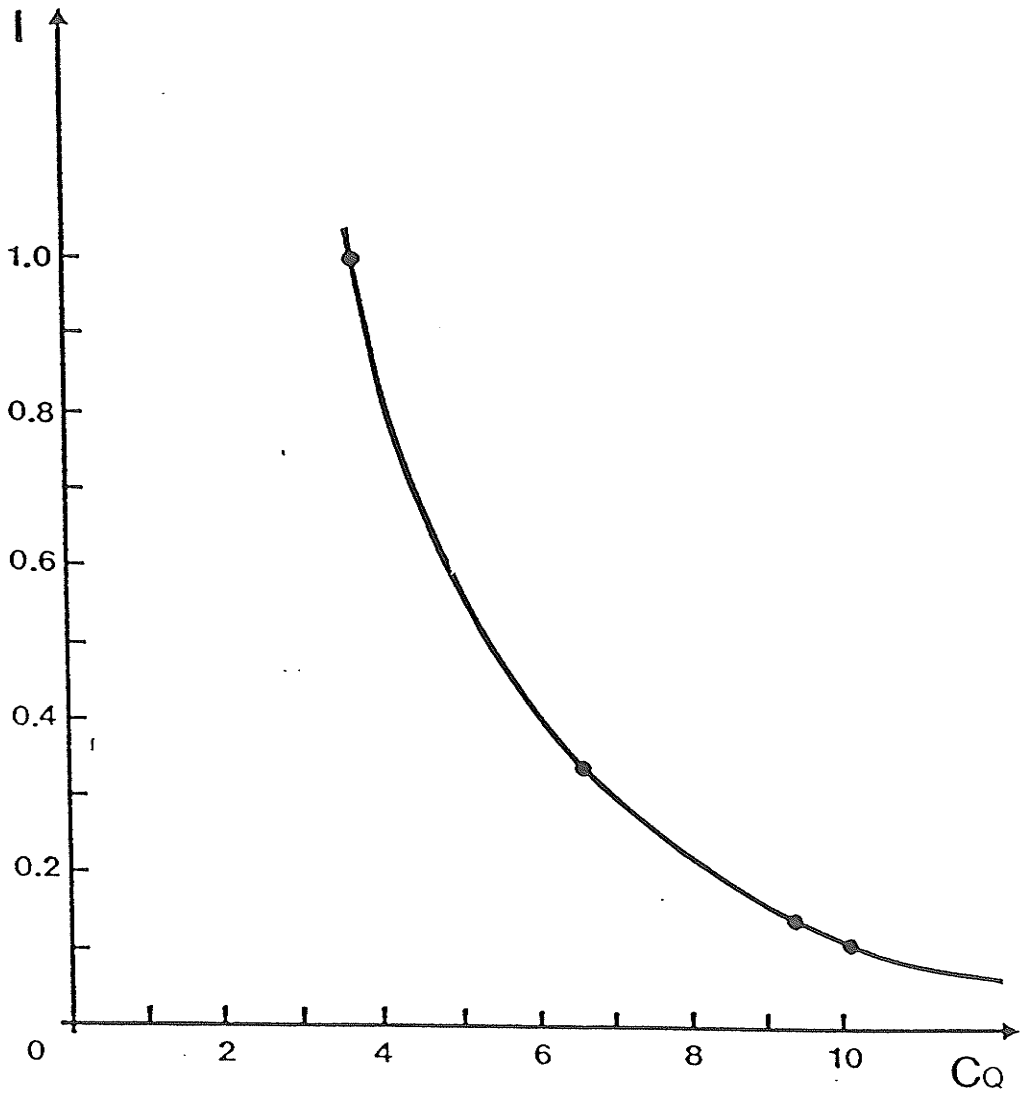

coupling constants of the sites.

5. 4. CONCLUSION

DOR techniques allow the resolution of four peaks in the ^{27}Al spectrum of kyanite due to the four octahedrally coordinated sites and of the two peaks relating to the octahedrally and tetrahedrally coordinated sites in sillimanite. In andalusite only the peak due to the five-coordinate site could be determined as the C_Q for the irregular octahedrally coordinated site is too large for the present technology of the DOR probe to resolve. Isotropic chemical shifts are calculated from quadrupolar parameters obtained from single crystal NMR and from the peak positions in the DOR spectra. The relative intensities of the peaks in the kyanite spectrum have an exponential relationship with the quadrupolar coupling constants.

REFERENCE FOR CHAPTER FIVE

[5.1] D. K. Kerrick : Reviews in Mineralogy. 22: The Al_2SiO_5 Polymorphs Mineral. Soc. Amer. (1990).

[5.2] C. W. Burnham : Refinement of the crystal structure of kyanite. Z. Kristallogr. **118**, 337 (1963).

[5.3] C. W. Burnham, M. J. Buerger : Refinement of the crystal structure of andalusite. Z. Kristallogr. **115**, 269 (1961).

[5.4] C. W. Burnham : Refinement of the crystal structure of sillimanite. Z. Kristallogr. **118**, 127 (1963).

[5.5] M. Raymond : Electric-field-gradient calculations in the aluminum silicates (Al_2SiO_5). Phys. Rev. B. **3**, 3692 (1971).

[5.6] L. B. Alemany, B. Massiot, B. L. Sherriff, M. E. Smith, F. Taulelle : Observation and accurate quantification of ^{27}Al MAS NMR spectra of some Al_2SiO_5 polymorphs Chem. Phys. Lett. **177**, 301 (1991).

[5.7] B. L. William (Sherriff): An investigation of the application of ^{29}Si MAS NMR in geology MSc thesis, Brock University, St Catharines, Ontario (1984).

[5.8] J. S. Hartman and B. L. Sherriff : ^{29}Si MAS NMR of the Aluminosilicate mineral kyanite: residual dipolar coupling to ^{27}Al and non-exponential spin -lattice relaxation J. Phys. Chem. **95**, 7575 (1991).

[5.9] J. Haase, H. Pfeifer, W. Oehme, J. Klinowski : Longitudinal NMR relaxation of ^{27}Al nuclei zeolites J. Chem. Phys. **150**, 189 (1988).

[5.10] K. T. Mueller, B. Q. Sun, C. G. Chingas, J. W. Zwanziger, T. Terao and A. Pines: Dynamic-angle spinning of quadrupolar nuclei J. Magn. Reson. **86**, 470 (1990).

[5.11] Y. Wu, B. Q. Sun, A. Pines : NMR with a new double rotor J. Magn. Reson. **89**, 297 (1990).

[5.12] A. Samoson, E. Lippmaa : Excitation phenomena and line intensities in high -resolution NMR powder spectra of half-integer quadrupolar nuclei Phys. Rev. B. **28**, 6567 (1983).

CHAPTER SIX. NMR STUDY ON QUADRUPOLAR NUCLEI IN THE SCAPOLITE MINERALS

6. 1. INTRODUCTION

Scapolites are framework aluminosilicates with tetragonal symmetry and a widespread geological occurrence.[6.1] They can be regarded as a solid solution between marialite (Ma), $Na_4Al_3Si_9O_{24}Cl$, and meionite (Me), $Ca_4Al_6Si_6O_{24}CO_3$.[6.1][6.2] Another known end-member is $Ca_4Al_6Si_6O_{24}SO_4$.[6.3][6.4] In this thesis only the scapolites within the Ma-Me solid solution series are studied. At compositions between these two end members scapolite is structurally complex. The general formula is established as $M_4T_{12}O_{24}\cdot A$,[6.5] where M = Na^+, Ca^{2+}, K^+ or Mg^{2+}, T = Si^{4+}, Al^{3+}, Fe^{3+} , and A = Cl^-, CO_3^{2-} or SO_4^{2-} anions plus OH^-.[6.1]

The main substitution is believed to be $Na^+ + Si^{4+} \leftrightarrow Ca^{2+} + Al^{3+}$ across the series. Shaw et al. [6.1] used percentage of meionite, % Me = $100\cdot Ca/(Na+Ca)$, as the chemical index to indicate the chemical compositions of scapolites.[6.1][6.6] Between 0 and 75% meionite, the substitution is between $Ca_3Al_2CO_3$ and Na_3Si_2Cl, but from 75% to 100% Me, it only involves CaAl and NaSi.[6.7] Ambiguities arise when only Me content is used as a composition index. At high Me content there is

Al deficiency, which means that the measured Al/Si ratio is smaller than that calculated from the theoretical solid solution. Also, the role of the hydrogens, present in scapolites, is not clear in the structure, as to whether they are present as (or in) cations, anions or molecules. Therefore, the calculation of Me content is not reliable. The problem is further complicated by the fact that samples with similar composition but different conditions of formation, may have structural differences. Samples from the same locality also showed up to 40% difference in Al/Si ratio when analyzed by separate groups. For example, sample MONT from Pianura, Monte Somma Vesuvius, has been analyzed by many groups. The Al/Si ratio of one sample worked on by Scherillo is 1.48 [6.8] while the Al/Si ratio of another sample from the same locality analyzed by Evans et al. is 1.09.[6.2] The same thing happens with sample ON8.[6.9][6.1a] For our study here, the samples are from the McMaster University and they have been carefully prepared and analyzed.

In terms of crystal structure, scapolites are interesting because of the presence of five-membered rings (Fig. 6. 2). The "unstable Al-O-Al linkage" [6.4] will form in scapolites with compositions greater than 37.5% Me and it is found that this "Al-linkage avoidance rule" is not the main factor to determine the crystal chemistry of scapolites. Also the unusual structural aspects, such as disordering of Al/Si framework and carbonate group in the voids and its effects on the crystal symmetry, has attracted the attention of many researchers.

Many techniques have been applied to analyze the scapolite minerals, including X-ray diffraction, wet chemistry, infrared spectroscopy, electron microprobe,

isotope composition[6.10], ion probe analysis[6.11], high-resolution transmission-electron microprobe[6.12], electron paramagnetic resonance (EPR)[6.13], MAS NMR[6.14]. Each technique has its own advantage and each provides complementary pieces of information. NMR can be used to observe directly the ordering of the Al/Si framework cations, alkali cations and anions.

The former NMR study by Sherriff et. al is based the fitting of some ^{29}Si MAS NMR and an ordering model has been established based mainly on this.[6.14] As the resolution of MAS NMR of ^{23}Na and ^{27}Al is low for scapolites, these spectra did not supply much additional information. In this study the new technique of DOR NMR is used to restudy ^{23}Na and ^{27}Al. Also the proton contents of ten samples are analyzed and ^{1}H NMR spectra obtained.

6. 2. THE CRYSTAL STRUCTURE OF SCAPOLITE

The first structure models of scapolite were reported by Pauling in 1930.[6.15] In the mid-1960's the structures of a Na-rich (19.4% meionite) and a Ca-rich (70.1% meionite) scapolite were refined in the space group of I4/m by Papike et al.[6.16][6.17] The space group of scapolite is a function of composition. In the early 1970's, Lin and Burley reported three additional structural refinements (21.3% Me, 52% Me and 93% Me) using the space group of $P4_2/n$.[6.18][6.19] Ulbrich also used this space group for a 93% Me scapolite .[6.20]

In these space groups there are three tetrahedral sites (T_1, T_2, T_3) among which Si and Al may be distributed. Each T cation is surrounded by four atoms of oxygen in tetrahedral coordination. The tetrahedral sites form two kinds of four-membered rings perpendicular to the c-axis: one only contain T_1 tetrahedra and the other alternating T_2 and T_3 sites. The four-membered rings also form two distinct types of oval-shaped channels parallel to the c-axis: the first of which contains either Na^+ or Ca^{2+} cations while the second contains the anions, such as CO_3^{2-}, Cl^- (Fig. 6. 1.). Viewed along the a-axis, a five-membered ring consisting of two T_2, two T_3 and one T_1 tetrahedra is presented (Fig. 6. 2). The T_2 and T_3 sites are geometrically identical in the I4/m space group and their positions are slight different in the $P4_2/n$ space group. From the view point of NMR environments, they are also magnetically equivalent.

Theoretically, the end-member, meionite, contains 50% Al and 50% Si atoms. Half of the five-membered rings must contain three Al and two Si tetrahedra, and half contain two Al and three Si tetrahedra. In the former case, one oxygen must connect two Al atoms and form an "Al-O-Al" linkage, which breaks Lowenstein's rule.[6.21] Actually, the Al-O-Al linkage is inevitable when [Al]/([Al] + [Si]) > 5/12.[6.22]

Al-Si ordering structure of the whole series have been presented by Lin and Burley[6.7]. Their models are mainly inferred from the Si-O bond lengths of T_1,T_2 and T_3 sites of single crystal X-ray diffraction refinement. According to their models, Al-Si has perfect ordering at 37% Me content. The Si/Al ratio is 2 : 1 and Al are

Fig. 6. 1. The structure of scapolite viewed along c-axis.[6.14]

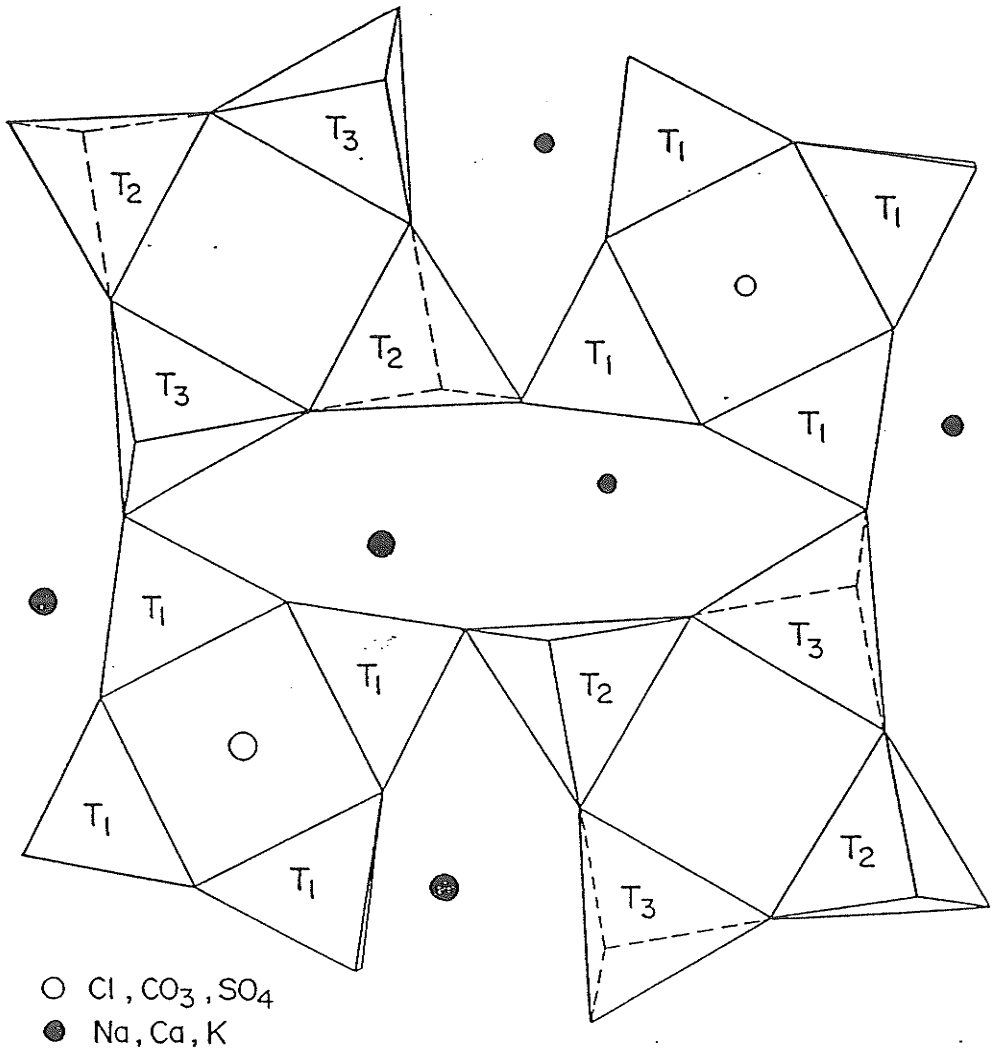

Fig. 6. 2. The structure of scapolite viewed along a-axis.[6.14]

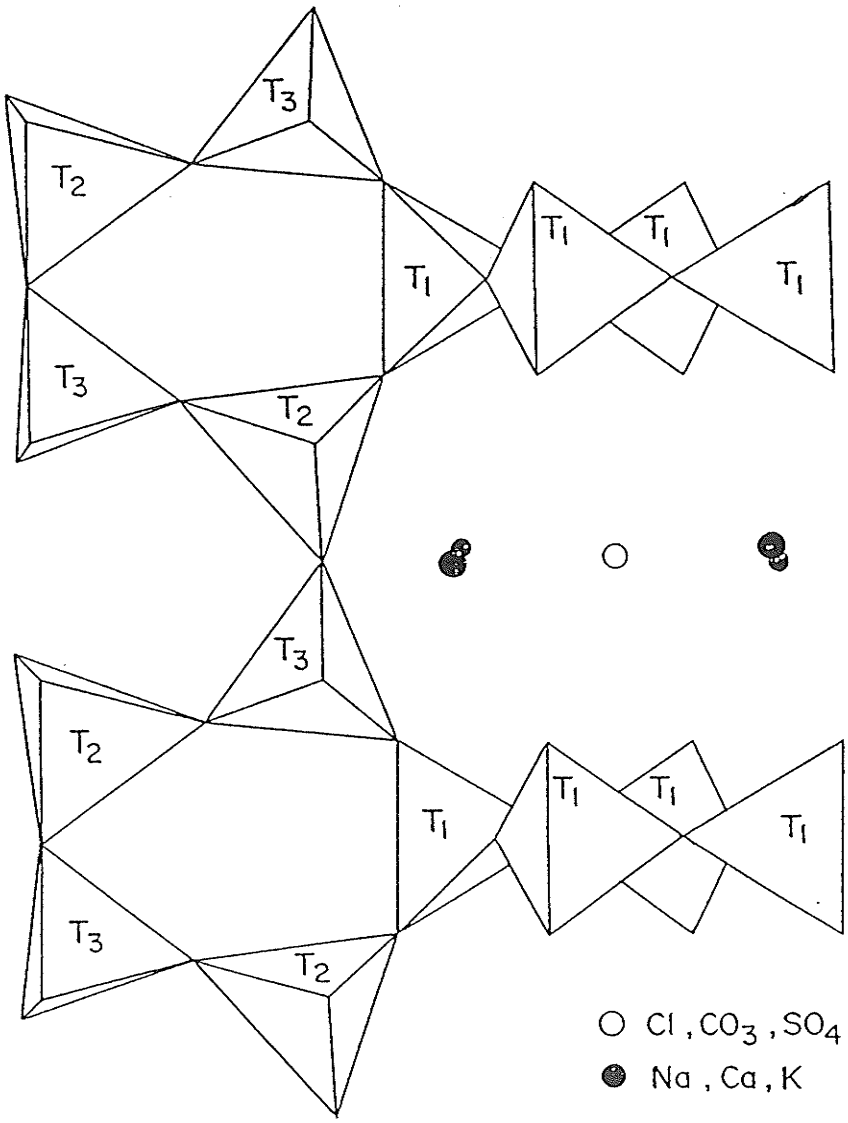

only in T_2 sites while T_1 and T_3 sites contain only Si. With smaller Me content (<37% Me), T_1 contains only Si, while Al and Si are disordered between T_2 and T_3. When Me content is higher than 37%, Al and Si are randomly distributed in all these T sites. For the end-member meionite, there are equal amount of Al and Si in all these three T sites.

6. 3. EXPERIMENTAL

6. 3. 1. Powder X-ray Diffraction Analysis

A series of powdered scapolite samples with compositions between 21.3% and 91.0% Me, covering the entire range of naturally occurring compositions, were used for this study (Table 6. 1). As scapolite is very difficult to separate from associated minerals, such as quartz, calcite, nepheline, alkali feldspar and plagioclase,[6.1] powder X-ray diffraction was done to check the purity of the samples. A SIEMENS Automated Powder Diffractometer System D5000, which is capable of filtering out the Cu $K\alpha_2$ line, line was used for the analysis ($K\alpha_1$ λ = 1.5406 Å). A slow scan of 0.02° per second in the 2θ range of 20 to 29° was used with a generator setting of 40 kV and 35 mA. The 2θ scan range was chosen to just cover the non-overlapping strong reflection peaks of nepheline, scapolite, feldspar, sodalite and NaCl in order to have good enough resolution to identify them. The results were compared with the published powder patterns of these minerals.

6. 3. 2. Water Content Measurement

Table 6. 1.

Scapolite samples used for NMR analysis[6.14]

Sample#	%Meionite	Rock Type	Locality	
ON8	21.3	syenite pegmatite	Gooderham, Glamorgan Twp. Ont.	*
TANZ	29.5	hbl.px.granulite	Morongoro, Tanzania.	**
ON7	33.3	calcareous gneiss	Monmouth Twp, Ontario.	*
GL	34.1	marble	Gib Lake, Pontiac Twp, Ontario	*
ON70	39.5	-	MpWapwa, Tanzania.	*
CA63A	44.5	Pegmatitic skarn	Grand Calumet Twp., Quebec.	*
MAD	45.2	-	Madagascar.	**
Q26	48.2	Pegmatitic skarn	Clapham Twp, Quebec	*
Q13	51.3	Px. gneiss	Huddersfield Twp.,Ontario	*
MIN	56.8	Skarn	Minden, Ontario.	**
ON27	59.3	Pegmatitic skarn	Olmsteadville, New York, U.S.A	*
Q85	65.2	Pegmatitic skarn	Huddersfield Twp., Quebec	*
BOLT	69.5	Marble pegmatite	Bolton, Mass., U.S.A.	**
ON47	79.6	Calc.silicate schist	Slyudyanka, Siberia, U.S.S.R	*
MONT	91.0	Vugs in limestone	Mount Vesuvius, Naples, Italy	**

* Donated by D. M. Shaw, McMaster University.
Chemical analyses from Evans et al. 1969.
Localities from Shaw 1960a

** Donated by D Moecher, University of Michigan.
Analyses from D Moecher (personal communication).

The water content of scapolite samples were measured with the Mitsubishi moisturemeter Model CA-06. About 100 mg of powder samples, contained in an open tube, were placed in an oven at 200°C for two days to drive off the surface water. During the measurements, the sample is heated in a furnace at 900°C so that water and hydroxyl could be driven out in less than 30 minutes. The water from the sample reacts with iodine which is generated electrolytically:

$$I_2 + SO_2 + H_2O \longleftrightarrow 2HI + SO_3$$

By measuring the electricity consumed in the reaction, the amount of iodine generated is known and therefore the water released from the sample can be calculated.

Water background was measured and calibrated between each three measurements. A standard sample was checked before and after all measurements, which showed the precision of the water measurement to be better than 5% (Table 6. 2).

6. 3. 3. NMR experiments

MAS spectra were acquired for ^{23}Na and ^{27}Al for all the samples at both the magnetic fields of 8.4 T and 11.7 T. The delay between pulses was 0.5 s and pulse lengths were 1 μs. Three thousand FID's were acquired for MAS experiments and the rotor spinning speeds were all about 7 kHz. ^{23}Na and ^{27}Al DOR spectra were acquired at 8.4 T for all the samples with outer rotor spinning speeds of 700 Hz and 800 Hz. The synchronization pulse technique was used to remove the odd number spinning sidebands (see Chapter Three). The circuit delays for 700 Hz and 800 Hz

Table 6. 2. Proton weight percentages in scapolites.

sample	Me%	sample weight (mg)	water weight (ug)	proton weight (ug)	proton weight concentration (100%)
TANZ	29.5	50.2	72.2	8.0	0.016
ON7	33.3	97.9	309.7	34.4	0.035
GL	34.1	93.0	328.9	36.5	0.039
ON70	39.5	93.6	98.9	11.0	0.012
CA63A	44.5	98.6	192.8	21.4	0.022
MAD	45.2	80.0	114.1	12.7	0.016
Q26	48.2	92.8	206.8	23.0	0.025
Q13	51.3	97.5	220.7	24.5	0.025
MIN	56.8	98.0	177.6	19.7	0.020
ON47	79.6	94.7	243.4	27.0	0.029

Checking with standard samples, the accuracy of water measurements is found to be about 5%. In terms of proton weight concentration, the error is smaller than 0.002%.

were47 μs and 40 μs, respectively. The delay between pulses was 1 s and the pulse lengths were 2 μs. About five hundred FID's were accumulated for each DOR experiment. ^{23}Na DOR NMR spectra were collected for twelve of the samples. ^{27}Al DOR NMR spectra were recorded for thirteen of the samples. The chemical shifts of ^{23}Na were measured with reference to 1 M aqueous solution of NaCl, and those of ^{27}Al, with reference to $[Al(H_2O)_6]^{3+}$ in a 1 M aqueous solution of $AlCl_3$.

^{1}H NMR spectra were measured on all the samples using a liquid NMR probe and varying the temperature from 375 K to 245 K. The spectrum of an empty rotor was measured and later subtracted from the ^{1}H spectra of scapolites to remove the background signal. The peaks were measured with reference to tetramethylsilane (TMS).

Peaks were fitted to the ^{27}Al DOR NMR spectra using a least-square iterative curve-fitting program "MDCON" written for the combination of Lorentzian and Gaussian line shapes on the Bruker AMX500 spectrometer. The width of the peaks at half height (PWHH) was not constrained by the program. Peak fitting was also done using the program "NMR286" on a 486 PC with constrained and unconstrained PWHH. In a fitting procedure with unconstrained PWHH, the estimated number of peaks, peak positions and PWHH are input as a starting point. Later the number of peaks, peak positions, peak intensities and PWHH are optimised by the program. For a constrained PWHH fitting procedure, PWHH is set at a certain value for all the peaks and the lineshape of each peak is chosen as Lorentzian.

6. 4. RESULTS AND DISCUSSION

Powder X-ray diffraction results showed that samples ON7, TANZ, ON70, MAD, CA63A, Q13, ON27 were pure; GL contains a significant amount of albite; Q26, MONT, ON8 and MIN have a small amount of albite; ON47 has an impurity which has not been identified; MIN and ON8 contain solid NaCl.

The ^{23}Na spectra are shown in Fig. 6. 3. and Fig. 6. 4. and the results are listed in Table 6. 3. From Fig. 6. 3, it can be seen that the DOR NMR spectral resolution is much higher than that of the MAS experiment and the peak widths of DOR spectra are reduced by a factor of three to four.

There is only one ^{23}Na DOR peak in the spectra of all the samples of scapolites. It is at about -20 ppm with a peak width of about 750 Hz. Sample GL (34.1% Me) has a second narrow peak at -28 ppm, which is considered to be ^{23}Na in the albite impurity in the sample. The broad width of the peaks could be caused by the disordering of Al/Si tetrahedra in the T sites, which are close to the Na cations. A similar effect has been observed in the analcime-pollucite mineral series.[6.24]

The ^{23}Na MAS NMR spectra at two magnetic field strengths have similar lineshapes and widths except for sample ON8, which has the highest Na content and a narrower peak. Assuming that there is only one Na crystallographic site in the structure, the quadrupolar parameter QCC ($C_Q(1+\eta^2/3)^{1/2}$) was calculated through the difference of the centre of gravity of the ^{23}Na MAS NMR peaks at the two magnetic field strengths (Table 6. 4), using the method described for tugtupite in

Fig. 6. 3. Comparison of ^{23}Na MAS and DOR NMR spectra of scapolite.

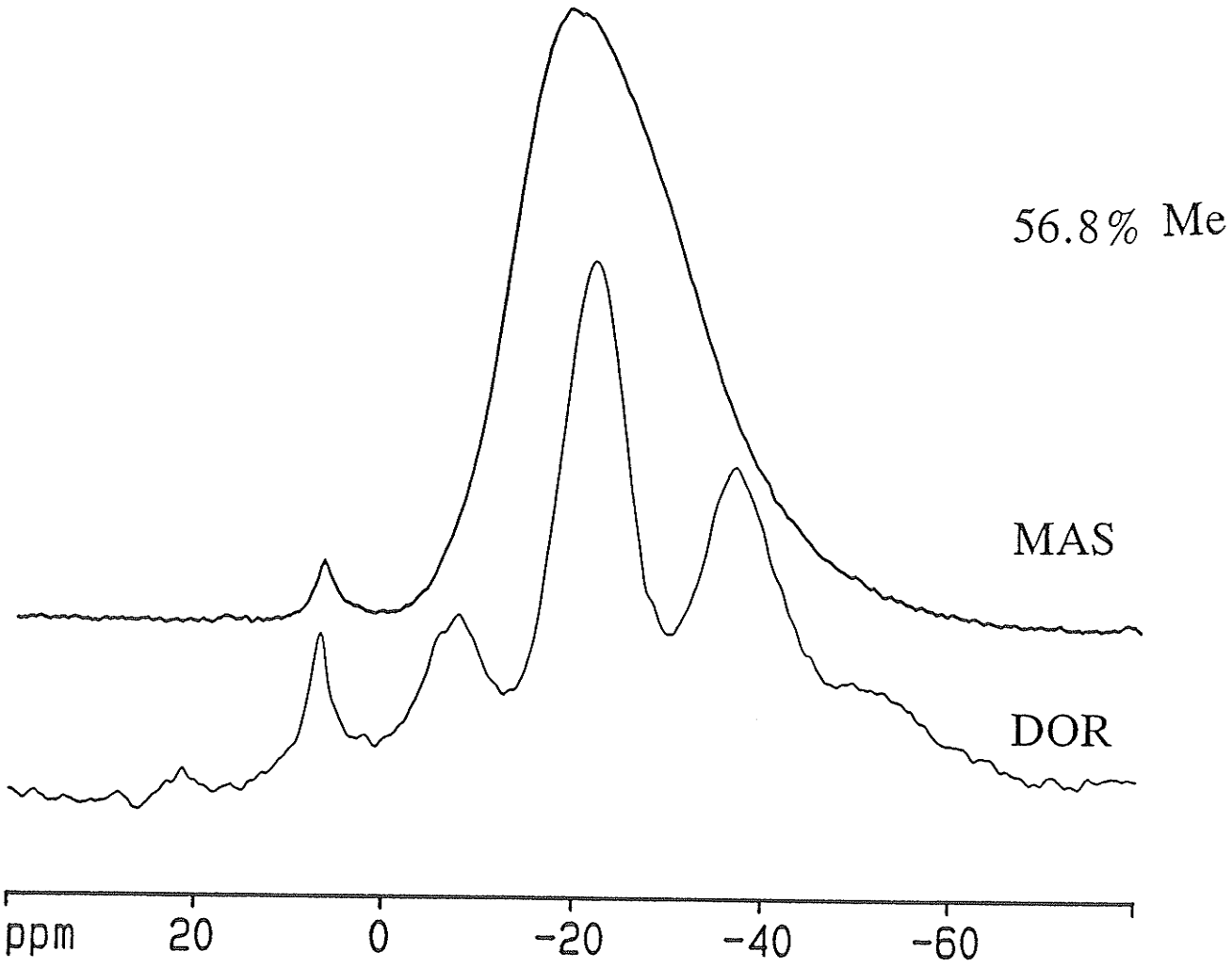

Fig. 6. 4. ^{23}Na DOR NMR spectra of scapolites.

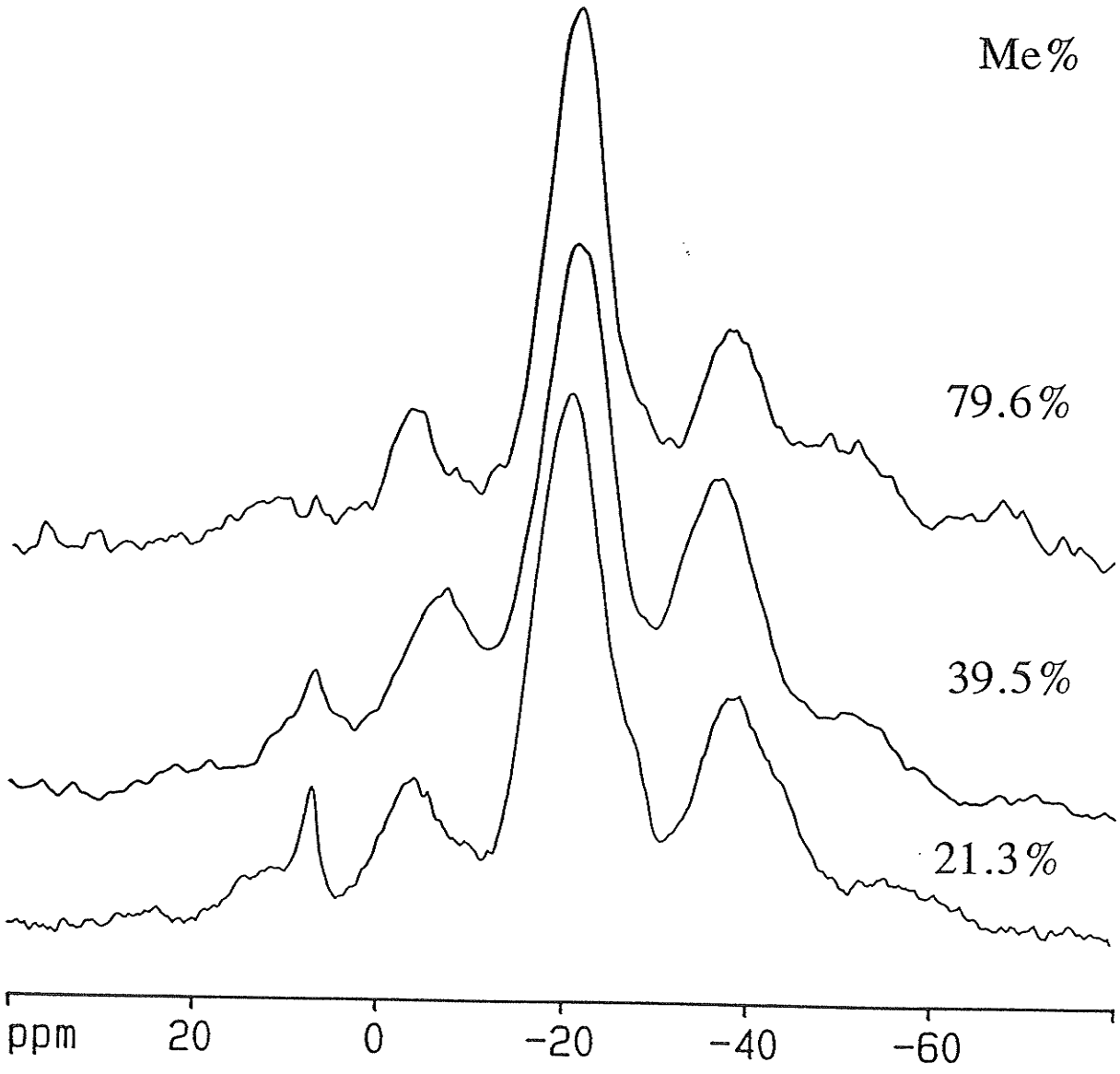

Table 6. 3. Comparison of ^{23}Na MAS and DOR Peak Width at Half Height.

sample	Me%	DOR (8.4 T): Hz	MAS (8.4 T): Hz	MAS (11.7 T): Hz
On8	21.3	830	1730	1290
TANZ	29.5	750	1950	1370
On7	33.3	740	1940	1410
GL	34.1	710	1920	1430
CA63A	44.5	860	2000	1460
Q26	48.2	860	1930	1440
Q13	51.3	740	1790	1400
Min	56.8	780	1970	1450
On47	79.6	640	1940	1400

Table 6. 4. ^{23}Na MAS and DOR Peak Positions.

sample	Me%	DOR (8.4T) ppm	MAS (8.4 T) ppm	MAS (11.7T) ppm	QCC (MHz)
On8	21.3	-19.9	-19.8	-13.7	2.1
TANZ	29.5	-21.4	-21.3	-14.2	2.3
On7	33.3	-21.5	-21.4	-14.4	2.3
GL	34.1	-21.7	-20.6	-14.6	2.1
CA63A	44.5	-21.5	-21.9	-14.7	2.3
Q26	48.2	-20.5	-20.3	-14.1	2.2
Q13	51.3	-21.2	-20.4	-14.6	2.1
MIN	56.8	-20.6	-21.0	-14.5	2.2
On47	79.6	-19.3	-20.3	-14.6	2.1

The difference ($\Delta\delta_Q$) of ^{23}Na peak positions in AMX500 and AMX360 is expressed as:

$$\Delta\delta_Q = 1.329 \cdot C_Q^2 \cdot (1 + \frac{\eta^2}{3}) = 1.329 \cdot (QCC)^2$$

$$QCC = \sqrt{\frac{\Delta\delta_Q}{1.329}}$$

Chapter Four. The QCC value of 2.2 $\pm$ 0.1 MHz means that there is a large electric field gradient at the Na nucleus, that the Na^+ cation is in a distorted environment and that the site symmetry does not appear to change substantially through the scapolite series. This agrees with the changes in symmetry of the Na site shown by bond-lengths and bond-angles from X-ray diffraction (Fig. 6. 5).[6.14]

Sample ON47 (79.6% Me) has a chlorine content of less than 0.1%, therefore, there could not be any Cl^- anions connected to Na^+ cations and Na^+ must be adjacent to a carbonate group. As the peak position and linewidth of ^{23}Na in ON47 are not significantly different from those for the other samples, there could be two possibilities : first, Na^+ cations are only connected to carbonate groups and Cl^- anions are bonded to Ca^{2+} cations or bonded to ^1H in HCO_3^- groups [6.23]; second, the peak position and linewidth of Na are not sensitive to the substitution of CO_3^{2-} for Cl^- anions. At the present time it is not possible to decide between these alternatives.

There is another distinct peak for ^{23}Na MAS and DOR spectra of sample ON8 and MIN. The position is 7.0 ppm. From the chemical shift, linewidth and the difference of observed chemical shifts in two magnetic fields (8.43 T and 11.7 T), it is found to be NaCl solid. The thin section of the two samples have been checked carefully under a microscope. No inclusions or small cubic crystals of NaCl are observed. It could be that there are NaCl structures within the voids of scapolite or some sort of sample contamination.

The resolution is much higher for ^{27}Al DOR spectra than from MAS NMR

Fig. 6. 5. (Na, Ca)-O bond lengths vs meionite content of scapolite.[6.14]

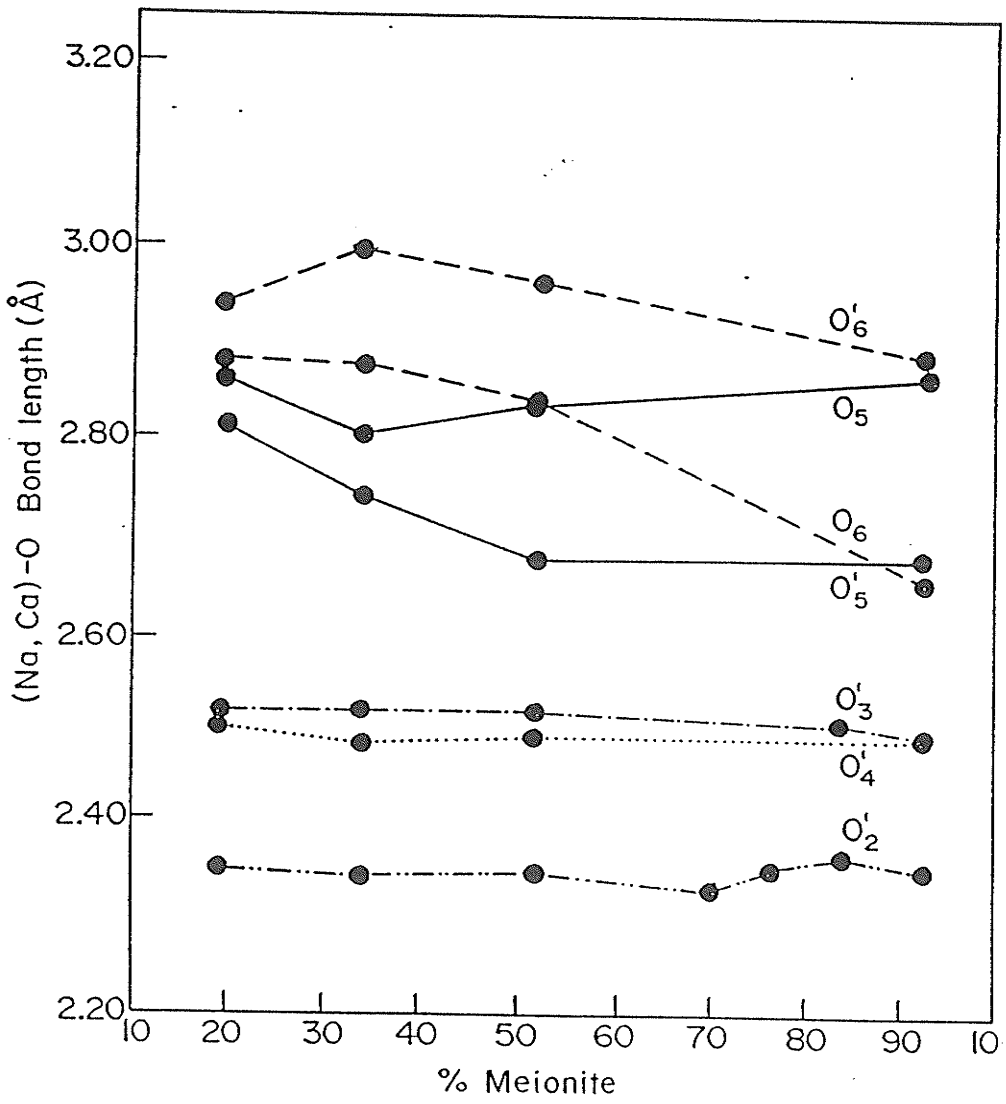

spectroscopy (Fig. 6. 6)[6.14] with two overlapping peaks resolved for eleven of the samples (Fig. 6. 7). As the DOR experiment averages the anisotropies of chemical shift, dipole-dipole and quadrupolar interactions to second-order, in the central band the remaining line broadening of the peaks are mainly due to the chemical shift distribution.

As mentioned before, T_2 and T_3 sites are magnetically equivalent and will give a single peak in NMR spectra. In the following discussion T_{23} is used to refer to both of the sites.

Al tetrahedra in T_{23} sites have two possible environments: Al(4Si) and Al(3Si 1Al), which means the next nearest tetrahedra are four Si and three Si one Al, respectively. For example, in sample ON7 (33.3% Me), according to the Si-O bond lengths from X-ray diffraction data, T_2 is mainly occupied by Al atoms, while T_1 and T_3 are full of Si atoms. Each T_2 site is connected to three T_3, and one T_1 sites (Fig. 6. 1, 6. 2). There should be mainly T_2Al(4Si) sites. However, as there is some Al substitution into T_1 sites, there should be some T_2Al(3Si 1Al) sites. Al(2Si 2Al) site is energetically unfavourable because it will form Al-O-Al bonds, which is against Lowenstein's Law.[6.21] Also there is a deficiency of Al content (smaller Al/Si ratio with respect to Me content) which further reduces the possibility of forming such kind of sites.[6.1] For high Me content, such as MONT (91.3% Me), there might be Al(2Si 2Al) or even Al(1Si 3Al) sites, but their intensities will probably be too weak to be observed. Therefore, only four magnetically non-equivalent Al sites are likely to be observed in the scapolite mineral series.

Fig. 6. 6. Comparison of ^{27}Al MAS and DOR NMR spectra of scapoite.

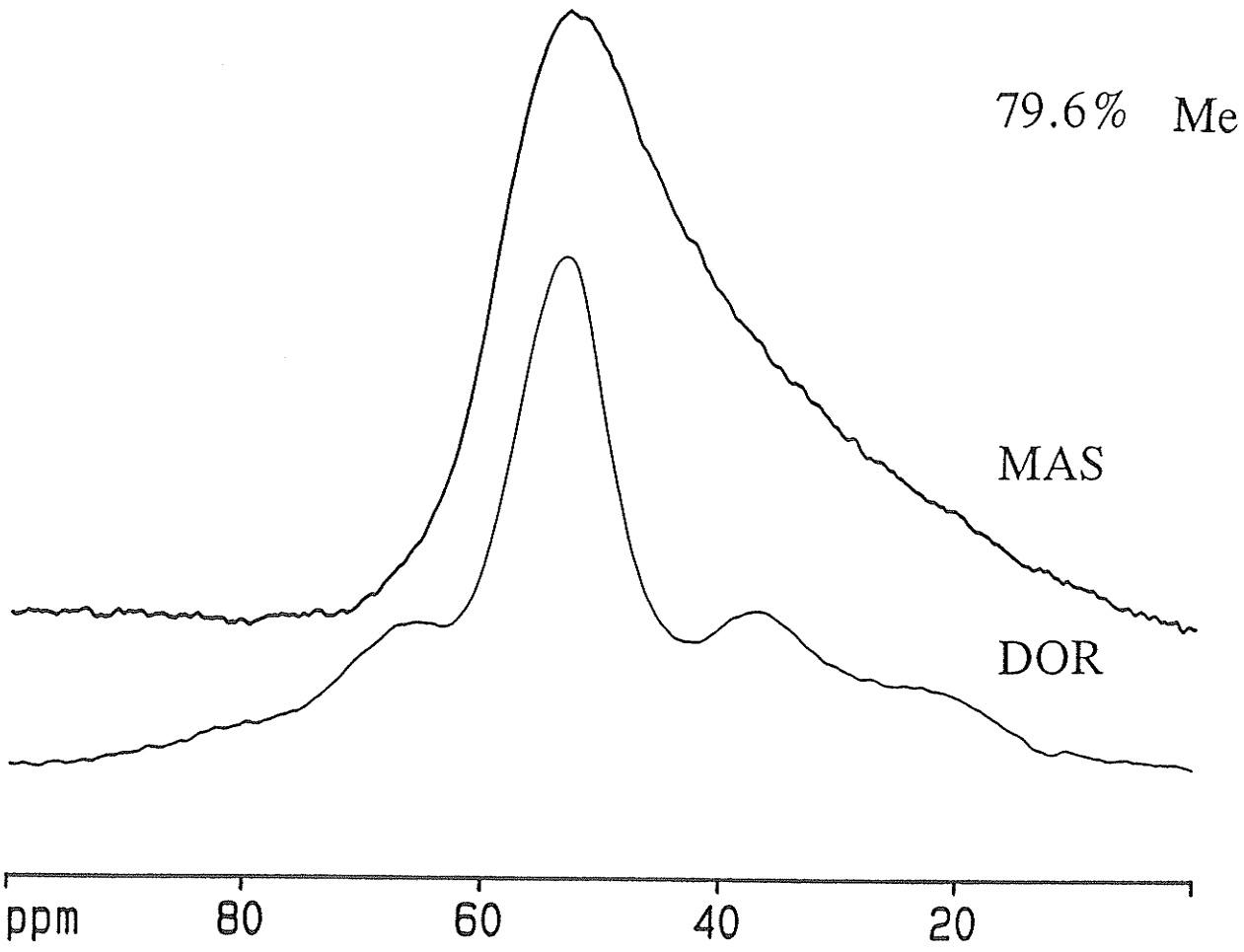

Fig. 6. 7. ^{23}Al DOR NMR spectra of scapolites.

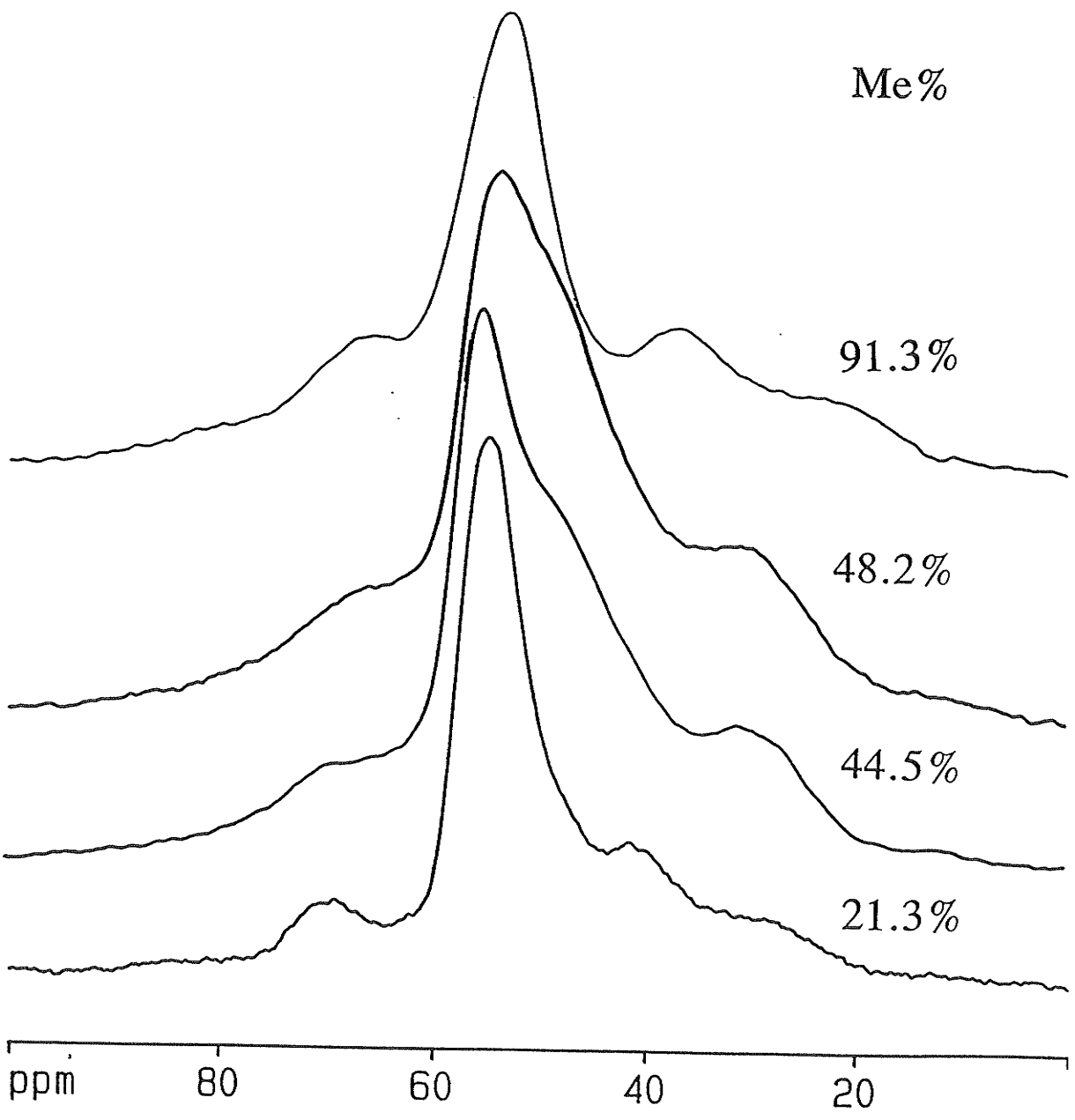

With four Si tetrahedra as next nearest neighbours, Al(4Si) is in a more symmetrical environment than that of Al(3Si 1Al) and thus is likely to have a smaller electric field gradient. The quadrupolar coupling constant of the Al(4Si) site should be smaller than that of the Al(3Si 1Al) site. Assuming Al(4Si) and Al(3Si 1Al) sites have similar isotropic chemical shifts, the negative quadrupolar shifts will move the observed position of the Al(3Si 1Al) site to a less shielded field (low field) than that of the Al(4Si) site.

Peak fitting was done using both "MDCON" and "NMR286" for all the ^{27}Al DOR spectra with unconstrained PWHH. The results are similar. For all the ^{27}Al DOR spectra of scapolites except ON47 (79.6% Me) and MONT (91.3% Me), two peaks were resolved: one has a PWHH of about 500 Hz and the position around 56 ppm while the other one has a PWHH from 1200 Hz to 1500 Hz and the position of 49 ppm (Table 6. 5). As the Me content increases, the intensity of the broad peak increases until the two peaks collapse to be one symmetrical peak at 79.6% and 91.0% Me and the peak position of 54 ppm is the average of the two.

X-ray results indicate that in a low Me content sample, such as ON8, there should be no Al in the T_1 site. The single narrow ^{27}Al peak of ON8 at 56 ppm must be assigned to T_{23} Al(4Si). Thus, the narrow ^{27}Al peak in all the DOR NMR spectra is due to T_{23} Al(4Si). The broader peak is considered to be the overlapping of three peaks : Al(3Si 1Al) site of T_{23}, Al(4Si) and Al(3Si 1Al) sites of T_1. In order to investigate the above hypothesis, further fittings with constrained PWHH using the "NMR286" program were performed for all the ^{27}Al DOR spectra. As in the

Table 6. 5. ^{27}Al DOR NMR fitting results with unconstrained PWHH.

sample	Me%	Position	(ppm)	Width	(Hz)	Relative	Intensity
		1	2	1	2	1	2
On8	21.3	55.7	50.9	470	860	0.6	0.4
TANZ	29.5	55.5	48.3	450	1270	0.4	0.6
On7	33.3	55.1	47.7	470	1420	0.4	0.6
GL	34.1	56.6	48.8	400	1110	0.5	0.5
On70	39.5	56.0	48.9	520	1300	0.3	0.7
CA63A	44.5	55.5	48.6	460	1330	0.3	0.7
Q26	48.2	55.2	49.1	550	1300	0.3	0.7
Q13	51.3	55.2	48.9	530	1240	0.3	0.7
MIN	56.8	54.9	48.9	580	1170	0.3	0.7
On27	59.3	54.8	48.2	700	1040	0.4	0.6

unconstrained fittings mentioned above there is a narrow peak of 500 Hz assigned to be Al(4Si) across the whole scapolite series; the PWHH was fixed at 500 Hz for all the four peaks in the central bands of the DOR spectra. The results are listed in Table 6. 6. As the ^{27}Al relative peak intensities depend on other factors besides the site occupancy ratio, such as the size of C_Q (Chapter Five) and rotor spinning speed,[6.24] these fittings give qualitative results, which will elucidate some of the Al/Si framework disordering structure.

As the T_1 site is quite different from T_{23}, peak one (57 ppm) and two (51 ppm) are assigned as Al(4Si) and Al(3Si 1Al) of T_{23}, and peak three (42 ppm) and four (33 ppm) for Al(4Si) and Al(3Si 1Al) of T_1, respective. With the increment of Me content, more Al goes into T_1 sites and the relative areas of T_1 sites increase from 35% (TANZ, 29.5% Me) to 45% (MIN, 56.8% Me). This increasing trend of Al in T_1 sites agrees with the X-ray diffraction results.

In a unit cell of scapolite, there are twelve T_1, six T_2 and six T_3 tetrahedra. In the end-member meionite there are equal amounts of Si and Al tetrahedra and Al is evenly distributed among T_1, T_2 and T_3 sites. Thus, as the Me content approaches 100%, the Al peak of T_1 and T_{23} should have equal intensities. They will form one symmetrical peak with the peak position at the average of the two. This happens in the ^{27}Al DOR NMR of sample ON47 and MONT. Another possible explanation is that ON47 and MONT have different structures from the other scapolites. As we study the DOR spectra of these samples, it is found that there are three different kinds of lineshapes: the first one is ON8, which has a symmetrical

Table 6. 6. Fitting results of ^{27}Al DOR spectra of scapolites with constrained PWHH of 500 Hz.

sample	ME %	peak positions (ppm)				relative intensity			
		1	2	3	4	1	2	3	4
ON8	23.1	58	52	44		0.43	0.37	0.20	
		58	53	48		0.40	0.38	0.22	
TANZ	29.5	57	52	43	34	0.38	0.27	0.19	0.16
		57	50	42	33	0.36	0.25	0.20	0.19
ON7	33.3	56	50	41	32	0.37	0.245	0.20	0.185
ON70	39.5	57	50	42	34	0.31	0.25	0.24	0.20
CA63A	44.5	56	50	41	31	0.35	0.25	0.22	0.18
Q26	48.2	58	52	46	38	0.29	0.28	0.23	0.20
Q13	51.3	57	51	43	35	0.30	0.27	0.24	0.19
		57	50	41	31	0.30	0.28	0.24	0.18
MIN	56.8	58	51	44	35	0.28	0.27	0.25	0.20
		59	52	45	37	0.29	0.27	0.24	0.20
ON27	59.3	58	51	44	37	0.29	0.30	0.23	0.18
ON47	79.6	61	55	50	44	0.22	0.31	0.27	0.20
		61	55	50	44	0.20	0.31	0.28	0.21
MONT	91.3	60	53	44	28	0.30	0.32	0.22	0.16
		63	57	51	44	0.23	0.32	0.27	0.17

peak around 57 ppm with a very small shoulder at the low field end (PWHH = 600 Hz); the next one is from Tanz to ON27, where all the ^{27}Al DOR spectra consist of two overlapping peaks, one broad and the other narrow; the third one is the DOR spectra of ON47 and MONT, which has a symmetrical broad peak (PWHH = 1100 Hz) around 55 ppm. It is more clear to see this from Table 6. 6. This distribution corresponds to the differences in the ^{29}Si MAS NMR spectra obtained by Sherriff.[6.]

Another interesting thing is that Al starts to go into T_1 tetrahedra at the Me content of 23.1%. This result is against the ordering model of Lin and Burley.[6.18] According to their model, there is no Al in T_1 sites until after 37.5% Me content and at 37.5% Me content the Al/Si framework is most ordered. As Si and Al atoms have similar X-ray diffraction scattering factors, it is difficult to detect a small amount of Al. Neutron diffraction data is needed to check our DOR NMR results.

The water contents of ten scapolite samples are listed in Table 6. 2. ^1H solid state NMR showed that there was a small peak at around 7 ppm superimposed on a broad base line peak for all the samples. If there are mobile water molecules in scapolite, they would give a strong narrow signal similar to the one seen in the zeolite chabasite.[6.25] Therefore the proton could be in the form of HCl, HCO_3^-, $(OH)^-$ or HSO_4^-. As the states of protons and their roles in charge balance are crucial in crystal chemistry calculations, such as bond valence calculations, ^1H MAS or even ^1H CRAMPS experiments are recommended to clarify this.

The Al/Si ordering model of Lin and Burley [6.7] needs to be revised in the light of this new data. However, the NMR data are insufficient to establish a new

model and further experiments, neutron diffraction data and even higher resolution NMR data are needed.

6. 5. CONCLUSION

The new NMR technique, DOR, is used to study the Al/Si framework and Na cation ordering problem in scapolites. Different ways of fitting peaks to the spectra have been done to investigate the possible explanations. The new data do not agree with the ordering model from single crystal X-ray diffraction. Al is believed to substitute into T_1 sites with Me content higher than 29%. The perfect ordering model at 37.5% of Lin et al. (1973) needs revising. New data on proton contents are obtained. Further experimental data are required to elucidate this challenging problem.

REFERENCE FOR CHAPTER SIX

[6.1] a. D. M. Shaw : The geochemistry of scapolite. Part I, Previous work and general mineralogy. J. Petrol. **1**, 218 (1960).

b. D. M. Shaw : The geochemistry of scapolite. Part II, Trace elements, petrology and general geochemistry. J. Petrol. **1**, 261 (1960).

[6.2] B. W. Evans, D. M. Shaw and D. R. Haughton : Scapolite stoichiometry Contrib. Mineral. Petrol. **24**, 293 (1969).

[6.3] J. F. Lovering and A. J. R. White : The significance of primary scapolite in granulitic inclusions from deep-seated pipes. J. Petrol. **5**, 195 (1964).

[6.4] B. W. Chappell and A. J. R. White : The X-ray spectrographic determination of sulphur coordination in scapolite. Amer. Mineral. **53**, 1735 (1968).

[6.5] a. B. J. Burley, E. B. Freeman and D. M. Shaw : Studies on scapolite Can. Mineral. **6**, 670 (1961).

b. D. M. Shaw, R. L. Moxham, R. H. Fily and W. W. Lapkowsky : The petrology and geochemistry of some Grenville skarns. Part II, geochemistry. Can. Mineral. **7**, 578 (1963).

c. C. O. Ingamells and J. Gittins : The stoichiometry of scapolite Can. Mineral. 45, 215 (1967).

[6.6] W. A. Deer, R. A. Howie and J. Zussman Rock-Forming Minerals, vol. 4, Longmas, London.

[6.7] a. S. B. Lin and B. J. Burley : Crystal structure of a sodium and chlorine-rich

scapolite. Acta. Crystallogr. **B29**, 1272 (1973).

b. S. B. Lin and B. J. Burley : On the weak reflections violating body centred symmetry in scapolites. Tschermaks Mineral. Petrogr. Mitt. **20**, 28 (1973).

[6.8] A. Scherillo : La meionite del Somma-Vesuvius. Period. Miner. **6**, 227 (1935).

[6.9] G. Graziani and S. Lucchesi : The thermal behaviour of scapolites. Amer. Mineral. **67**, 1229 (1982).

[6.10] J. Hoefs, J. J. Coolen and J. Touret : The sulphur and carbon isotope composition of scapolite-rich granulites from southern Tanzania Contrib. Mineral. Petrol. **78**, 332 (1981).

[6.11] A. P. Jones and J. V. Smith : Ion probe analysis of H, Li, B, F, and Ba in micas, with additional data for metamorphic amphibole, scapolite and pyroxene N. Jb. Miner. Mh. **H5**, 228 (1984).

[6.12] I. Hassan and P. R. Buseck : HRTEM characterization of scapolite solid solutions Amer. Mineral. **73**, 119 (1988).

[6.13] A. B. Vassilikou-Dova : An EPR study of scapolite Cryst. Res. Technol. **26**, 135 (1991).

[6.14] B. L. Sherriff, H. D. Grundy and J. S. Hartman : Occupancy of T-sites in the scapolite series. A multinuclear NMR study using magic angle spinning. Can. Mineral. **25**, 717 (1987).

[6.15] L. Pauling : The structure of some sodium and calcium alumino-silicates. Proc. Wash. Acad. Sci. **16**, 453 (1930).

[6.16] a. J. J. Papike and T. Zoltai : The crystal structure of a marialite scapolite. Amer. Mineral. **50**, 641 (1965).

b. J. J. Papike and N. C. Stephenson : The crystal structure of mizzonite, a calcium- and carbonate-rich scapolite. Amer. Mineral. **51**, 1014 (1966).

[6.17] L. Levien and J. J. Papike : Scapolite crystal chemistry: aluminum-silicon distribution, carbonate group disorder and thermal expansion. Amer. Mineral. **61**, 864 (1976).

[6.18] S. B. Lin and B. J. Burley : The crystal structure of meionite. Acta. Crystallogr. **B29**, 2024 (1973).

[6.19] S. B. Lin and B. J. Burley : The crystal structure of an intermediate scapolite-wernerite. Acta. Crystallogr. **B31**, 1806 (1975).

[6.20] H. H. Ulbrich : Crystallographic data and refractive indices of scapolites. Amer. Mineral. **58**, 81 (1973).

[6.21] W. Lowenstein : The distribution of aluminum in the tetrahedra of silicates and aluminosilicates. Amer. Mineral. **39**, 92 (1954).

[6.22] W. E. Klee : Al/Si distribution in tectosilicates: Scapolites Z. Kristallogr. **140**, 163 (1974).

[6.23] G. Donnay, C. F. Shaw, I. S. Butler and J. R. O'Neil : The presence of HCl in scapolite Can. Mineral. **16**, 341 (1978).

[6.24] D. Massiot, C. Bessada, J. P. Coutures and F. Taulelle : A quantitative study of ^{27}Al MAS NMR in crystalline YAG J. Magn. Reson. **90**, 231 (1990).

[6.25] D. K. Teertstra, B. L. Sherriff, Z. Xu and P. Cerny : MAS and DOR NMR

study of ordering in the analcime-pollucite series. Can. Mineral., in print.